Fractionalization of Forchheimer’s correction to Darcy’s law in porous media in large deformations

Fractionalization of Forchheimer's correction to Darcy's law in porous media in large deformations

Sachin Gunda[1], Alessandro Giammarini[2], Ariel Ramírez-Torres[3], Sundararajan Natarajan[1], Olga Barrera[4,5], and Alfio Grillo[2*]

[1]Department of Mechanical Engineering, Indian Institute of Technology Madras, Chennai, Tamil Nadu, India.
[2]Dip. di Scienze Matematiche "G. L. Lagrange", Politecnico di Torino, Corso Duca degli Abruzzi 24, 10129, Torino, Italia.
[3]School of Mathematics & Statistics, Mathematics & Statistics Building, University Place, Glasgow, G12 8QQ, UK.
[4]School of Engineering, Computing and Mathematics, Oxford Brookes University, Headington, Oxford OX3 0BP, UK.
[5]Department of Engineering Science, University of Oxford, Parks Road, OX1 3PJ, Oxford, UK.

Abstract

This work presents a theoretical and numerical study of the flow of the interstitial fluid saturating a porous medium, principally aimed at modeling a bio-mimetic material and assumed to experience a dynamic regime different from the Darcian one, as is typically hypothesized in biomechanical scenarios. The main aspect of our research is the conjecture according to which, for a particular mechanical state of the porous medium, the fluid exhibits two types of deviation from Darcy's law. One is due to the inertial forces characterizing the pore scale dynamics of the fluid. This aspect can be resolved by turning to the *Forchheimer correction* to Darcy's law, which introduces non-linearities in the relationship between the fluid filtration velocity and the dissipative forces describing the interactions between the fluid and the solid matrix. The second source of discrepancies from classical Darcy's law emerges, for example, when pore scale disturbances to the flow, such as obstructions of the fluid path or clogging of the pores, result in a time delay between drag force and filtration velocity. Recently, models have been proposed in which such delay is described through constitutive laws featuring fractional operators. Whereas, to the best of our knowledge, the above-mentioned behaviors have been studied separately or in small deformations, we present a model of fluid flow in a deformable porous medium undergoing large deformations in which the fluid motion obeys a fractionalized Forchheimer's correction. After reviewing Forchheimer's formulation, we present a fractionalization of the Darcy-Forchheimer law, and we explain the numerical procedure adopted to solve the highly non-linear boundary value problem resulting from the presence of the two considered deviations from the Darcian regime. We complete our study by highlighting the way in which the fractional order of the model tunes the magnitude of the pore pressure and fluid filtration velocity.

Keywords: Flow in deformable porous media; Darcy's law; Forchheimer's correction; Media with memory; Integro-differential constitutive equations; Fractional Calculus; Fractional integrals and derivatives.

1 Introduction

According to a rather consolidated modeling picture in the biomechanical literature[1], a biological tissue classified as *soft* and *hydrated* is regarded, at least, as a biphasic medium[2], constituted by a sufficiently

*Corresponding author: Alfio Grillo, Dipartimento di Scienze Matematiche "G. L. Lagrange", Politecnico di Torino, Torino, 10129.
Email: alfio.grillo@polito.it

compliant solid porous matrix and a fluid that participates in a variety of biophysical, biochemical, and mechanical processes, all essential for sustaining the tissue itself[2, 3, 4, 1, 5].

The characterization of the mechanical properties of the solid matrix of soft tissues, be they hydrated or not, has been the subject of several studies with increasing level of complexity: whereas the first, pioneering models looked at the essence of phenomenology, and, for their purposes, considered tissues (see, e.g.,[2] for articular cartilage) homogeneous and isotropic, more recent works studied the consequences of inhomogeneity and anisotropy, especially in connection with the presence of reinforcing collagen fibers[6, 7, 8, 9, 10, 11], often assumed to be statistically oriented[12, 13, 14, 15, 16, 17, 18].

Collagen fibers represent a very important chapter in the mechanical and hydraulic analysis of biological tissues. Indeed, besides exerting a structural action that contributes to the overall mechanical response of a given tissue, they influence considerably also the tendency of the tissue to enhance, or to inhibit, the circulation of fluid in its interior. At the macroscale, this property is referred to as *permeability*. For example, in the case of articular cartilage, Maroudas and Bullough[6] have hypothesized that the tissue's permeability depends on the distribution and orientation of the collagen fibers. Subsequent studies in this direction, conceived to examine Maroudas and Bullough's hypothesis[6] have been conducted, e.g., in[19, 20], and set themselves in a line of research dedicated to the theoretical and numerical modeling of the biomechanics of fiber-reinforced, anisotropic tissues[8, 21, 22, 23, 24, 25, 26, 17, 27, 18].

To the authors' knowledge, since Holmes and Mow's permeability model[2] for articular cartilage, the explicit coupling between this transport property and the tissue's deformation has been a leading topic in many other publications on the subject (see, e.g.,[21, 22, 24, 20]). In all these works, emphasis is put on the importance of understanding how the mechanics of the tissue combines with its permeability in order to provide acceptable descriptions of the fluid's behavior, especially in terms of its mechanical state. This is motivated by the fact that being able to predict, for example, the fluid pressure allows to estimate possible remarkable aspects of a tissue, like its global health[28, 7, 29].

Rather typical approaches having the purpose of studying the mechanics of soft and hydrated tissues, like articular cartilage, and, above all, of giving prominence to the coupling discussed above, are based on several formulations of poro-elasticity, in terms either of Biot's or of biphasic theory [1, 22, 19, 24, 20, 17, 30, 31]. A common feature of the majority of these approaches is that they rely on the hypothesis that the flow of the fluid obeys Darcy's law (see, e.g.,[32, 33, 34, 1, 22]), thereby presuming, in the most classical formulation, a linear relationship between the fluid filtration velocity and the pressure gradient realized in the tissue. More precisely, the filtration velocity is obtained by multiplying the medium permeability (which, in general, is a second-order tensor field) by the opposite of the pressure gradient. The resulting flow model has the advantage of being computationally cheap, because of the linearity of this relationship with respect to the pressure gradient, and it is sufficient to capture the coupling between flow and deformation through a suitable definition of the permeability tensor (see, e.g., [2]). In fact, this coupling is also capable of considering nonlinear deformations. In spite of this capability, however, in the literature there have also been attempts to elaborate flow models that account for non-Darcian behaviors of the fluid, like, for instance, those predicted by Forchheimer or Brinkman's corrections to Darcy's law (see, e.g.,[35, 36, 30]).

In the context of articular cartilage, in[36, 30], the authors have hypothesized that, under certain loading conditions, as could be the case in compression tests in which the load is applied with a relatively high velocity, the mechanical behavior of the fluid is better approximated by the Darcy-Forchheimer model of the flow. In fact, adopting Forchheimer's correction means accounting for non-linear terms in the constitutive relationships between the filtration velocity and the drag force that may generally result in slower flows and higher pressures than those predicted by Darcy's law. This, in turn, calls for the introduction of additional parameters to describe the flow, the identification of which may depend on the structure of the porous medium[37], the model of permeability[22, 19], and the experimental procedure employed to estimate the numerical values of the quantities at hand. In addition, it has been shown in[30] that resorting to the Darcy-Forchheimer law may be used to switch from a model of permeability to another one by attributing the resulting variations in the behavior of the fluid to the correction of the flow rather than to different assumptions on the permeability.

Another phenomenon that is not accounted for in the "classical" formulation of the Darcy or Darcy-Forchheimer models is the anomalous "diffusion" of the fluid flow (see, e.g.,[38]). In particular, Darcy's law has proved to be non appropriate for fluid flow in high porosity media due to the influence of inertial, thermal, and convective terms, and because of solid-fluid boundary effects that are not contemplated in Darcy's model[39].

Recently, a body of work has gone into collecting experimental evidence of anomalous "diffusion" (another type of non-Darcian behavior) for different classes of porous media, from tissues, such meniscal tissue[40], to rocks and porous building materials[41]. The predominant matter is the explicit time-dependence of the permeability, which results in an explicitly time-dependent flow rate.

In [42], clogging of the pores and explicit time-dependence of the permeability of hydro-geological porous media are described by means of an integro-differential operator that keeps track of the time history of permeability. This study offers a very important point of departure for the introduction of Fractional Calculus in modeling flow in porous media, especially for describing deviations from Darcian transport, as is the case for subdiffusion or superdiffusion processes, both observable experimentally[38, 43].

Confined compression tests in meniscal tissues have shown that anomalous transport phenomena are well captured by fractional poroelastic models (e.g., of Biot-type) in which the pore pressure diffusion equation results from a modified version of Darcy's law involving fractional derivatives[40, 44, 45]. The diffusion is then anomalous and the order of the fractional derivatives involved in the models rules the fluid flow. Fittings of experimental data proved to be better than adopting classical Biot or biphasic models, and the fractional poroelastic model has been —for the first time— validated [44]. The values of the fractional order, obtained by fitting the experimental data across various samples, vary in the range $[0.51, 0.73]$[44], and are considerably higher than the ones found by Bulle et al.[40]. Hence, the memory effects related to the fluid flow in the meniscus seem to be, in general, not negligible. In addition, since the model in[44] is transversely isotropic for both the fractional and the standard case, the fractional derivative captures the deviation from classical Darcy's law triggered by the presence of a hierarchical network of collagen channels in the meniscus, which is not inherently related to the anisotropy of the medium. By our understanding, this result shows that biological tissues can exhibit a behavior well captured by the methods of Fractional Calculus, and related to the tortuosity of the pores. Moreover, the model developed in[44] accounts only for small deformations. In this sense, one of the aims of our work is to provide the mathematical infrastructure to deal with temporal fractional derivatives within a large deformation setting, while complying with the principle of objectivity.

Other studies[46, 47] highlight the role of poroelasticity in the anomalous "diffusion" processes that can be observed on meniscus samples. In the literature, some investigations have been done to capture the relationship between the memory effects of the flow of interstitial fluid, which are due to the interactions between the fluid and the pore network, and the behavior of the solid phase. In particular, in[31] a fractional Darcy's law was studied in the setting of small elastic strains, while in[48] classical Darcy's law was coupled with a solid phase experiencing *"material hereditariness"*[49, 50, 51], i.e., dependence of the stress on the past history of strain, which was described by means of a fractional-order *"hereditariness"* model[52, 53, 54, 55].

With respect to the review of literature done above, the novelty of our work resides in the search for memory effects associated with a *fractional Darcy-Forchheimer* flow model developed in the framework of *finite deformations*. After presenting the constitutive theory on which our study relies, we simulate an unconfined compression test, performed over a cylindrical specimen of a hypothetical tissue that has "borrowed" some properties from articular cartilage[7, 9, 29, 56, 20], but is assumed here to be homogeneous and isotropic. Note also that we speak of a "hypothetical tissue" because, for the time being, we do not have experimental values for the parameters defining the fractional operators adopted in the sequel. We take the elastic coefficients of articular cartilage because of the studies available in the literature that address explicitly memory effects in this tissue and employ Fractional Calculus (see e.g.[57, 58], although the framework established therein is very different from ours). In addition, we select the unconfined compression test since this is a rather standard experimental set-up and is able to provide information in quite a simple manner about the relationship between specimen deformation and

fluid flow.

As remarked above, the assumption of homogeneity and isotropy is not realistic, but we need it now in order to focus on the novelties of our model without having to deal with other sources of computational complications. However, a generalization to an inhomogeneous and anisotropic medium, with statistical orientation of reinforcing collagen fibers, is not too demanding from the modeling point of view, since the literature in the field is quite rich[8, 21, 22, 23, 24, 25, 26, 17, 27, 18], although it necessarily increases the computational burden.

Before proceeding, we clarify that, at the moment, we *are not* aiming at reproducing any experiment conducted on a real medium, be it a bio-mimetic scaffold or a true biological tissue. Rather, we are presenting a study that is meant to indicate, through numerical simulations, new research directions in the field of Fractional Calculus applied to Biomechanics. In this sense, the numerical simulations presented in the sequel may provide guidance in devising experimental procedures that aim at quantifying the presence of possible memory effects in the flow of the interstitial fluid of the medium under study. The model and the associated simulations, in fact, should act like a magnifying glass on the internal mechanics of the medium and of the memory effects (non-local in time) taking place in it. We believe that such information could aid in designing experiments.

Our principal results are: (i) the formulation of a fractional constitutive equation that expresses the dissipative drag force stemming from the fluid-solid interactions as a functional of the fluid filtration velocity; and (ii) the numerical procedure developed to solve this equation together with the momentum and mass balance laws characterizing the fractional Darcy-Forchheimer model in finite deformations. The main outcomes of our simulations predict the influence of the fractionalization of Forchheimer's correction on pore pressure and on the magnitude of the fluid filtration velocity.

2 Kinematics of biphasic mixtures

In this section, we briefly present the kinematics of solid-fluid mixtures in the framework delineated in [59, 60]. The solid and the fluid phase are represented by two smooth material manifolds $\mathcal{M}_\mathrm{s}$ and $\mathcal{M}_\mathrm{f}$, and the embedding of the solid phase in the three dimensional Euclidean space $\mathcal{S}$ is called *reference placement* of the solid phase $\mathcal{B} \subset \mathcal{S}$.

The class of media taken as target in this work refers mainly to bio-mimetic scaffolds, to be employed, for example, in the replacement of injured tissues, as could be the case of articular cartilage, which comprises cells, extracellular matrix, and collagen fibers. Although such target media may feature complicated internal structures a simplified approach is followed in the sequel. This is done because, for a given target tissue, the focus of our work is not a detailed description of the tissue's structure.

In this work, we adhere to the description of the solid phase put forward in[30]. For each instant of time t of the time window $\mathcal{I} \subset]0, +\infty[$ in which we keep track of the evolution of the system, the motion $\chi(\,\cdot\,, t) : \mathcal{B} \to \mathcal{S}$ of the solid phase maps the reference placement $\mathcal{B}$ into the *current placement* $\chi(\mathcal{B}, t)$. This description can be extended also to the case in which the solid phase features several constituents (e.g., extracellular matrix, cells, and collagen fibers) by hypothesizing, as is often done in this context, that the "points" of $\mathcal{M}_\mathrm{s}$ share the same motion. Furthermore, for each $t \in \mathcal{I}$, the motion of the fluid is described by means of a one-parameter family of embeddings $\mathfrak{f}(\,\cdot\,, t) : \mathcal{M}_\mathrm{f} \to \mathcal{S}$ that attaches fluid particles $\mathfrak{X}_\mathrm{f} \in \mathcal{M}_\mathrm{f}$ to a point in the Euclidean space $\mathcal{S}$. The portion of $\mathcal{S}$ in which the solid and the fluid phases coexist is denoted by $\mathcal{B}_t := \chi(\mathcal{B}, t) \cap \mathfrak{f}(\mathcal{M}_\mathrm{f}, t)$[59, 60] and constitutes the solid-fluid mixture. Furthermore, for each time $t \in \mathcal{I}$, we assume, with a slight abuse of notation, that the inverse mapping in space $[\chi(\,\cdot\,, t)]^{-1} : \mathcal{B}_t \to \mathcal{B}$ is surjective with respect to the reference placement of the solid phase, so that for each point of the mixture there is a corresponding point in the reference placement of the solid phase (since $\chi(\,\cdot\,, t)$ is injective but nor surjective, the inverse $[\chi(\,\cdot\,, t)]^{-1}$ has to be understood, with an abuse of notation, as the inverse of the auxiliary map $\hat{\chi}(\,\cdot\,, t) : \mathcal{B} \to \mathcal{B}_t$, with $\hat{\chi}(X, t) \equiv \chi(X, t)$).

In summary, the hydrated media considered hereafter, even with multiple solid constituents, are seen at the macroscale as mixtures with a solid component and a fluid one. In particular, following [61, 20], and under the hypothesis that the heterogeneities at the medium's fine scale do not affect the behavior

of the medium at the macroscale [62], we introduce an admissible representative element [62] and the fraction of relative volume which is occupied by the solid or by the fluid phase. These quantities are called, respectively, the solid volumetric fraction and the fluid volumetric fraction, and are denoted by $\phi_\alpha : \mathscr{B}_t \rightarrow]0,1[$, with $\alpha = \mathrm{s}, \mathrm{f}$.

For each point $x \in \mathscr{B}_t$ in the current placement and each point $X \in \mathscr{B}$ in the reference placement, we introduce the tangent spaces $T_x\mathscr{S}$ and $T_X\mathscr{B}$, and the dual spaces $T^*_x\mathscr{S}$ and $T^*_X\mathscr{B}$, respectively, as well as the tangent bundles $T\mathscr{S} := \bigsqcup_{x\in\mathscr{B}_t} T_x\mathscr{S}$ and $T\mathscr{B} := \bigsqcup_{X\in\mathscr{B}} T_X\mathscr{B}$. Similarly, we define the cotangent bundles $T^*\mathscr{S} := \bigsqcup_{x\in\mathscr{B}_t} T^*_x\mathscr{S}$ and $T^*\mathscr{B} := \bigsqcup_{X\in\mathscr{B}} T^*_X\mathscr{B}$ (see e.g. [63] for further details).

The velocity of a solid particle passing at the time t through the spatial point $x = \chi(X,t)$ is denoted by $\boldsymbol{v}_\mathrm{s}(x,t) = \dot{\chi}(X,t) \in T_x\mathscr{S}$, with the superimposed dot meaning partial differentiation with respect to time, while the velocity of a fluid particle passing through the same spatial point $x \in \mathscr{B}_t$ is obtained as $\boldsymbol{v}_\mathrm{f}(x,t) = \dot{\mathfrak{f}}(\mathfrak{X}_\mathrm{f},t) \in T_x\mathscr{S}$. The above defined velocities $\boldsymbol{v}_\mathrm{s}$ and $\boldsymbol{v}_\mathrm{f}$ are also known as *spatial* velocities, while the relative motion of the fluid with respect to the solid phase is described by the relative velocity as $\boldsymbol{w}_\mathrm{fs}(x,t) := \boldsymbol{v}_\mathrm{f}(x,t) - \boldsymbol{v}_\mathrm{s}(x,t)$. For the fluid phase, we also introduce the *filtration velocity* $\boldsymbol{q}(x,t) := \phi_\mathrm{f}(x,t)\boldsymbol{w}_\mathrm{fs}(x,t) \in T_x\mathscr{S}$, which represents the specific mass flux vector of fluid passing through $x \in \mathscr{B}_t$ at time t (i.e., the mass flux vector normalized by the fluid true mass density ϱ_f)[33].

Finally, we introduce the tangent map of the motion of the solid phase, $\boldsymbol{F}(X,t) = T\chi(X,t) \equiv D\chi(X,t)$, where $D\chi$ is the Jacobian tensor associated with χ, known as the *deformation gradient tensor* $\boldsymbol{F}(X,t) : T_X\mathscr{B} \rightarrow T_{\chi(X,t)}\mathscr{S}$, which transforms vectors of $T_X\mathscr{B}$ into vectors of $T_x\mathscr{S}$, with $x = \chi(X,t)$. In order for a motion to be admissible, the determinant of $\boldsymbol{F}$ is required to satisfy the condition $J(X,t) := \det\boldsymbol{F}(X,t) > 0$, for all $X \in \mathscr{B}$ and $t \in \mathscr{I}$, so that $\boldsymbol{F}$ is non-singular. Similarly, we define the inverse, the transpose, and the inverse transpose tensors of $\boldsymbol{F}$, that is, $\boldsymbol{F}^{-1}(x,t) : T_x\mathscr{S} \rightarrow T_X\mathscr{B}$, $\boldsymbol{F}^{\mathrm{T}}(x,t) : T^*_x\mathscr{S} \rightarrow T^*_X\mathscr{B}$, and $\boldsymbol{F}^{-\mathrm{T}}(X,t) : T^*_X\mathscr{B} \rightarrow T^*_x\mathscr{S}$, respectively, with $X = [\chi(\,\cdot\,,t)]^{-1}(x)$. As usual, the Cauchy-Green deformation tensor $\boldsymbol{C}(X,t) : T_X\mathscr{B} \rightarrow T^*_X\mathscr{B}$ is defined as $\boldsymbol{C}(X,t) = \boldsymbol{F}^{\mathrm{T}}(x,t)\boldsymbol{\eta}(x)\boldsymbol{F}(X,t)$, with $x = \chi(X,t)$, and $\boldsymbol{\eta}(x) : T_x\mathscr{S} \rightarrow T^*_x\mathscr{S}$ being the spatial metric tensor attached at the spatial point $x \in \mathscr{S}$[63]. When there is no room for confusion, also the less rigorous notations $\boldsymbol{C} = \boldsymbol{F}^{\mathrm{T}}.\boldsymbol{F} \equiv \boldsymbol{F}^{\mathrm{T}}\boldsymbol{\eta}\boldsymbol{F}$ will be employed, in which the dot "." is an abbreviation for the spatial metric tensor field $\boldsymbol{\eta}$.

Remark 1 (Composition of maps and notation).
To pass from the current placement to the reference placement, we compose any field $\varsigma : \mathscr{B}_t \times \mathscr{I} \rightarrow \mathbb{S}$, valued in $\mathbb{S} \equiv \mathbb{R}$ or in higher-order vector or tensor spaces, with χ and the time map $\mathfrak{T} : \mathscr{B} \times \mathscr{I} \rightarrow \mathscr{I}$, so that it holds that $\varsigma \circ (\chi, \mathfrak{T}) : \mathscr{B} \times \mathscr{I} \rightarrow \mathbb{S}$ (the formalism is adapted from [64]).

In the sequel, in order to lower the notational complexity, we will omit the explicit composition with $(\chi, \mathfrak{T})$ and drop the dependency on X and t whenever the reported expressions are already well-established in the literature. For example, the material volumetric fraction of the α-th phase, which is defined as $\Phi_\alpha(X,t) := J(X,t)\phi_\alpha(\chi(X,t),t)$, will be simply indicated as $\Phi_\alpha := J\phi_\alpha$.

3 Fundamental balance equations

In this section, we recall the fundamental balance equations for the modeling problem at hand, i.e., the balance of mass and the balance of linear momentum for the solid and for the fluid phase.

Our target material, assumed to represent, e.g., a bio-mimetic tissue, is viewed as a solid-fluid mixture, in which the solid phase comprises all the solid constituents of the tissue (in the present framework, these could be identified with the extracellular matrix and the structural components of the cells), while the fluid phase accounts for the interstitial fluid that flows through the pores.

As is often the case in the biomechanical modeling of soft hydrated tissues[1, 22, 20, 36, 30], both the solid and the fluid phase are regarded as incompressible (more specifically, we will assume that their true mass densities are constant), and their presence in the mixture under study is measured by their *volumetric fractions*, denoted by ϕ_s and ϕ_f, respectively. Through these quantities, we define the *apparent mass densities* $\varrho_\mathrm{s}\phi_\mathrm{s}$ and $\varrho_\mathrm{f}\phi_\mathrm{f}$, with ϱ_s and ϱ_f being the constant mass densities of the solid and the fluid. Since the mixture considered in our work is saturated, the condition $\phi_\mathrm{s} + \phi_\mathrm{f} = 1$ applies.

By composing the mass balances for the fluid and solid phase in the current placement (see Remark 1 and Appendix A) with the pair of maps $(\chi, \mathfrak{T}) : \mathscr{B} \times \mathscr{T} \to \mathscr{S} \times \mathscr{T}$, the mass balance laws for the solid phase and for the mixture as a whole can be written with respect to the reference placement as

$$\dot{\Phi}_{\mathrm{s}} = 0, \qquad \text{in } \mathscr{B}, \tag{1a}$$

$$\dot{J} + \mathrm{Div}\boldsymbol{Q} = 0, \qquad \text{in } \mathscr{B}, \tag{1b}$$

where, with a slight abuse of notation, $\Phi_{\mathrm{s}} := J\phi_{\mathrm{s}}$ and $\boldsymbol{Q} := J\boldsymbol{F}^{-1}\boldsymbol{q}$ are the solid phase *material volumetric fraction* and the *material filtration velocity* representing the pull-backs of ϕ_{s} and $\boldsymbol{q}$, respectively[5, 20, 30]. It follows from Equation (1a) that Φ_{s} is constant in time. Hence, we set $\Phi_{\mathrm{s}}(X, t) \equiv \Phi_{\mathrm{sR}}(X)$ (see Appendix 1).

We emphasize that, in spite of the terminology "filtration velocity", $\boldsymbol{q}$ *is not* a true velocity. Rather, it is a *specific mass flux vector*, i.e., a mass flux vector defined by the multiplication of the velocity of the fluid relative to the solid, i.e., $\boldsymbol{w}_{\mathrm{fs}}$, by the volumetric fraction of the fluid ϕ_{f}. As remarked in [65], this is an important clarification, since it predicts how $\boldsymbol{q}$ transforms. Indeed, since $\boldsymbol{q}$ is a flux vector, it has to be identified with a *pseudo-vector* and, as such, its material counterpart, obtained by computing its backward Piola transformation, reads $\boldsymbol{Q} = J\boldsymbol{F}^{-1}\boldsymbol{q}$ [66, 20, 65, 30].

In the present framework, the balance of linear momentum (see Appendix A) can be reformulated in the reference placement as

$$\mathrm{Div}(\boldsymbol{T}_{\mathrm{s}} + \boldsymbol{T}_{\mathrm{f}}) + [\Phi_{\mathrm{s}}\varrho_{\mathrm{s}} + (J - \Phi_{\mathrm{s}})\varrho_{\mathrm{f}}]\boldsymbol{g} = \boldsymbol{0}, \tag{2a}$$

$$\mathrm{Div}\boldsymbol{T}_{\mathrm{f}} + \boldsymbol{F}^{-\mathrm{T}}\boldsymbol{\Pi}_{\mathrm{f}} + (J - \Phi_{\mathrm{s}})\varrho_{\mathrm{f}}\boldsymbol{g} = \boldsymbol{0}, \tag{2b}$$

where $\boldsymbol{T}_{\alpha} := J\boldsymbol{\sigma}_{\alpha}\boldsymbol{F}^{-\mathrm{T}}$, with $\alpha \in \{\mathrm{s}, \mathrm{f}\}$, is the first Piola-Kirchhoff stress tensor associated with the αth phase, $\boldsymbol{\Pi}_{\mathrm{f}} = J\boldsymbol{F}^{\mathrm{T}}\boldsymbol{\pi}_{\mathrm{f}} \in T^{*}_{X}\mathscr{B}$ is the pull-back of $\boldsymbol{\pi}_{\mathrm{f}}$ to the reference placement, with $\boldsymbol{\pi}_{\mathrm{f}}$ being the force density due to the exchanges of linear momentum between the fluid and the solid phase.

4 General constitutive relations

In view of the computational burden that will be introduced for describing the flow, for the purposes of our present study we assume that the solid phase is isotropic, homogeneous, and characterized by a Neo-Hookean hyperelastic strain energy density function $\Psi_{\mathrm{s}}(\boldsymbol{C})$[67], which, written per unit volume of the reference placement, takes on the form

$$\Psi_{\mathrm{s}}(\boldsymbol{C}) = \tfrac{1}{2}\Phi_{\mathrm{s}}\mu_{\mathrm{s}}[I_1 - 3] - \tfrac{1}{2}\Phi_{\mathrm{s}}\mu_{\mathrm{s}}\,\log I_3 + \tfrac{1}{8}\Phi_{\mathrm{s}}\lambda_{\mathrm{s}}\,[\log I_3]^2, \tag{3}$$

where λ_{s} and μ_{s} are Lamé's parameters, and $I_1 = \mathrm{tr}\boldsymbol{C}$, and $I_3 = \det\boldsymbol{C} = J^2$ are two of the three principal invariants of the Cauchy-Green tensor $\boldsymbol{C}$ (we recall that the second principal invariant is $I_2 = \frac{1}{2}\{[\mathrm{tr}\boldsymbol{C}]^2 - \mathrm{tr}\boldsymbol{C}^2\}$).

Before going further, it is important to remark that, for biological tissues, there exist strain energy densities that are more appropriate than the Neo-Hookean one. A rather typical example is the Holmes&Mow[2] strain energy density function, which has been extensively used and generalized in many works addressing the mechanics of articular cartilage in the biphasic context, especially when fibers are included in order to make the model at least transversely isotropic [8, 23, 13, 16, 19, 24, 20, 25, 26, 30, 17, 27, 18].

By viewing I_1 and I_3 as functions of $\boldsymbol{C}$, and $\boldsymbol{C}$ as a function of $\boldsymbol{F}$, we can rewrite $\Psi_{\mathrm{s}}(\boldsymbol{C})$ as $\Psi_{\mathrm{s}}(\boldsymbol{C}) \equiv W_{\mathrm{s}}(\boldsymbol{F})$, and, thus, we determine $\boldsymbol{T}_{\mathrm{sc}}$ as

$$\boldsymbol{T}_{\mathrm{sc}} = \frac{\partial W_{\mathrm{s}}}{\partial \boldsymbol{F}}(\boldsymbol{F}) = \boldsymbol{\eta}\boldsymbol{F}\left[2\frac{\partial \Psi_{\mathrm{s}}}{\partial \boldsymbol{C}}(\boldsymbol{C})\right]. \tag{4}$$

In the sequel, $\boldsymbol{T}_{\mathrm{sc}}$ will be referred to as the *constitutive part of the first Piola-Kirchhoff stress tensor* associated with the solid phase. Its explicit expression will be supplied below, when discussing some

numerical aspects of the problem at hand. Here, we simply notice that, since $\boldsymbol{T}_{\rm sc}$ is defined constitutively, $\boldsymbol{T}_{\rm s}$ is fully defined in terms of $\boldsymbol{T}_{\rm sc}$ and of the pore pressure $P(X,t) = p(\chi(X,t),t)$ (i.e., the pore pressure expressed as a function of the points of $\mathscr{B}$ and of time), and since $\boldsymbol{T}_{\rm f}$ depends only on P ((as is customary in the Darcy-Forchheimer model, the fluid stress tensor does not feature any dissipative part)), then all the stresses featuring in the balance laws of interest are completely expressed in terms of the unknowns χ (through the deformation gradient tensor) and P.

In fact, the structure of the inner part of stress, i.e., $\boldsymbol{\sigma}_{\rm I} = \boldsymbol{\sigma}_{\rm s} + \boldsymbol{\sigma}_{\rm f}$ (see Appendix B), yields the inner first and second Piola-Kirchhoff stress tensors $\boldsymbol{T}_{\rm I} = -JP\boldsymbol{F}^{-\rm T} + \boldsymbol{T}_{\rm sc}$, and $\boldsymbol{S}_{\rm I} = -JP\boldsymbol{C}^{-1} + \boldsymbol{S}_{\rm sc}$, where $\boldsymbol{S}_{\rm sc}$ is the constitutive part of the solid phase second Piola-Kirchhoff stress tensor and is defined as $\boldsymbol{S}_{\rm sc} = J\boldsymbol{F}^{-1}\boldsymbol{\eta}^{-1}\boldsymbol{\sigma}_{\rm sc}\boldsymbol{F}^{-\rm T}$. Moreover, since the solid phase is assumed to be hyperelastic, $\boldsymbol{S}_{\rm I}$ can be determined by differentiating an *augmented* strain energy density $\Psi_{\rm s}^{\rm a}$, obtained through the addition of the pressure term $-[J-1]P$ to $\Psi_{\rm s}(\boldsymbol{C})$, i.e.,

$$\Psi_{\rm s}^{\rm a}(\boldsymbol{C},P) := \Psi_{\rm s}(\boldsymbol{C}) - [J-1]P = \tfrac{1}{2}\Phi_{\rm s}\mu_{\rm s}[{\rm tr}\boldsymbol{C} - 3] - \Phi_{\rm s}\mu_{\rm s}\log J + \tfrac{1}{2}\Phi_{\rm s}\lambda_{\rm s}\,[\log J]^2 - [J-1]P, \tag{5a}$$

$$\boldsymbol{S}_{\rm I} = 2\frac{\partial\Psi_{\rm s}^{\rm a}}{\partial\boldsymbol{C}}(\boldsymbol{C},P) = -JP\boldsymbol{C}^{-1} + \boldsymbol{S}_{\rm sc} = -JP\boldsymbol{C}^{-1} + 2\frac{\partial\Psi_{\rm s}}{\partial\boldsymbol{C}}(\boldsymbol{C}). \tag{5b}$$

For future use, we also introduce the strain energy density $W_{\rm s}^{\rm a}(\boldsymbol{F},P) \equiv \Psi_{\rm s}^{\rm a}(\boldsymbol{C},P)$.

There remains to determine $\boldsymbol{\pi}_{\rm fd}$ and, to do so, we proceed with the study of the dissipation inequality[32, 68, 34, 22, 5, 30].

5 Constitutive representation of the dissipative forces

We are interested here in evaluating the influence that the fluid phase non-Darcian dynamics may have on the medium's overall mechanical behavior. In particular, to account for loading conditions that do not fully justify the hypothesis of negligibility of inertial forces, we consider Forchheimer's correction to Darcy's law[62, 69, 32, 70, 35, 33]. Moreover, to account for dissipative flow features that, in the literature (see e.g[71, 72, 73, 74, 38]), have conducted to flow laws non-local in time, we propose a fractionalization of Forchheimer's correction. To this end, we suggest a relation between the fluid phase filtration velocity and pressure gradient that is highly non-linear, and is expressed through integro-differential operators of fractional type describing a possible non-locality in time in the constitutive representation of the drag forces as functionals of the fluid filtration velocity.

Under the hypotheses done so far, by assuming that the sole source of energetic loss is due to the momentum exchanged between the fluid and the solid phase, and adhering to the frameworks developed in[32, 34], and, subsequently, in[5], it can be proven that the local form of the residual dissipation per unit of volume of $\mathscr{B}_t$ is given by

$$\mathfrak{D}^{(\rm a)} = -\boldsymbol{\pi}_{\rm fd}\boldsymbol{w}_{\rm fs} = -\boldsymbol{\pi}_{\rm fd}\phi_{\rm f}^{-1}\boldsymbol{q} \geq 0. \tag{6}$$

We recall that, throughout this work, all the force densities, and, thus, also $\boldsymbol{\pi}_{\rm fd}$, are identified as pseudo co-vectors, while all the velocities are defined as vectors. Hence, $\boldsymbol{\pi}_{\rm fd}(x,t)$ has to be regarded as a linear map that, whenever evaluated over a vector $\boldsymbol{u} \in T_x\mathscr{B}_t$, returns a pseudo-scalar value. In particular, the juxtapositions $\boldsymbol{\pi}_{\rm fd}\boldsymbol{w}_{\rm fs}$ and $\boldsymbol{\pi}_{\rm fd}\boldsymbol{q}$ in Equation (6) are to be understood, in index notation, as $\boldsymbol{\pi}_{\rm fd}\boldsymbol{w}_{\rm fs} = [\boldsymbol{\pi}_{\rm fd}]_a[\boldsymbol{w}_{\rm fs}]^a$ and $\boldsymbol{\pi}_{\rm fd}\boldsymbol{q} = [\boldsymbol{\pi}_{\rm fd}]_a q^a$, where Einstein's convention of summation over repeated indices applies, unless stated otherwise.

Expressions similar to Equation (6) can be found in several publications (see e.g. [32, 34, 1, 5, 30]) and, thus, its full derivation will not be reported here. However, we recall that the superscript "(a)" in $\mathfrak{D}^{(\rm a)}$ stands for "augmented", since, to obtain Equation (6), the constraint of incompressibility, imposed to each phase of the mixture, and reflected by the mass balance law (1b), is appended to the local form of the dissipation inequality, multiplied by the pore pressure p. This latter field, thus, acquires the meaning of the Lagrange multiplier[34, 5] associated with the given constraint. For the advantages related with this procedure, the reader is referred to[75, 34].

We hypothesize that the dissipative force density $\boldsymbol{\pi}_{\mathrm{fd}}$ can be expressed constitutively, up to the sign, as the result of some suitably defined operator $\mathcal{O}_{\boldsymbol{q}}$, applied to $\boldsymbol{q}$, and in which the subscript "$\boldsymbol{q}$" indicates that, in general, the operator may depend on $\boldsymbol{q}$ itself. Hence, we impose a relationship of the kind

$$\boldsymbol{\pi}_{\mathrm{fd}} \equiv -\mathcal{O}_{\boldsymbol{q}}\boldsymbol{q}. \tag{7}$$

Such relationship is nonlinear in general, and, for consistency with Equation (6), it imposes that $\mathcal{O}_{\boldsymbol{q}}$ complies with the dissipation inequality, so that the condition $\mathfrak{D}^{(\mathrm{a})} = \phi_{\mathrm{f}}^{-1}[\mathcal{O}_{\boldsymbol{q}}\boldsymbol{q}]\boldsymbol{q} \geq 0$ must be respected at all times and at all points of the region of space occupied by the mixture. Furthermore, by substituting the relationship (7) into the balance law of linear momentum in the spatial placement (see Appendix 2), we find the following operator equation in the unknown $\boldsymbol{q}$:

$$-\mathcal{O}_{\boldsymbol{q}}\boldsymbol{q} = \phi_{\mathrm{f}}[\operatorname{grad} p - \varrho_{\mathrm{f}}\boldsymbol{g}]. \tag{8}$$

Among the various possible definitions of $\mathcal{O}_{\boldsymbol{q}}$, each of which depends on the biphasic medium that has to be modeled, we require $\mathcal{O}_{\boldsymbol{q}}$ to be such that it vanishes identically for the null filtration velocity $\boldsymbol{q}_0 \equiv \boldsymbol{0}$, i.e.,

$$\mathcal{O}_{\boldsymbol{q}}\boldsymbol{q} = \mathcal{O}_{\boldsymbol{q}_0}\boldsymbol{q}_0 \equiv \boldsymbol{0}. \tag{9}$$

In addition, we require that the null vector field $\boldsymbol{q}_0 \equiv \boldsymbol{0}$ is the unique solution to the equation $\mathcal{O}_{\boldsymbol{q}}\boldsymbol{q} = \boldsymbol{0}$. By doing so, when the pressure field solves $\operatorname{grad} p - \varrho_{\mathrm{f}}\boldsymbol{g} = \boldsymbol{0}$, so that also the left-hand side of Equation (8) has to vanish, the solution is $\boldsymbol{q} = \boldsymbol{q}_0$. This requirement is important in view of the fact that a "modified" Caputo derivative will feature in the definition of the operator $\mathcal{O}_{\boldsymbol{q}}\boldsymbol{q}$, thereby implying that a field $\boldsymbol{q}$ with non-vanishing initial value $\boldsymbol{q}(x, t_{\mathrm{in}}) \neq \boldsymbol{0}$ is, in general, a nontrivial solution of the equation $\mathcal{O}_{\boldsymbol{q}}\boldsymbol{q} = \boldsymbol{0}$ (see Equation (15)). Hence, to maintain the uniqueness of the solution $\boldsymbol{q}_0 \equiv \boldsymbol{0}$, we will always assume that $\boldsymbol{q}$ has null initial value.

The considerations on $\mathcal{O}_{\boldsymbol{q}}\boldsymbol{q}$ done above imply that also the right-hand side of Equation (8) must vanish for $\boldsymbol{q} = \boldsymbol{q}_0$, thereby recovering Stevin's law of the statics of fluids, i.e., $\operatorname{grad} p - \varrho_{\mathrm{f}}\boldsymbol{g} = \boldsymbol{0}$. Moreover, several other fluid behaviors are ruled out, like those characterized by non-null values of $\boldsymbol{\pi}_{\mathrm{fd}}$ for $\boldsymbol{q} = \boldsymbol{q}_0$. In the latter case, indeed, by denoting by $\boldsymbol{\pi}_{\mathrm{fd}}^{\mathrm{st}}$ the value of $\boldsymbol{\pi}_{\mathrm{fd}}$ in static conditions, the statics of the fluid under consideration is governed by the force balance $\boldsymbol{\pi}_{\mathrm{fd}}^{\mathrm{st}} - \phi_{\mathrm{f}}\operatorname{grad} p + \phi_{\mathrm{f}}\varrho_{\mathrm{f}}\boldsymbol{g} = \boldsymbol{0}$, which determines $\boldsymbol{\pi}_{\mathrm{fd}}^{\mathrm{st}}$ as $\boldsymbol{\pi}_{\mathrm{fd}}^{\mathrm{st}} = \phi_{\mathrm{f}}[\operatorname{grad} p - \varrho_{\mathrm{f}}\boldsymbol{g}]$[1] without constitutive prescriptions.

For the sake of clarity, before describing the operator $\mathcal{O}_{\boldsymbol{q}}$ in detail for the case that characterizes the main novelty of this work, we briefly discuss the (classical) definitions of $\mathcal{O}_{\boldsymbol{q}}$ that return Darcy's law and Forchheimer's correction to Darcy's law. In doing this, since gravity is not expected to play a relevant role for the problems that will be investigated in the sequel, we shall drop the buoyancy term $\varrho_{\mathrm{f}}\boldsymbol{g}$ from here on.

5.1 Darcy's law

Although Darcy's law is well-known, we find it useful to briefly review its origin and the range of its applicability in order to give context to the need for Forchheimer's correction and for its fractionalization.

Darcy's law is widely employed in the mechanics of porous media of environmental, industrial, and biological interest (see e.g. [69, 33, 34, 1, 22, 76], to mention just a few) to describe, at the *macroscale*, the flow of a fluid through the pores of a given porous medium. Here, by "macroscale", it is meant the scale at which the porous medium and the fluid are viewed as a mixture.

Darcy's regime is satisfactory when the following two main hypotheses are met:

(i) The stress tensor of the fluid is well approximated by its so-called equilibrium part, so that any contribution due to the fluid viscosity is negligible and one can write the fluid's Cauchy stress tensor as $\boldsymbol{\sigma}_{\mathrm{f}} = -\phi_{\mathrm{f}} p \boldsymbol{\imath}^{\mathrm{T}}$.

[1] Note that this equation is different from Equation (103b) (see Appendix B) in that it applies in static conditions, whereas Equation (103b) holds true in dynamic regime, but in the limit of negligible inertial forces.

(ii) Inertial forces are negligible both at the macroscale and at the microscale. At the macroscale, this assumption implies that no inertial effects are accounted for in the fluid's macroscopic momentum balance law. For what concerns the microscale, instead, the assumption of negligible inertial effects has two meanings. On the one hand, it requires that such effects are one or more orders of magnitude smaller than those of the other forces contributing to the flow, and, on the other hand, that the linear momentum exchanged between the fluid and the solid at their interface does not depend appreciably on the dynamic part of the overall mechanical stress (see e.g. [70]). In particular, this latter statement is reflected by the fact that, at the macroscale, and in the cases in which $\boldsymbol{\pi}_{\mathrm{fd}}$ can be expressed constitutively, one can prescribe $\boldsymbol{\pi}_{\mathrm{fd}}$ to be a linear function of $\boldsymbol{q}$ (see e.g. [69, 33, 34, 1]), i.e.,

$$\boldsymbol{\pi}_{\mathrm{fd}} = \boldsymbol{\mathcal{G}}^{\boldsymbol{\pi}_{\mathrm{fd}}}(\boldsymbol{q}, \ldots) := \boldsymbol{\mathcal{G}}^{\boldsymbol{r}}(\ldots)\boldsymbol{q} = -\boldsymbol{r}\boldsymbol{q}, \tag{10}$$

where $\boldsymbol{\mathcal{G}}^{\boldsymbol{\pi}_{\mathrm{fd}}}(\boldsymbol{q}, ...)$ is the constitutive law expressing $\boldsymbol{\pi}_{\mathrm{fd}}$, $\boldsymbol{r}$ is a second-order tensor field, referred to as *resistivity tensor*, and $\boldsymbol{\mathcal{G}}^{\boldsymbol{r}}(\ldots)$ is its constitutive representation (here, the ellipsis means that the considered constitutive functions depend, in general, on variables that are left unspecified at the moment). In passing, we recall that there exist generalizations to Darcy's law that involve threshold phenomena, according to which, for example, relationships similar to Equation (10) can be written only when the norm of $\boldsymbol{\pi}_{\mathrm{fd}}$ exceeds a certain value (see e.g. [33]). However, these circumstances are out of the scopes of our present work.

According to Equation (10), in the case of Darcy's law the identification $\mathcal{O}_{\boldsymbol{q}}\boldsymbol{q} \equiv \boldsymbol{r}\boldsymbol{q}$ applies, so that the operator $\mathcal{O}_{\boldsymbol{q}}$ is represented by $\boldsymbol{r}$ and is, thus, independent of $\boldsymbol{q}$. Furthermore, by substituting Equation (10) into the residual dissipation inequality (6), one obtains

$$\begin{aligned}\mathfrak{D}^{(\mathrm{a})} &= -\boldsymbol{\pi}_{\mathrm{fd}}\,\phi_{\mathrm{f}}^{-1}\boldsymbol{q} = [\boldsymbol{r}\boldsymbol{q}]\phi_{\mathrm{f}}^{-1}\boldsymbol{q} = \phi_{\mathrm{f}}^{-1}[\mathrm{sym}(\boldsymbol{r})\boldsymbol{q}]\boldsymbol{q} \\ &= \phi_{\mathrm{f}}^{-1}\,\mathrm{tr}\{\mathrm{sym}(\boldsymbol{r})[\boldsymbol{q}\otimes\boldsymbol{q}]\} = \phi_{\mathrm{f}}^{-1}[\mathrm{sym}(\boldsymbol{r})]_{ab}[\boldsymbol{q}]^{a}[\boldsymbol{q}]^{b} \geq 0,\end{aligned} \tag{11}$$

which requires *per se* the symmetric part of the resistivity tensor, $\mathrm{sym}(\boldsymbol{r})$, to be positive semi-definite. Typically, however, one aims at obtaining an expression for $\boldsymbol{q}$ in closed form by substituting Equation (10) into the spatial balance law of linear momentum for the fluid phase, and solving for $\boldsymbol{q}$. Hence, to do this, one assumes that $\mathrm{sym}(\boldsymbol{r})$ is positive definite (which is also consistent with the condition $\mathcal{O}_{\boldsymbol{q}_0}\boldsymbol{q}_0 \equiv \boldsymbol{0}$) and, often, it is also hypothesized from the outset that the resistivity tensor $\boldsymbol{r}$ is symmetric, so that the identity $\boldsymbol{r} \equiv \mathrm{sym}(\boldsymbol{r})$ is stated. Under these hypotheses, indeed, one achieves Darcy's law in the "popular" form

$$\boldsymbol{q} = -\frac{\boldsymbol{k}}{\mu}\mathrm{grad}\,p \equiv \boldsymbol{q}_{\mathrm{D}}, \qquad \boldsymbol{r} := \phi_{\mathrm{f}}\mu\boldsymbol{k}^{-1}, \tag{12}$$

where $\boldsymbol{k}$ is a second-order tensor field referred to as *permeability tensor*, μ is the fluid's viscosity, and $\boldsymbol{q}_{\mathrm{D}}$ stands for "Darcy's velocity".

With respect to the reference placement of the medium, Equation (12) transforms as

$$\boldsymbol{Q} = -\frac{\boldsymbol{K}}{\mu}\mathrm{Grad}\,P \equiv \boldsymbol{Q}_{\mathrm{D}}, \tag{13}$$

where P is the pore pressure written as a function of the points X of the reference placement and of time, i.e., $P = p \circ (\chi, \mathfrak{T})$, while $\boldsymbol{K}$ is referred to as *material permeability tensor* and is related to $\boldsymbol{k}$ through the backward Piola transformation $\boldsymbol{K} = J\boldsymbol{F}^{-1}\boldsymbol{k}\boldsymbol{F}^{-\mathrm{T}}$. Hence, the Darcian material filtration velocity $\boldsymbol{Q}_{\mathrm{D}}$ can be expressed in terms of the pore pressure and deformation gradient tensor.

Finally, having neglected the buoyancy terms in Equations (2a) and (2b), the equations to be solved in the case of validity of Darcy's regime can be summarized as

$$\mathrm{Div}(-JP\boldsymbol{F}^{-\mathrm{T}} + \boldsymbol{T}_{\mathrm{sc}}) = \boldsymbol{0}, \tag{14a}$$

$$\dot{J} = \mathrm{Div}\left[\frac{\boldsymbol{K}}{\mu}\mathrm{Grad}P\right], \tag{14b}$$

where $\boldsymbol{T}_{\mathrm{sc}} = \eta\boldsymbol{F}\boldsymbol{S}_{\mathrm{sc}}$, with $\boldsymbol{S}_{\mathrm{sc}}$ being deducible from Equation (5b), is determined constitutively as shown in Equation (4), while the permeability tensor $\boldsymbol{K}$ is specified in Equation (36) below. Moreover, the material volumetric fractions Φ_{s} and Φ_{f}, which feature in the definitions of $\boldsymbol{T}_{\mathrm{sc}}$ and $\boldsymbol{K}$, are $\Phi_{\mathrm{s}} = J\phi_{\mathrm{s}} = \Phi_{\mathrm{sR}}$ and $\Phi_{\mathrm{f}} = J\phi_{\mathrm{f}}$, and Φ_{sR} is regarded as known. In the system of Equations (14a) and (14b), the unknowns are pressure P and the motion χ. The latter is accounted for by $\boldsymbol{F}$ and $J = \det\boldsymbol{F}$, and Φ_{f} is expressed as $\Phi_{\mathrm{f}} = J - \Phi_{\mathrm{s}}$ by virtue of the backward Piola transformation of the saturation condition.

Before proceeding, the following two remarks are in order:

Remark 2. In the literature on the mechanics of fluid-saturated porous media, models have been proposed that, although assuming the Darcian regime for the fluid, account for memory in the description of the flow (see, e.g.,[38]). These models have the purpose of describing, for instance, non-mechanical, micro-structural interactions of the fluid with the pores, such as chemical processes[38], that contribute to hinder the flow. Often, this phenomenology is studied by adopting integro-differential operators in time that introduce a delay in the purely Darcian linear relationship between pressure gradient and filtration velocity. For example, Deseri and Zingales[38] used operators based on the fractional Caputo derivative, so that, under some simplifying hypotheses, classical Darcy's law can be replaced by

$$\boldsymbol{q}(t) + \frac{\alpha\, t_{\mathrm{c}}^{\alpha}}{\Gamma(1-\alpha)}\int_{t_{\mathrm{in}}}^{t}\frac{\dot{\boldsymbol{q}}(\tau)}{(t-\tau)^{\alpha}}\mathrm{d}\tau = \boldsymbol{q}_{\mathrm{D}}(t). \tag{15}$$

Equation (15) is a generalized Cattaneo's model conceived for porous media that either do not undergo deformation or are in the regime of infinitesimal deformations[77, 38, 78, 31]. Indeed, when the deformations have to be regarded as finite, relationships of the type provided in Equation (15) are not objective because of the presence of the time derivative of $\boldsymbol{q}$ featuring inside the integral. To avoid this problem, we take advantage of the property of $\boldsymbol{q}$ of being a pseudo-vector and, consequently, we have recourse to the most natural way to describe its time evolution, i.e., to its Truesdell rate (see[79] for a recent discussion on this topic).

Remark 3 (Caputo fractional derivative, frame indifference and Truesdell rate).
Caputo's fractional derivative[80, 42] in time cannot be employed directly to obtain constitutive relations that satisfy the principle of frame indifference, since the time derivative is not an objective rate. In particular, by introducing a proper orthogonal tensor $\boldsymbol{R}$ ($\det\boldsymbol{R} = 1$), such that a given vector field $\boldsymbol{v}$ transforms as $\tilde{\boldsymbol{v}} = \boldsymbol{R}\boldsymbol{v}$, the Caputo derivative yields

$${}^{C}D_{t}^{\alpha}\tilde{\boldsymbol{v}} = {}^{C}D_{t}^{\alpha}(\boldsymbol{R}\boldsymbol{v}) = \frac{1}{\Gamma(1-\alpha)}\int_{t_{\mathrm{in}}}^{t}\frac{1}{(t-\tau)^{\alpha}}\dot{\overline{\boldsymbol{R}\boldsymbol{v}}}\,\mathrm{d}\tau = \frac{1}{\Gamma(1-\alpha)}\int_{t_{\mathrm{in}}}^{t}\frac{1}{(t-\tau)^{\alpha}}(\dot{\boldsymbol{R}}\boldsymbol{v} + \boldsymbol{R}\dot{\boldsymbol{v}})\,\mathrm{d}\tau, \tag{16}$$

where $\dot{\boldsymbol{R}}\boldsymbol{v}$ is the term that spoils objectivity.

Conversely, since in our work we need to make sure that the fractional derivative employed in the fractionalization of constitutive relations respects objectivity, we replace the time derivative in the integral with an appropriate objective rate. In particular, an objective rate suitable for our purposes is the Truesdell rate, because it is conceived for fluxes and, in fact, we have to compute the derivative of $\boldsymbol{q}$, which is a flux. Such a modification of the Caputo fractional derivative will satisfy a relation of the type

$${}^{\bar{C}}D_{t}^{\alpha}\tilde{\boldsymbol{q}} = \frac{1}{\Gamma(1-\alpha)}\int_{t_{\mathrm{in}}}^{t}\frac{1}{(t-\tau)^{\alpha}}\mathcal{T}_{\mathrm{s}}\tilde{\boldsymbol{q}}\,\mathrm{d}\tau = \frac{1}{\Gamma(1-\alpha)}\int_{t_{\mathrm{in}}}^{t}\frac{1}{(t-\tau)^{\alpha}}\boldsymbol{R}\mathcal{T}_{\mathrm{s}}\boldsymbol{q}\,\mathrm{d}\tau, \tag{17}$$

in which $\mathcal{T}_{\mathrm{s}}$ is the Truesdell rate and the bar over "C" in the left-hand side indicates a "modified" Caputo derivative. We recall that, in the present context, the Truesdell rate of $\boldsymbol{q}$ can be computed as[2]

$$\mathcal{T}_{\mathrm{s}}\boldsymbol{q}(\chi(X,\tau),\tau) \equiv \frac{1}{J(X,\tau)}\boldsymbol{F}(X,\tau)\,\mathrm{D}_{\mathrm{s}}\left[\frac{1}{\det\boldsymbol{F}^{-1}}\boldsymbol{F}^{-1}\boldsymbol{q}\right](\chi(X,\tau),\tau), \tag{18}$$

[2]In fact, the right-hand side of Equation (18) is *not* the *definition* of the Truesdell rate of $\boldsymbol{q}$, but just a simple way for computing it. A more rigorous way of writing it can be found e.g. in [79].

where D_s is the substantial derivative with respect to the solid phase motion. In the spatial description, Equation (18) produces the result

$$\begin{aligned}\mathcal{T}_\mathrm{s}\boldsymbol{q} &= [\operatorname{div}\boldsymbol{v}_\mathrm{s}]\boldsymbol{q} - [\operatorname{grad}\boldsymbol{v}_\mathrm{s}]\boldsymbol{q} + \mathrm{D}_\mathrm{s}\boldsymbol{q}\\ &= [\operatorname{div}\boldsymbol{v}_\mathrm{s}]\boldsymbol{q} - [\operatorname{grad}\boldsymbol{v}_\mathrm{s}]\boldsymbol{q} + [\operatorname{grad}\boldsymbol{q}]\boldsymbol{v}_\mathrm{s} + \partial_t\boldsymbol{q}.\end{aligned} \tag{19}$$

However, since we are interested in the material description of the flow, we express $\mathcal{T}_\mathrm{s}\boldsymbol{q}$ as

$$\mathcal{T}_\mathrm{s}\boldsymbol{q}(\chi(X,\tau),\tau) \equiv \frac{1}{J(X,\tau)}\boldsymbol{F}(X,\tau)\dot{\boldsymbol{Q}}(X,\tau), \tag{20}$$

where we recall the definition of *material filtration velocity* $\boldsymbol{Q}(X,t) = [(\det\boldsymbol{F}^{-1})^{-1}\boldsymbol{F}^{-1}\boldsymbol{q}](\chi(X,t),t)$.

5.2 Forchheimer's correction

Following [70], Forchheimer's correction to Darcy's law becomes necessary when the hypothesis (ii) of the section 5.1 is not satisfied. Indeed, as remarked in [70], the correction accounts for the inertial effects that characterize the pore scale dynamics of the fluid, and for those that take part to the momentum exchange between the fluid and the solid phase. In fact, it can be shown that (see e.g.[81]), at the macroscale, the consideration of the inertial effects mentioned above can be expressed in terms of a non-linear relationship between $\boldsymbol{\pi}_\mathrm{fd}$ and $\boldsymbol{q}$ of the type (see e.g. [70, 68, 82, 36, 30])

$$\boldsymbol{\pi}_\mathrm{fd} = \boldsymbol{\mathcal{G}}^{\boldsymbol{\pi}_\mathrm{fd}}(\boldsymbol{q},\ldots) = \boldsymbol{\mathcal{G}}^{\boldsymbol{r}_\mathrm{F}}(\boldsymbol{q},\ldots)\boldsymbol{q} = -\,\boldsymbol{r}_\mathrm{F}(\|\boldsymbol{q}\|)\boldsymbol{q}, \tag{21}$$

where $\boldsymbol{r}_\mathrm{F}(\|\boldsymbol{q}\|)$ can be thought of as a $\boldsymbol{q}$-dependent resistivity tensor. Note that, here and in the following, the subscript "F" stands for "Forchheimer", and is introduced in order to highlight that the current description differs from the Darcian one. In addition, as suggested by the identification $\boldsymbol{\mathcal{G}}^{\boldsymbol{r}_\mathrm{F}}(\boldsymbol{q},\ldots) \equiv -\boldsymbol{r}_\mathrm{F}(\|\boldsymbol{q}\|)$, the resistivity tensor depends, in general, aside from $\|\boldsymbol{q}\|$, also on other parameters characterizing the flow, although we do not report them here explicitly for the sake of a lighter notation. We recall and clarify the procedure undertaken in[30, 36, 82] for the characterization of Forchheimer's correction in the spatial setting and we extend it to the reference placement through the appropriate backward Piola transformations. In fact, although the derivations are similar, the aim in[30] was to rephrase Forchheimer's correction as a scalar coefficient that multiplies the permeability tensor, whilst the aim of this section is to provide a clear material description for Forchheimer's coefficient.

As reported in[70, 68, 82, 36, 30], the resistivity tensor $\boldsymbol{r}_\mathrm{F}(\|\boldsymbol{q}\|)$ can be defined as

$$\boldsymbol{r}_\mathrm{F}(\|\boldsymbol{q}\|) = \boldsymbol{r} + \|\boldsymbol{q}\|\mathfrak{a}\boldsymbol{r} = \phi_\mathrm{f}\mu[\boldsymbol{k}^{-1} + \|\boldsymbol{q}\|\mathfrak{a}\boldsymbol{k}^{-1}], \tag{22}$$

where $\mathfrak{a}$, in general, is a second-order tensor field denominated *Forchheimer's coefficient*, having physical dimensions of the inverse of a characteristic velocity, and that is to be assigned constitutively (see Equation (32) below).

By comparing Equation (22) with the general definition (7), we obtain the identification

$$O_{\boldsymbol{q}} \equiv \phi_\mathrm{f}\mu[\boldsymbol{k}^{-1} + \|\boldsymbol{q}\|\mathfrak{a}\boldsymbol{k}^{-1}] = \phi_\mathrm{f}\mu\boldsymbol{k}^{-1}[\boldsymbol{\imath} + \|\boldsymbol{q}\|\boldsymbol{k}\mathfrak{a}\boldsymbol{k}^{-1}]. \tag{23}$$

Moreover, by substituting Equation (23) into the constitutive representation (21) of $\boldsymbol{\pi}_\mathrm{fd}$, using the resulting expression into the force balance (8), neglecting gravity, and invoking the definition (12) of Darcy's velocity $\boldsymbol{q}_\mathrm{D}$, we find that $\boldsymbol{q}$ must satisfy the algebraic equation

$$\phi_\mathrm{f}\mu\boldsymbol{k}^{-1}[\boldsymbol{\imath} + \|\boldsymbol{q}\|\boldsymbol{k}\mathfrak{a}\boldsymbol{k}^{-1}]\boldsymbol{q} = \phi_\mathrm{f}\mu\boldsymbol{k}^{-1}\boldsymbol{q}_\mathrm{D}, \tag{24}$$

which can be put in the equivalent form (see [30], in which a slightly different notation is employed)

$$[\boldsymbol{\imath} + \|\boldsymbol{q}\|\boldsymbol{k}\mathfrak{a}\boldsymbol{k}^{-1}]\boldsymbol{q} = \boldsymbol{q}_\mathrm{D}. \tag{25}$$

The backward Piola transformation of Equation (25) produces [30]

$$[\boldsymbol{I} + \|\boldsymbol{Q}\|_{\boldsymbol{C}} \boldsymbol{K}\boldsymbol{\mathcal{A}}\boldsymbol{K}^{-1}]\boldsymbol{Q} = \boldsymbol{Q}_{\mathrm{D}}, \tag{26}$$

where $\boldsymbol{I}$ is the material identity tensor, $\|\boldsymbol{Q}\|_{\boldsymbol{C}} := J^{-1}\sqrt{[\boldsymbol{C} : (\boldsymbol{Q} \otimes \boldsymbol{Q})]}$ is the $\boldsymbol{C}$-norm of $\boldsymbol{Q}$, i.e., the norm of $\boldsymbol{Q}$ computed with respected to the deformed metric tensor induced by the right Cauchy-Green deformation tensor $\boldsymbol{C}$, while

$$\boldsymbol{\mathcal{A}}(X,t) := \boldsymbol{F}^{\mathrm{T}}(\chi(X,t),t)\mathfrak{a}(\chi(X,t),t)\boldsymbol{F}^{-\mathrm{T}}(X,t) \tag{27}$$

is the backward Piola transform of Forchheimer's coefficient. Note that the norm $\|\boldsymbol{Q}\|_{\boldsymbol{C}}$ arises because of the identity $\|\boldsymbol{q}(x,t)\| = \|\boldsymbol{Q}(X,t)\|_{\boldsymbol{C}}$ (an equivalent formulation of equation (26) can be obtained by redefining $\|\boldsymbol{Q}\|_{\boldsymbol{C}}$ as $J\|\boldsymbol{q}\|$, so as to emphasize that $\|\boldsymbol{q}\|$ transforms as a pseudo-scalar, and $\boldsymbol{\mathcal{A}}$ as $J^{-1}\boldsymbol{F}^{\mathrm{T}}\mathfrak{a}\boldsymbol{F}^{-\mathrm{T}}$).

Finally, we notice that a rather suggestive reformulation of Equation (26) reads

$$\boldsymbol{R}_{\mathrm{F}}(\|\boldsymbol{Q}\|_{\boldsymbol{C}})\boldsymbol{Q} = \Phi_{\mathrm{f}}\mu\,\boldsymbol{K}^{-1}\boldsymbol{Q}_{\mathrm{D}}, \tag{28}$$

where we have introduced the material resistivity tensor

$$\boldsymbol{R}_{\mathrm{F}}(\|\boldsymbol{Q}\|_{\boldsymbol{C}}) := \Phi_{\mathrm{f}}\mu\boldsymbol{K}^{-1}\left[\boldsymbol{I} + \|\boldsymbol{Q}\|_{\boldsymbol{C}}\boldsymbol{K}\boldsymbol{\mathcal{A}}\boldsymbol{K}^{-1}\right], \tag{29}$$

related to $\boldsymbol{r}_{\mathrm{F}}(\|\boldsymbol{q}\|)$ through $\boldsymbol{R}_{\mathrm{F}}(\|\boldsymbol{Q}\|_{\boldsymbol{C}}) = \boldsymbol{F}^{\mathrm{T}}[\boldsymbol{r}_{\mathrm{F}}(\|\boldsymbol{q}\|)]\boldsymbol{F}$. The tensor function $\boldsymbol{R}_{\mathrm{F}}$ depends also on the deformation gradient tensor $\boldsymbol{F}$ through Φ_{f} and $\boldsymbol{K}$, although we prefer not to emphasize this dependence here, both for notational convenience and for highlighting the fact that, since $\boldsymbol{R}_{\mathrm{F}}$ is the backward Piola transformation of $\boldsymbol{r}_{\mathrm{F}}$, it depends on the $\boldsymbol{C}$-norm of the material filtration velocity $\boldsymbol{Q}$.

Although there exists some interest for the impact of Forchheimer's correction in porous media of biological relevance (see e.g. [35, 36, 30]), to the best of our knowledge the majority of the studies devoted to the identification of Forchheimer coefficient $\mathfrak{a}$ come from hydrogeology[33] and petroleum engineering[83, 84]. In fact, $\mathfrak{a}$ is often expressed through (semi-)empirical laws. For instance, Wang et al. [85] provided an expression for $\mathfrak{a}$ that, in our formalism, reads

$$\mathfrak{a} := \varrho_{\mathrm{f}}\boldsymbol{\eta}\mu^{-1}\boldsymbol{k}\boldsymbol{\beta}, \tag{30}$$

where the tensor field $\boldsymbol{\beta}$ is said to be *non-Darcy coefficient* [85]. As done in [30], we take an empirical formula from Thauvin and Mohanty [37] and we adapt it to our purposes, thereby expressing $\boldsymbol{\beta}$ as

$$\boldsymbol{\beta} = c_0\phi_{\mathrm{f}}^{c_1}[\boldsymbol{\eta}\boldsymbol{k}]^{c_2}, \tag{31}$$

in which c_0, c_1, and c_2 are empirical (real) constants, with c_0 having to be non-negative. We remark that there are at least two ways to assign c_0, either in a theoretical way, on the basis of the geometrical features of the pores (see e.g. [86]), or by calculating it through the fitting of the experimental data (see e.g. [87]). A third approach, which interprets c_0 as a parameter prescribed to switch from a permeability model to another[30], is discussed at the end of the section.

By substituting Equation (31) into Equation (30), and exploiting the positivity of all the eigenvalues of $\boldsymbol{k}$, we obtain

$$\mathfrak{a} = c_0\varrho_{\mathrm{f}}\phi_{\mathrm{f}}^{c_1}\mu^{-1}[\boldsymbol{\eta}\boldsymbol{k}]^{1+c_2}. \tag{32}$$

A strong simplification is achieved when the porous medium under consideration is assumed to be isotropic and, in particular, *"unconditionally isotropic"*[22]. In this case, indeed, the spatial permeability tensor $\boldsymbol{k}$ reduces to $\boldsymbol{k} = k_{\mathrm{iso}}\boldsymbol{\eta}^{-1}$, where k_{iso} is referred to as *scalar permeability*; the material permeability tensor becomes $\boldsymbol{K} = \kappa_{\mathrm{iso}}\boldsymbol{C}^{-1}$, with $\kappa_{\mathrm{iso}} := Jk_{\mathrm{iso}}$; the Forchheimer coefficient $\mathfrak{a}$ reduces to

$\mathfrak{a} = c_0 \varrho_\mathrm{f} \phi_\mathrm{f}^{c_1} \mu^{-1} k_\mathrm{iso}^{1+c_2} \boldsymbol{\imath}^\mathrm{T}$, and the material Forchheimer coefficient $\boldsymbol{\mathcal{A}}$ can be written as $\boldsymbol{\mathcal{A}} = \mathcal{A}_\mathrm{iso} \boldsymbol{I}^\mathrm{T}$, whereby it is fully represented by the scalar quantity

$$\mathcal{A}_\mathrm{iso} = c_0 \varrho_\mathrm{f} \left[\frac{\Phi_\mathrm{f}}{J}\right]^{c_1} \frac{1}{\mu} \left[\frac{\kappa_\mathrm{iso}}{J}\right]^{1+c_2}, \qquad \text{with } \Phi_\mathrm{f} > 0,\ k_\mathrm{iso} > 0, \text{ and } \mu > 0. \tag{33}$$

By substituting this result into Equation (26), and following a procedure similar to the one described in [82, 36, 30], we can express $\boldsymbol{Q}$ as a function of $\boldsymbol{Q}_\mathrm{D}$, i.e.,

$$\boldsymbol{Q} = \mathfrak{F} \boldsymbol{Q}_\mathrm{D} = -\frac{\mathfrak{F} \boldsymbol{K}}{\mu} \mathrm{Grad} P, \qquad \mathfrak{F} := \frac{2}{1 + \sqrt{1 + 4 \mathcal{A}_\mathrm{iso} \|\boldsymbol{Q}_\mathrm{D}\|_{\boldsymbol{C}}}}, \tag{34}$$

where $\mathfrak{F}$ is referred to as *material friction factor*[82, 36, 30] (note that, in[82, 36, 30], Equation (34) is obtained in the spatial description and, thus, in the models presented therein the adjective *"material"* is not present).

A relevant consequence of Equation (34) is that, for an *"unconditionally isotropic"*[22] porous medium, $\boldsymbol{Q}$ can be understood as a reformulation of Darcy's law, in which the permeability is multiplicatively rescaled by means of $\mathfrak{F}$, which, in turn, depends again on the $\boldsymbol{C}$-norm of material Darcy's velocity $\|\boldsymbol{Q}_\mathrm{D}\|_{\boldsymbol{C}}$ as well as on κ_iso, porosity, and the other flow parameters accounted for in the model. Therefore, under the hypothesis of *"unconditionally isotropic"* medium, the governing equations read as

$$\mathrm{Div}(-JP\boldsymbol{F}^{-\mathrm{T}} + \boldsymbol{T}_\mathrm{sc}) = \boldsymbol{0}, \tag{35a}$$

$$\dot{J} = \mathrm{Div}\left[\frac{\mathfrak{F} \boldsymbol{K}}{\mu} \mathrm{Grad} P\right]. \tag{35b}$$

In the sequel, we adopt an expression of κ_iso taken from Holmes&Mow[2], given by

$$\kappa_\mathrm{iso} = J k_\mathrm{ref} \left[\frac{J - \Phi_\mathrm{s}}{1 - \Phi_\mathrm{s}}\right]^{m_0} \exp\left(\frac{m_1}{2}[J^2 - 1]\right), \tag{36}$$

where k_ref is a reference permeability, while m_0 and m_1 are non-negative material parameters.

5.3 Fractional Forchheimer's correction

From the point of view of mathematical modeling, this section is the heart of the present work since we propose here a fractionalization of the constitutive law (21), which we provide in the form

$$\boldsymbol{\pi}_\mathrm{fd}(t) := -\boldsymbol{r}_\mathrm{F}(\|\boldsymbol{q}(t)\|)\boldsymbol{q}(t) - \frac{\alpha\, t_\mathrm{c}^\alpha}{\Gamma(1-\alpha)} \int_{t_\mathrm{in}}^{t} \frac{\boldsymbol{r}_\mathrm{F}(\|\boldsymbol{q}(\tau)\|)}{(t-\tau)^\alpha} \mathcal{T}_\mathrm{s} \boldsymbol{q}(\tau) \mathrm{d}\tau, \tag{37}$$

where $\boldsymbol{r}_\mathrm{F}(\|\boldsymbol{q}(t)\|)$ is defined in Equation (22), t_c is a characteristic time scale of the flow, $\alpha \in]0, 1[$ another characteristic parameter of the flow, and $\mathcal{T}_\mathrm{s}\boldsymbol{q}(\tau)$ denotes the *Truesdell rate* of $\boldsymbol{q}$, computed with respect to the velocity of the solid phase, and evaluated at time $\tau \in [t_\mathrm{in}, t[$. Note that, with the exception of α, t_c, and the independent variables t and τ, all the quantities featuring in Equation (37) have to be understood as functions of spatial points and time, although we report explicitly the sole dependence on time for the sake of a lighter notation. Equation (37), which, to the best of our knowledge, is novel and constitutes the starting point of the fractionalization of Forchheimer's correction, has been inspired by the works[38, 31], in which similar models have been proposed to fractionalize Darcy's law.

By substituting Equation (37) into the force balance $-\phi_\mathrm{f} \,\mathrm{grad} p + \boldsymbol{\pi}_\mathrm{fd} = \boldsymbol{0}$, we obtain

$$\boldsymbol{r}_\mathrm{F}(\|\boldsymbol{q}(t)\|)\boldsymbol{q}(t) + \frac{\alpha\, t_\mathrm{c}^\alpha}{\Gamma(1-\alpha)} \int_{t_\mathrm{in}}^{t} \frac{\boldsymbol{r}_\mathrm{F}(\|\boldsymbol{q}(\tau)\|)}{(t-\tau)^\alpha} \mathcal{T}_\mathrm{s} \boldsymbol{q}(\tau) \mathrm{d}\tau = \phi_\mathrm{f}(t) \mu\, \boldsymbol{k}^{-1}(t) \boldsymbol{q}_\mathrm{D}(t), \tag{38}$$

which, by virtue of Equation (20), can be recast in the form

$$\boldsymbol{R}_\mathrm{F}(\|\boldsymbol{Q}(t)\|_{\boldsymbol{C}(t)})\boldsymbol{Q}(t) + \frac{\alpha\, t_\mathrm{c}^\alpha}{\Gamma(1-\alpha)} \int_{t_\mathrm{in}}^{t} \frac{J(t)}{J(\tau)} \frac{\boldsymbol{F}^\mathrm{T}(t)\boldsymbol{F}^{-\mathrm{T}}(\tau)\boldsymbol{R}_\mathrm{F}(\|\boldsymbol{Q}(\tau)\|_{\boldsymbol{C}(\tau)})}{(t-\tau)^\alpha} \dot{\boldsymbol{Q}}(\tau) \mathrm{d}\tau$$

$$= \Phi_{\mathrm{f}}(t)\mu\, \boldsymbol{K}^{-1}(t)\boldsymbol{Q}_{\mathrm{D}}(t). \tag{39}$$

With reference to Remark 2, we notice that, due to the natural choice of employing the Truesdell rate, the backward Piola transformation of Equation (38) to the medium's reference placement yields Equation (39), which features the time derivative of the material filtration velocity $\boldsymbol{Q}$. In this case, because of the presence of the deformation, Cattaneo equation is not directly recovered under the sole assumptions that $\mathfrak{a}$ is null and that ϕ_{f}, μ, and $\boldsymbol{k}$ are constant in time.

In the case of *"unconditionally isotropic"*[22] porous medium, the resistivity tensor given in Equation (29) reads

$$\boldsymbol{R}_{\mathrm{F}}(\|\boldsymbol{Q}\|_{\boldsymbol{C}}) = \frac{\Phi_{\mathrm{f}}\mu}{\kappa_{\mathrm{iso}}}[1 + \mathcal{A}_{\mathrm{iso}}\|\boldsymbol{Q}\|_{\boldsymbol{C}}]\boldsymbol{C} = \mathcal{R}_{\mathrm{F}}(\boldsymbol{F},\boldsymbol{Q})\boldsymbol{C}, \tag{40}$$

where $\mathcal{A}_{\mathrm{iso}}$ is defined in Equation (33), and $\mathcal{R}_{\mathrm{F}}(\boldsymbol{F},\boldsymbol{Q})$ is a *scalar resistivity coefficient* defined by

$$\mathcal{R}_{\mathrm{F}}(\boldsymbol{F},\boldsymbol{Q}) := \frac{\Phi_{\mathrm{f}}\mu}{\kappa_{\mathrm{iso}}}[1 + \mathcal{A}_{\mathrm{iso}}\|\boldsymbol{Q}\|_{\boldsymbol{C}}]. \tag{41}$$

Therefore, after some algebraic passages, Equation (39) becomes

$$\begin{aligned}&\mathcal{R}_{\mathrm{F}}(\boldsymbol{F}(t),\boldsymbol{Q}(t))\boldsymbol{Q}(t) + \frac{\alpha\, t_{\mathrm{c}}^{\alpha}}{\Gamma(1-\alpha)}\int_{t_{\mathrm{in}}}^{t}\frac{J(t)}{J(\tau)}\frac{\mathcal{R}_{\mathrm{F}}(\boldsymbol{F}(\tau),\boldsymbol{Q}(\tau))}{(t-\tau)^{\alpha}}\boldsymbol{F}^{-1}(t)\boldsymbol{F}(\tau)\dot{\boldsymbol{Q}}(\tau)\mathrm{d}\tau\\ &= \mathcal{R}_{\mathrm{D}}(\boldsymbol{F}(t))\boldsymbol{Q}_{\mathrm{D}}(t),\end{aligned} \tag{42}$$

with $\mathcal{R}_{\mathrm{D}}(\boldsymbol{F}) := \Phi_{\mathrm{f}}\mu/\kappa_{\mathrm{iso}}$, and $\mathcal{R}_{\mathrm{D}}$ depending on $\boldsymbol{F}$ being through Φ_{f} and κ_{iso}.

In conclusion, for the fractional version of Forchheimer's correction analyzed in this section, the model equations to be solved are given by

$$\mathrm{Div}(-JP\boldsymbol{F}^{-\mathrm{T}} + \boldsymbol{T}_{\mathrm{sc}}) = \boldsymbol{0}, \tag{43a}$$

$$\dot{J} + \mathrm{Div}\boldsymbol{Q} = 0, \tag{43b}$$

$$\begin{aligned}&\mathcal{R}_{\mathrm{F}}(\boldsymbol{F}(t),\boldsymbol{Q}(t))\frac{1}{J(t)}\boldsymbol{F}(t)\boldsymbol{Q}(t) + \frac{\alpha\, t_{\mathrm{c}}^{\alpha}}{\Gamma(1-\alpha)}\int_{t_{\mathrm{in}}}^{t}\frac{\mathcal{R}_{\mathrm{F}}(\boldsymbol{F}(\tau),\boldsymbol{Q}(\tau))}{(t-\tau)^{\alpha}}\frac{1}{J(\tau)}\boldsymbol{F}(\tau)\dot{\boldsymbol{Q}}(\tau)\mathrm{d}\tau\\ &= \mathcal{R}_{\mathrm{D}}(\boldsymbol{F}(t))\frac{1}{J(t)}\boldsymbol{F}(t)\boldsymbol{Q}_{\mathrm{D}}(t).\end{aligned} \tag{43c}$$

Equations (43a)-(43c) are equivalent to a set of seven scalar equations in the seven unknowns represented by the three components of the solid phase motion χ, pore pressure P (which features both in the momentum balance law (43a) and in Darcy's velocity $\boldsymbol{Q}_{\mathrm{D}}$, as specified in Equation (13)), and the three components of the filtration velocity $\boldsymbol{Q}$. Thus, to close the model, it suffices to assign the solid phase volumetric fraction in the reference placement, i.e., Φ_{s}, which is independent of time in the present study, and, as it was already done in the previous sections, to prescribe constitutively the first Piola-Kirchhoff stress tensor of the solid phase, i.e., $\boldsymbol{T}_{\mathrm{sc}}$, the scalar permeability κ_{iso}, and the coefficient c_0.

6 Numerical implementation of the model equations

In this section, we introduce the most fundamental aspects of the determination of the numerical solution of the fractional Darcy-Forchheimer model (43a)-(43c). We split our study into two parts: first, we concentrate on the discretization in time of Equation (43c) and, subsequently, we present the main introductory steps to the finite element implementation of the whole system (43a)-(43c).

6.1 Time discretization of the fractional Darcy-Forchheimer model

The starting point for the numerical implementation of Equation (43c) is the renaming $\alpha = 1 - \beta$, so that

$$\frac{1}{\Gamma(1-\alpha)} \int_{t_{\text{in}}}^{t} \frac{1}{(t-\tau)^{\alpha}} \boldsymbol{h}(\tau) \mathrm{d}\tau \underbrace{=}_{1-\alpha=\beta} \frac{1}{\Gamma(\beta)} \int_{t_{\text{in}}}^{t} \frac{1}{(t-\tau)^{1-\beta}} \boldsymbol{h}(\tau) \mathrm{d}\tau, \tag{44}$$

where $\boldsymbol{h}$ is a scalar- or tensor-valued function for which the considered integrals exist. By direct inspection of Equation (43c), the function $\boldsymbol{h}$ is identified with the expression

$$\boldsymbol{h}(\tau) \equiv \mathcal{R}_{\text{F}}(\boldsymbol{F}(\tau), \boldsymbol{Q}(\tau)) \frac{1}{J(\tau)} \boldsymbol{F}(\tau) \dot{\boldsymbol{Q}}(\tau), \tag{45}$$

with $\mathcal{R}_{\text{F}}(\boldsymbol{F}, \boldsymbol{Q})$ given in Equation (41).

The next step is the representation of the fractional operator featuring in Equation (43c) in the form suggested by Podlubny[80] for the numerical approximation of the Grünwald-Letnikov fractional derivative, which, for our purposes, we slightly modify as follows:

$$\begin{aligned} \frac{1}{\Gamma(\beta)} \int_{t_{\text{in}}}^{t} (t-\tau)^{\beta-1} \boldsymbol{h}(\tau) \mathrm{d}\tau &= \lim_{N \to \infty} \left(\frac{t - t_{\text{in}}}{N} \right)^{\beta} \sum_{n=0}^{N} \begin{bmatrix} \beta \\ n \end{bmatrix} \boldsymbol{h}\left(t - n \frac{t - t_{\text{in}}}{N} \right) \\ &\approx \left(\frac{t - t_{\text{in}}}{N_0} \right)^{\beta} \sum_{n=0}^{N_0} \begin{bmatrix} \beta \\ n \end{bmatrix} \boldsymbol{h}\left(t - n \frac{t - t_{\text{in}}}{N_0} \right), \end{aligned} \tag{46}$$

for $\beta \in]0, 1[$, where $\boldsymbol{h}$ is assumed to be continuous over the interval $[t_{\text{in}}, t]$, $N \in \mathbb{N}$ is the number of sub-intervals partitioning $[t_{\text{in}}, t]$, $N_0 \in \mathbb{N}$ is a sufficiently large value of N above which the value of the sum in the limit does not change appreciably within a given tolerance, and the symbol

$$\begin{bmatrix} \beta \\ 0 \end{bmatrix} = 1 \qquad \text{and} \qquad \begin{bmatrix} \beta \\ n \end{bmatrix} = \frac{\prod_{i=1}^{n} (\beta + i - 1)}{n!}, \quad \text{for } n \geq 1, \tag{47}$$

generalizes the binomial factor to the case in which β is not a natural number[80].

We notice that, in our simulations, the value of N_0 that truncates the series representing the Grünwald-Letnikov fractional derivative of $\boldsymbol{h}$, as specified in Equation (46), will be taken as a function of the instant of time at which the corresponding sum is evaluated. To proceed, we introduce two time grids: one discretizes the time interval $[t_{\text{in}}, t_{\text{fin}}]$ over which the system is observed, and is given by $\mathcal{T} := \{t_0, \ldots, t_m, \ldots, t_M\} \subseteq [t_{\text{in}}, t_{\text{fin}}]$, so that $t_0 \equiv t_{\text{in}}$, $t_M \equiv t_{\text{fin}}$, and $m = 0, \ldots, M$, with $M \in \mathbb{N}$, $M > 1$, being the number of sub-intervals by which $[t_0, t_{\text{M}}]$ is partitioned, and $\Delta t := t_m - t_{m-1}$ being the *constant* time step; the other grid is used to handle the fractional integral (46) numerically, and discretizes each interval $[t_0, t_m]$, $m = 1, \ldots, M$, in $\hat{N}_0(t_m) > m$ sub-intervals of uniform amplitude

$$s = \frac{t_m - t_0}{\hat{N}_0(t_m)}. \tag{48}$$

With reference to the second grid, the nodes are enumerated as $t_{m,n} = t_m - ns$, with $n = 0, \ldots, \hat{N}_0(t_m)$, so that $t_{m,0} = t_m$, and $t_{m,\hat{N}_0(t_m)} = t_m - \hat{N}_0(t_m)s = t_0$. Moreover, we subdivide each interval $[t_{m-1}, t_m]$ uniformly, we denote by $n_\sigma \in \mathbb{N}$, $n_\sigma > 1$, the number of sub-intervals partitioning $[t_{m-1}, t_m]$, and we have $n_\sigma s = \Delta t$, and $t_m - ns \in [t_{m-1}, t_m]$, for $n = 0, \ldots, n_\sigma$. Specifically, we obtain $(t_m - t_{m-1})/n_\sigma = \Delta t / n_\sigma = s$ and $\hat{N}_0(t_m) = n_\sigma m$, for all $m = 1, ..., M$.

According to the discretization outlined above, Equation (46), evaluated at $t = t_m$ and rewritten for $\beta = 1 - \alpha$, becomes:

$$\frac{1}{\Gamma(1-\alpha)} \int_{t_0}^{t_m} \frac{1}{(t_m - \tau)^{\alpha}} \frac{\mathcal{R}_{\text{F}}(\boldsymbol{F}(\tau), \boldsymbol{Q}(\tau))}{J(\tau)} \boldsymbol{F}(\tau) \dot{\boldsymbol{Q}}(\tau) \mathrm{d}\tau$$

$$\approx \left(\frac{t_m - t_0}{\hat{N}_0(t_m)}\right)^{1-\alpha} \sum_{n=0}^{\hat{N}_0(t_m)} \begin{bmatrix} 1-\alpha \\ n \end{bmatrix} \boldsymbol{h}\left(t_m - n\,\frac{t_m - t_0}{\hat{N}_0(t_m)}\right)$$

$$= s^{1-\alpha}\boldsymbol{h}(t_m) + s^{1-\alpha} \sum_{n=1}^{n_\sigma - 1} \begin{bmatrix} 1-\alpha \\ n \end{bmatrix} \boldsymbol{h}(t_m - ns) + s^{1-\alpha} \sum_{n=n_\sigma}^{\hat{N}_0(t_m)} \begin{bmatrix} 1-\alpha \\ n \end{bmatrix} \boldsymbol{h}(t_m - ns). \tag{49}$$

The crucial point of the procedure described by Equation (49) is that $\boldsymbol{h}(t_m)$ and $\boldsymbol{h}(t_m - ns)$ feature the time derivatives $\dot{\boldsymbol{Q}}(t_m)$ and $\dot{\boldsymbol{Q}}(t_m - ns)$. However, the numerical scheme that we use for this work provides an explicit expression for such derivatives only at the nodes of the *coarser* time grid $\mathcal{T} = \{t_0, \ldots, t_m, \ldots, t_M\}$, i.e., only for $\dot{\boldsymbol{Q}}(t_m)$, which we approximate as

$$\dot{\boldsymbol{Q}}(t_m) \approx \dot{\boldsymbol{Q}}_{\text{app}}(t_m) = \frac{\boldsymbol{Q}(t_m) - \boldsymbol{Q}(t_{m-1})}{\Delta t}. \tag{50}$$

Hence, $\boldsymbol{h}(t_m)$ reads

$$\boldsymbol{h}(t_m) = \frac{\mathcal{R}_{\text{F}}(\boldsymbol{F}(t_m), \boldsymbol{Q}(t_m))}{J(t_m)} \boldsymbol{F}(t_m) \frac{\boldsymbol{Q}(t_m) - \boldsymbol{Q}(t_{m-1})}{\Delta t}, \tag{51}$$

where all the quantities evaluated at t_m are unknown, and $\boldsymbol{Q}(t_m)$ is *the* unknown for which the discretized version of Equation (43c) has to be solved. On the other hand, the quantity $\boldsymbol{h}(t_m - ns)$ as a whole, for $m = 2, \ldots, M$, is computed through the interpolation

$$\boldsymbol{h}(t_m - ns) = \begin{cases} \left(1 - \frac{ns}{\Delta t}\right)\boldsymbol{h}(t_m) + \frac{ns}{\Delta t}\boldsymbol{h}(t_{m-1}), & \text{if } n = 0, \ldots, n_\sigma - 1, \\ \boldsymbol{h}(t_m - p\Delta t), & \text{if } n = pn_\sigma,\ p = 1, \ldots, m, \\ \left(1 - \frac{ls}{\Delta t}\right)\boldsymbol{h}(t_{m-p}) + \frac{ls}{\Delta t}\boldsymbol{h}(t_{m-p-1}), & \text{if } n = pn_\sigma + l,\ p = 1, \ldots, m-1,\ l = 1, \ldots, n_\sigma - 1, \end{cases} \tag{52}$$

where $\boldsymbol{h}(t_{m-1}), \boldsymbol{h}(t_{m-2}), \ldots$ are obtained by applying Equation (51) recursively. Note that, for $m = 1$, only the first two rows of Equation (52) apply, with $p = 1$.

Following a convergence study (data not shown) in which we solved the discretized poroelastic system (see Equations (87a) and (87b) below), we set $n_\sigma = 5$ for all $m = 1, \ldots, M$.

By enforcing the scheme outlined so far, the second addend on the left-hand side of Equation (43c) is approximated as

$$\frac{\alpha\, t_{\text{c}}^\alpha}{\Gamma(1-\alpha)} \int_{t_0}^{t_m} \frac{1}{(t_m - \tau)^\alpha} \frac{\mathcal{R}_{\text{F}}(\boldsymbol{F}(\tau), \boldsymbol{Q}(\tau))}{J(\tau)} \boldsymbol{F}(\tau)\dot{\boldsymbol{Q}}(\tau)\mathrm{d}\tau$$

$$\approx \alpha\, t_{\text{c}}^\alpha s^{1-\alpha}\boldsymbol{h}(t_m) + \alpha\, t_{\text{c}}^\alpha s^{1-\alpha} \sum_{n=1}^{n_\sigma - 1} \begin{bmatrix} 1-\alpha \\ n \end{bmatrix} \boldsymbol{h}(t_m - ns) + \alpha\, t_{\text{c}}^\alpha s^{1-\alpha} \sum_{n=n_\sigma}^{\hat{N}_0(t_m)} \begin{bmatrix} 1-\alpha \\ n \end{bmatrix} \boldsymbol{h}(t_m - ns)$$

$$= \alpha\, t_{\text{c}}^\alpha s^{1-\alpha}\boldsymbol{h}(t_m) + \alpha\, t_{\text{c}}^\alpha s^{1-\alpha} \sum_{n=1}^{n_\sigma - 1} \begin{bmatrix} 1-\alpha \\ n \end{bmatrix} \left\{\left(1 - \frac{ns}{\Delta t}\right)\boldsymbol{h}(t_m) + \frac{ns}{\Delta t}\boldsymbol{h}(t_{m-1})\right\}$$

$$+ \alpha\, t_{\text{c}}^\alpha s^{1-\alpha} \sum_{n=n_\sigma}^{\hat{N}_0(t_m)} \begin{bmatrix} 1-\alpha \\ n \end{bmatrix} \boldsymbol{h}(t_m - ns)$$

$$= \alpha\, t_{\text{c}}^\alpha s^{1-\alpha}\zeta_\alpha \boldsymbol{h}(t_m) + \alpha\, t_{\text{c}}^\alpha \boldsymbol{\mathcal{F}}_\alpha(t_m), \tag{53}$$

where we define

$$\zeta_\alpha := 1 + \sum_{n=1}^{n_\sigma - 1} \begin{bmatrix} 1-\alpha \\ n \end{bmatrix} \left(1 - \frac{ns}{\Delta t}\right) = \sum_{n=0}^{n_\sigma - 1} \begin{bmatrix} 1-\alpha \\ n \end{bmatrix} \left(1 - \frac{ns}{\Delta t}\right), \tag{54a}$$

$$\boldsymbol{\mathcal{F}}_\alpha(t_m) := s^{1-\alpha} \left(\sum_{n=1}^{n_\sigma - 1} \begin{bmatrix} 1-\alpha \\ n \end{bmatrix} \frac{ns}{\Delta t} \right) \frac{\mathcal{R}_{\text{F}}(\boldsymbol{F}(t_{m-1}), \boldsymbol{Q}(t_{m-1}))}{J(t_{m-1})} \boldsymbol{F}(t_{m-1})\dot{\boldsymbol{Q}}_{\text{app}}(t_{m-1})$$

$$+ s^{1-\alpha} \sum_{n=n_\sigma}^{\hat{N}_0(t_m)} \begin{bmatrix} 1-\alpha \\ n \end{bmatrix} \boldsymbol{h}(t_m - ns). \tag{54b}$$

In conclusion, by collecting the results obtained so far, the time discretized form of Equation (43c), or equivalently, of Equation (42), reads:

$$\begin{aligned} &\mathcal{R}_{\mathrm{F}}(\boldsymbol{F}(t_m), \boldsymbol{Q}(t_m))\boldsymbol{Q}(t_m) + \alpha\, t_{\mathrm{c}}^{\alpha}\, s^{1-\alpha}\, \zeta_\alpha \mathcal{R}_{\mathrm{F}}(\boldsymbol{F}(t_m), \boldsymbol{Q}(t_m))\, \dot{\boldsymbol{Q}}_{\mathrm{app}}(t_m) + \alpha\, t_{\mathrm{c}}^{\alpha}\, J(t_m)\boldsymbol{F}^{-1}(t_m)\boldsymbol{\mathcal{F}}_\alpha(t_m) \\ &= \mathcal{R}_{\mathrm{D}}(\boldsymbol{F}(t_m))\boldsymbol{Q}_{\mathrm{D}}(t_m). \end{aligned} \tag{55}$$

Moreover, to single out the unknown to be determined through the solution of Equation (55), i.e., $\boldsymbol{Q}(t_m)$, and in view of the linearization procedure that will be employed for the finite element simulations performed in the sequel, we take into account the expression of $\dot{\boldsymbol{Q}}_{\mathrm{app}}$ in Equation (50), we highlight the dependence of $\boldsymbol{Q}_{\mathrm{D}}$ on $\boldsymbol{F}$ and Grad$P$ by writing $\boldsymbol{Q}_{\mathrm{D}} = \boldsymbol{\mathcal{G}}^{\boldsymbol{Q}_{\mathrm{D}}}(\boldsymbol{F}, \mathrm{Grad}P)$, and we recast Equation (55) as

$$\begin{aligned} \boldsymbol{\mathcal{Z}}(\boldsymbol{F}_m, \mathrm{Grad}P_m, \boldsymbol{Q}_m) :=& \left(1 + \frac{\alpha t_{\mathrm{c}}^{\alpha} s^{1-\alpha} \zeta_\alpha}{\Delta t}\right) \mathcal{R}_{\mathrm{F}}(\boldsymbol{F}_m, \boldsymbol{Q}_m)\boldsymbol{Q}_m - \frac{\alpha t_{\mathrm{c}}^{\alpha} s^{1-\alpha} \zeta_\alpha}{\Delta t} \mathcal{R}_{\mathrm{F}}(\boldsymbol{F}_m, \boldsymbol{Q}_m)\boldsymbol{Q}_{m-1} \\ &+ \alpha t_{\mathrm{c}}^{\alpha} J_m \boldsymbol{F}_m^{-1} \boldsymbol{\mathcal{F}}_\alpha(t_m) - \mathcal{R}_{\mathrm{D}}(\boldsymbol{F}_m)\boldsymbol{\mathcal{G}}^{\boldsymbol{Q}_{\mathrm{D}}}(\boldsymbol{F}_m, \mathrm{Grad}P_m) = \boldsymbol{0}, \end{aligned} \tag{56}$$

where, for any generic physical quantity Ψ, the notation $\Psi(t_m) \equiv \Psi_m$ has been employed to express that it is evaluated at time t_m (the dependence on X is omitted, but understood).

We remark that, by performing some lengthy algebraic manipulations, Equation (56) can be solved analytically for $\boldsymbol{Q}_m$ by turning it into a polynomial equation of grade four in $\boldsymbol{Q}_m$. This property descends from the dependence of $\mathcal{R}_{\mathrm{F}}(\boldsymbol{F}_m, \boldsymbol{Q}_m)$ on $\boldsymbol{Q}_m$ being through the $\boldsymbol{C}_m$-norm $||\boldsymbol{Q}_m||_{\boldsymbol{C}_m}$. However, although the four roots of an equation of this type can be computed analytically, it is very difficult to ascertain, for generic values of $\boldsymbol{F}_m$ and GradP_m, which solutions are physically admissible. Moreover, if more than one physically admissible solutions exist, the problem of non-uniqueness of the solution arises, and, even in the case in which the solution were unique, its analytical expression would be too complicated to study it in conjunction with the other two equations of the model. For all these reasons, we prefer to proceed with the search for a unique numeric solution, to be found through a Newton-Raphson method around a "good" initial guess. These considerations lead us to the adoption of the following procedure.

6.2 Linearization of the fractional Darcy-Forchheimer model

The discretized, fractional Darcy-Forchheimer equation (56) should be studied in conjunction with the discretized version of the balance laws (43a) and (43b), put in weak form in view of their finite element implementation. In this respect, we notice that we have conducted the numerical simulations of our work in ABAQUS®, partially writing our own code for solving Equations (43a), (43b) and (56), but not for the whole implementation. Thus, although we do not have complete control over the numerical procedures employed by the commercial software, some properties of Equations (43a), (43b), and (56) can be discussed, even without entering the details of their numerical analysis.

As anticipated above, we neglect gravity, and to render the weak forms of Equations (43a) and (43b) as simple as possible, we consider the case in which their associated boundary terms are identically zero. To comply with these conditions, we partition the boundary of $\mathcal{B}$, for the motion χ, into the disjoint union of a traction-free part and Dirichlet part, and, for the pressure P, into the disjoint union of a flux-free part and, again, of a Dirichlet part. Then, within this setting, we take the procedure adopted in[66] for the purely Darcian, hyperelastic, and isotropic case, and extended in[88] for poroplasticity, and in[17] for anisotropic, fiber-reinforced porous media. In the sequel, we show the most fundamental steps of its generalization to our model, which, although being isotropic and homogeneous, takes into account Forchheimer's correction to Darcy's law and the interactions between the fluid and the solid phase arising because of such correction.

To begin with, we consider a three-field formulation of the problem at hand, which involves Equation (56) and the time-discrete, weak forms of Equations (43a) and (43b). This leads to the system

$$A(\chi_m, P_m, \boldsymbol{Q}_m; \boldsymbol{V}_\mathrm{v}) := \int_{\mathscr{B}} \left\{ - J_m P_m \boldsymbol{F}_m^{-\mathrm{T}} + \boldsymbol{\mathcal{G}}^{\boldsymbol{T}_{\mathrm{sc}}}(\boldsymbol{F}_m) \right\} : \mathrm{Grad}\boldsymbol{V}_\mathrm{v} - \int_{\partial_\mathrm{N}^\chi \mathscr{B}} \left(\boldsymbol{T}_{\mathrm{Im}} \boldsymbol{N}\right) \boldsymbol{V}_\mathrm{v} = 0, \tag{57a}$$

$$B(\chi_m, P_m, \boldsymbol{Q}_m; P_\mathrm{v}) := - \int_{\mathscr{B}} \frac{J_m - J_{m-1}}{\Delta t} P_\mathrm{v} + \int_{\mathscr{B}} \boldsymbol{Q}_m \mathrm{Grad} P_\mathrm{v} - \int_{\partial_\mathrm{N}^P \mathscr{B}} \left(\boldsymbol{Q}_m \boldsymbol{N}\right) P_\mathrm{v} = 0, \tag{57b}$$

$$\begin{aligned} \boldsymbol{\mathcal{Z}}(\boldsymbol{F}_m, \mathrm{Grad}P_m, \boldsymbol{Q}_m) := & \left(1 + \frac{\alpha t_\mathrm{c}^\alpha s^{1-\alpha} \zeta_\alpha}{\Delta t}\right) \mathcal{R}_\mathrm{F}(\boldsymbol{F}_m, \boldsymbol{Q}_m) \boldsymbol{Q}_m - \frac{\alpha t_\mathrm{c}^\alpha s^{1-\alpha} \zeta_\alpha}{\Delta t} \mathcal{R}_\mathrm{F}(\boldsymbol{F}_m, \boldsymbol{Q}_m) \boldsymbol{Q}_{m-1} \\ & + \alpha t_\mathrm{c}^\alpha J_m \boldsymbol{F}_m^{-1} \boldsymbol{\mathcal{F}}_\alpha(t_m) - \mathcal{R}_\mathrm{D}(\boldsymbol{F}_m) \boldsymbol{\mathcal{G}}^{\boldsymbol{Q}_\mathrm{D}}(\boldsymbol{F}_m, \mathrm{Grad}P_m) = \boldsymbol{0}, \end{aligned} \tag{57c}$$

in the unknowns χ_m, P_m, and $\boldsymbol{Q}_m$. To obtain Equations (57a) and (57b), we have introduced: the test functions $\boldsymbol{V}_\mathrm{v}$ and P_v, identifiable with an arbitrary virtual velocity and an arbitrary virtual pressure, respectively; the constitutive representation $\boldsymbol{\mathcal{G}}^{\boldsymbol{T}_{\mathrm{sc}}}(\boldsymbol{F}_m) \equiv \boldsymbol{T}_{\mathrm{sc}}(t_m)$, at time t_m, of the first Piola-Kirchhoff stress tensor of the solid phase; the portions $\partial_\mathrm{N}^\chi \mathscr{B}$ and $\partial_\mathrm{N}^P \mathscr{B}$ of the boundary of $\mathscr{B}$, i.e., $\partial\mathscr{B}$, on which Neumann boundary conditions on the solid phase motion and on the pressure field are enforced, respectively; and the field of co-normals $\boldsymbol{N}$ associated with the boundary of $\mathscr{B}$. We remark that, although we have reported the boundary terms in Equations (57a) and (57b), these are identically null in our setting.

The system (57a)-(57c) is highly non-linear in the motion χ_m and in the filtration velocity $\boldsymbol{Q}_m$, and it will be solved by employing a linearization procedure. One possible way is to perform, for each time t_m, a Newton-Raphson method in a neighborhood of an initially *guessed* triple $(\chi_m^0, P_m^0, \boldsymbol{Q}_m^0)$, with unknown increments $(\delta\chi_m^1, \delta P_m^1, \delta\boldsymbol{Q}_m^1)$, and then, by iteration, to construct the sequence of triples

$$(\chi_m^k = \chi_m^{k-1} + \delta\chi_m^k, P_m^k = P_m^{k-1} + \delta P_m^k, \boldsymbol{Q}_m^k = \boldsymbol{Q}_m^{k-1} + \delta\boldsymbol{Q}_m^k), \quad \text{for } k \geq 1. \tag{58}$$

At each time t_m and iteration $k \geq 1$, such a method requires the determination of the three increments $\delta\chi_m^k$, δP_m^k, and $\delta\boldsymbol{Q}_m^k$, for each of which it is necessary to provide a suitable spatial interpolation. However, rather than proceeding this way, we find it more convenient to follow a different path, as explained below.

Two-field-approach by means of Dini's implicit function Theorem. In this paragraph we present a numerical procedure that shares similarities with the one elaborated in[89]. We notice that, for $m \geq 1$, there exists a non-empty open set Ω_m of triples

$$(\boldsymbol{F}_m, \mathrm{Grad}P_m, \boldsymbol{Q}_m) \in [T\mathscr{B}_t \otimes T^*\mathscr{B}] \times T^*\mathscr{B} \times T\mathscr{B}, \qquad \text{with } \boldsymbol{Q}_m \neq \boldsymbol{0}, \tag{59}$$

such that the function $\boldsymbol{\mathcal{Z}}$ defined by the right-hand side of Equation (57c) is of class $C^1(\Omega_m; T\mathscr{B})$. Then, we assume that there exists a non-empty subset of Ω_m, hereafter denoted by $\Sigma_m \subset \Omega_m$, that consists of all the triples $(\boldsymbol{F}_m, \mathrm{Grad}P_m, \boldsymbol{Q}_m) \in \Omega_m$ that satisfy Equation (57c) as an identity, i.e., that constitute the intersection between Ω_m and the set of all the solutions of $\boldsymbol{\mathcal{Z}}(\boldsymbol{F}_m, \mathrm{Grad}P_m, \boldsymbol{Q}_m) = \boldsymbol{0}$, and for which the partial derivative of $\boldsymbol{\mathcal{Z}}$ with respect to $\boldsymbol{Q}_m$ is a non-singular second-order tensor. Hence, by setting $(\sharp) := (\boldsymbol{F}_m, \mathrm{Grad}P_m, \boldsymbol{Q}_m)$, it holds by hypothesis that $\det[\partial_{\boldsymbol{Q}_m} \boldsymbol{\mathcal{Z}}(\sharp)] \neq 0$ for all $(\boldsymbol{F}_m, \mathrm{Grad}P_m, \boldsymbol{Q}_m) \in \Sigma_m$, and $\partial_{\boldsymbol{Q}_m} \boldsymbol{\mathcal{Z}}(\sharp)$ is given by

$$\begin{aligned} \partial_{\boldsymbol{Q}_m} \boldsymbol{\mathcal{Z}}(\sharp) &= \mathcal{R}_\mathrm{F}(\boldsymbol{F}_m, \boldsymbol{Q}_m) \left[1 + \frac{\alpha t_\mathrm{c}^\alpha s^{1-\alpha} \zeta_\alpha}{\Delta t}\right] \boldsymbol{I} + \left\{\boldsymbol{Q}_m + \frac{\alpha t_\mathrm{c}^\alpha s^{1-\alpha} \zeta_\alpha}{\Delta t} [\boldsymbol{Q}_m - \boldsymbol{Q}_{m-1}]\right\} \otimes \frac{\partial \mathcal{R}_\mathrm{F}}{\partial \boldsymbol{Q}_m}(\boldsymbol{F}_m, \boldsymbol{Q}_m) \\ &= \mathcal{R}_\mathrm{F}(\boldsymbol{F}_m, \boldsymbol{Q}_m) \left[1 + \frac{\alpha t_\mathrm{c}^\alpha s \zeta_\alpha}{s^\alpha \Delta t}\right] \boldsymbol{I} + \frac{\Phi_{\mathrm{f}m} \mu}{\kappa_{\mathrm{iso}m}} \mathcal{A}_{\mathrm{iso}m} \left\{\boldsymbol{Q}_m + \frac{\alpha t_\mathrm{c}^\alpha s \zeta_\alpha}{s^\alpha \Delta t} [\boldsymbol{Q}_m - \boldsymbol{Q}_{m-1}]\right\} \otimes \frac{J_m^{-2} \boldsymbol{C}_m \boldsymbol{Q}_m}{||\boldsymbol{Q}_m||_{\boldsymbol{C}_m}}, \end{aligned} \tag{60}$$

where $\Phi_{\mathrm{f}m} \equiv J_m - \Phi_{\mathrm{sR}}$ is the pull-back of the fluid phase volumetric fraction evaluated at time t_m, while $\kappa_{\mathrm{iso}m}$ and $\mathcal{A}_{\mathrm{iso}m}$ denote κ_{iso} and $\mathcal{A}_{\mathrm{iso}}$ at time t_m.

In fact, all the properties of $\boldsymbol{\mathcal{Z}}$ and of $\partial_{\boldsymbol{Q}_m}\boldsymbol{\mathcal{Z}}$ enunciated so far constitute the hypotheses of Dini's Implicit Function Theorem for vector-valued functions of multiple arguments. Therefore, by selecting one triple $(\bar{\sharp}) \equiv (\bar{\boldsymbol{F}}_m, \mathrm{Grad}\bar{P}_m, \bar{\boldsymbol{Q}}_m) \in \Sigma_m$ (for which, thus, $\boldsymbol{\mathcal{Z}}(\bar{\sharp}) = \boldsymbol{0}$, and $\det[\partial_{\boldsymbol{Q}_m}\boldsymbol{\mathcal{Z}}(\bar{\sharp})] \neq 0$), there exists a neighborhood $\mathscr{V}(\bar{\boldsymbol{F}}_m, \mathrm{Grad}\bar{P}_m, \bar{\boldsymbol{Q}}_m) \subset \Omega_m$ of such triple such that, for the elements of the intersection $\mathscr{V}(\bar{\boldsymbol{F}}_m, \mathrm{Grad}\bar{P}_m, \bar{\boldsymbol{Q}}_m) \cap \Sigma_m \neq \emptyset$ it is possible to express $\boldsymbol{Q}_m$ as a function of $\boldsymbol{F}_m$ and $\mathrm{Grad}\, P_m$ for some neighborhood $\mathscr{U}(\bar{\boldsymbol{F}}_m, \mathrm{Grad}\bar{P}_m) \subset [T\mathscr{B}_t \otimes T^*\mathscr{B}] \times T^*\mathscr{B}$ of the pair $(\bar{\boldsymbol{F}}_m, \mathrm{Grad}\bar{P}_m)$. By denoting this vector-valued function by

$$\boldsymbol{\mathcal{G}}^{\boldsymbol{Q}_m} : \mathscr{U}(\bar{\boldsymbol{F}}_m, \mathrm{Grad}\bar{P}_m) \to T\mathscr{B}, \qquad (\boldsymbol{F}_m, \mathrm{Grad}\, P_m) \mapsto \boldsymbol{\mathcal{G}}^{\boldsymbol{Q}_m}(\boldsymbol{F}_m, \mathrm{Grad}\, P_m) = \boldsymbol{Q}_m, \tag{61}$$

Equation (57c) is identically satisfied by replacing $\boldsymbol{Q}_m$ with $\boldsymbol{\mathcal{G}}^{\boldsymbol{Q}_m}(\boldsymbol{F}_m, \mathrm{Grad}\, P_m)$, thereby obtaining

$$\hat{\boldsymbol{\mathcal{Z}}}(\boldsymbol{F}_m, \mathrm{Grad}P_m) \equiv \boldsymbol{\mathcal{Z}}(\boldsymbol{F}_m, \mathrm{Grad}P_m, \boldsymbol{\mathcal{G}}^{\boldsymbol{Q}_m}(\boldsymbol{F}_m, \mathrm{Grad}\, P_m)) = \boldsymbol{0}, \tag{62}$$

for all $(\boldsymbol{F}_m, \mathrm{Grad}\, P_m) \in \mathscr{U}(\bar{\boldsymbol{F}}_m, \mathrm{Grad}\bar{P}_m)$. Hence, the just defined function $\hat{\boldsymbol{\mathcal{Z}}} : \mathscr{U}(\bar{\boldsymbol{F}}_m, \mathrm{Grad}\bar{P}_m) \to T\mathscr{B}$ is constant in the neighborhood $\mathscr{U}(\bar{\boldsymbol{F}}_m, \mathrm{Grad}\bar{P}_m)$ and, since it is also of class C^1 therein, it has vanishing differential. In fact, upon setting $\boldsymbol{Y}_m := \mathrm{Grad}P_m$ and $(\natural) := (\boldsymbol{F}_m, \mathrm{Grad}P_m) \equiv (\boldsymbol{F}_m, \boldsymbol{Y}_m) \in \mathscr{U}(\bar{\boldsymbol{F}}_m, \mathrm{Grad}\bar{P}_m)$, from the condition of annihilation of the differential of $\hat{\boldsymbol{\mathcal{Z}}}$ along any pair of admissible increments $(\delta\boldsymbol{F}_m, \delta\boldsymbol{Y}_m)$, we find:

$$\begin{aligned}
\mathrm{d}\hat{\boldsymbol{\mathcal{Z}}}(\natural)(\delta\boldsymbol{F}_m, \delta\boldsymbol{Y}_m) =& [\partial_{\boldsymbol{F}_m}\hat{\boldsymbol{\mathcal{Z}}}(\natural)] : \delta\boldsymbol{F}_m + [\partial_{\boldsymbol{Y}_m}\hat{\boldsymbol{\mathcal{Z}}}(\natural)]\delta\boldsymbol{Y}_m \\
=& [\partial_{\boldsymbol{F}_m}\boldsymbol{\mathcal{Z}}(\sharp)] : \delta\boldsymbol{F}_m + [\partial_{\boldsymbol{Y}_m}\boldsymbol{\mathcal{Z}}(\sharp)]\delta\boldsymbol{Y}_m \\
&+ [\partial_{\boldsymbol{Q}_m}\boldsymbol{\mathcal{Z}}(\sharp)][\partial_{\boldsymbol{F}_m}\boldsymbol{\mathcal{G}}^{\boldsymbol{Q}_m}(\natural)] : \delta\boldsymbol{F}_m + [\partial_{\boldsymbol{Q}_m}\boldsymbol{\mathcal{Z}}(\sharp)][\partial_{\boldsymbol{Y}_m}\boldsymbol{\mathcal{G}}^{\boldsymbol{Q}_m}(\natural)]\delta\boldsymbol{Y}_m \\
=& \left\{\partial_{\boldsymbol{F}_m}\boldsymbol{\mathcal{Z}}(\sharp) + [\partial_{\boldsymbol{Q}_m}\boldsymbol{\mathcal{Z}}(\sharp)][\partial_{\boldsymbol{F}_m}\boldsymbol{\mathcal{G}}^{\boldsymbol{Q}_m}(\natural)]\right\} : \delta\boldsymbol{F}_m \\
&+ \left\{\partial_{\boldsymbol{Y}_m}\boldsymbol{\mathcal{Z}}(\sharp) + [\partial_{\boldsymbol{Q}_m}\boldsymbol{\mathcal{Z}}(\sharp)][\partial_{\boldsymbol{Y}_m}\boldsymbol{\mathcal{G}}^{\boldsymbol{Q}_m}(\natural)]\right\}\delta\boldsymbol{Y}_m = 0.
\end{aligned} \tag{63}$$

Accordingly, the coefficients of $\delta\boldsymbol{F}_m$ and $\delta\boldsymbol{Y}_m$ must vanish independently from one another, i.e.,

$$\partial_{\boldsymbol{F}_m}\boldsymbol{\mathcal{Z}}(\sharp) + [\partial_{\boldsymbol{Q}_m}\boldsymbol{\mathcal{Z}}(\sharp)][\partial_{\boldsymbol{F}_m}\boldsymbol{\mathcal{G}}^{\boldsymbol{Q}_m}(\natural)] = \boldsymbol{O} \quad \Rightarrow \quad \partial_{\boldsymbol{F}_m}\boldsymbol{\mathcal{G}}^{\boldsymbol{Q}_m}(\natural) = -[\partial_{\boldsymbol{Q}_m}\boldsymbol{\mathcal{Z}}(\sharp)]^{-1}\partial_{\boldsymbol{F}_m}\boldsymbol{\mathcal{Z}}(\sharp), \tag{64a}$$

$$\partial_{\boldsymbol{Y}_m}\boldsymbol{\mathcal{Z}}(\sharp) + [\partial_{\boldsymbol{Q}_m}\boldsymbol{\mathcal{Z}}(\sharp)][\partial_{\boldsymbol{Y}_m}\boldsymbol{\mathcal{G}}^{\boldsymbol{Q}_m}(\natural)] = \boldsymbol{0} \quad \Rightarrow \quad \partial_{\boldsymbol{Y}_m}\boldsymbol{\mathcal{G}}^{\boldsymbol{Q}_m}(\natural) = -[\partial_{\boldsymbol{Q}_m}\boldsymbol{\mathcal{Z}}(\sharp)]^{-1}\partial_{\boldsymbol{Y}_m}\boldsymbol{\mathcal{Z}}(\sharp), \tag{64b}$$

where $\boldsymbol{O}$ is the null element in the space of third-order tensors.

The result reported in Equation (61) permits to rephrase the system (57a)-(57c) as a system consisting of its first two equations only, i.e.[66, 88, 17],

$$\hat{A}(\chi_m, P_m; \boldsymbol{V}_\mathrm{v}) := \int_{\mathscr{B}} \left\{ -J_m P_m \boldsymbol{F}_m^{-\mathrm{T}} + \boldsymbol{\mathcal{G}}^{\boldsymbol{T}_{\mathrm{sc}}}(\boldsymbol{F}_m)\right\} : \mathrm{Grad}\boldsymbol{V}_\mathrm{v} = 0, \tag{65a}$$

$$\hat{B}(\chi_m, P_m; P_\mathrm{v}) := -\int_{\mathscr{B}} \frac{J_m - J_{m-1}}{\Delta t} P_\mathrm{v} + \int_{\mathscr{B}} \boldsymbol{\mathcal{G}}^{\boldsymbol{Q}_m}(\boldsymbol{F}_m, \mathrm{Grad}P_m)\mathrm{Grad}P_\mathrm{v} = 0, \tag{65b}$$

where the functionals $\hat{A}$ and $\hat{B}$ are highly non-linear both in χ_m and in P_m.

Remark 4. It is important to remark that the function $\boldsymbol{\mathcal{G}}^{\boldsymbol{Q}_m}$, although it exists, is not determined explicitly, since its determination would constitute a very demanding task. However, it is not necessary to find it in closed form. This is because we are going to solve Equations (65a) and (65b) through a Newton-Raphson linearization procedure, which, to determine the unknown increments of χ_m and P_m at each iteration, only requires the knowledge of the partial derivatives of $\boldsymbol{\mathcal{G}}^{\boldsymbol{Q}_m}$ at the values of $\boldsymbol{F}_m$ and $\mathrm{Grad}\, P_m$ obtained at the preceding iteration. In this respect, we emphasize that, since an expression of $\boldsymbol{\mathcal{G}}^{\boldsymbol{Q}_m}$ as a function of $\boldsymbol{F}_m$ and $\mathrm{Grad}\, P_m$ is not available, the writing $\hat{B}(\chi_m, P_m; P_\mathrm{v})$ has to be regarded as merely formal. More specifically, it has to be understood as $\hat{B}(\chi_m, P_m; P_\mathrm{v}) \equiv B(\chi_m, P_m, \boldsymbol{Q}_m; P_\mathrm{v})$, in which χ_m and P_m are the solutions to Equations (65a) and (65b), obtained by means of the procedure just mentioned, while $\boldsymbol{Q}_m$ will be determined separately through an additional Newton-Raphson method applied to Equation (57c), once $\boldsymbol{F}_m$ and $\mathrm{Grad}\, P_m$ are known (see also [89]).

Newton-Raphson method applied to Equations (65a) and (65b). To sketch the linearization procedure adopted to solve Equations (65a) and (65b), we set $k \geq 1$, with $k \in \mathbb{N}$, and we introduce both for χ_m and for P_m the values inherited from the $(k-1)$th iteration, i.e., χ_m^{k-1} and P_m^{k-1}, which are regarded as known, and the *unknown* increments $\delta\chi_m^k$ and δP_m^k. Hence, we write[66, 88, 17]

$$\chi_m^k := \chi_m^{k-1} + \delta\chi_m^k \qquad \Rightarrow \qquad \delta \boldsymbol{F}_m^k = \mathrm{Grad}\delta\chi_m^k, \tag{66a}$$

$$P_m^k := P_m^{k-1} + \delta P_m^k \qquad \Rightarrow \qquad \delta\mathrm{Grad}P_m^k = \mathrm{Grad}\delta P_m^k. \tag{66b}$$

Then, to shorten the notation, we define $\mathsf{u}_m^{k-1} := (\chi_m^{k-1}, P_m^{k-1})$ and the *approximated* functionals

$$\hat{A}_{\mathrm{app}}(\delta\chi_m^k, \delta P_m^k; \boldsymbol{V}_{\mathrm{v}}) := \hat{A}(\mathsf{u}_m^{k-1}; \boldsymbol{V}_{\mathrm{v}}) + \mathcal{D}_\chi \hat{A}(\mathsf{u}_m^{k-1}; \boldsymbol{V}_{\mathrm{v}})[\delta\chi_m^k] + \mathcal{D}_P \hat{A}(\mathsf{u}_m^{k-1}; \boldsymbol{V}_{\mathrm{v}})[\delta P_m^k], \tag{67a}$$

$$\hat{B}_{\mathrm{app}}(\delta\chi_m^k, \delta P_m^k; P_{\mathrm{v}}) := \hat{B}(\mathsf{u}_m^{k-1}; P_{\mathrm{v}}) + \mathcal{D}_\chi \hat{B}(\mathsf{u}_m^{k-1}; P_{\mathrm{v}})[\delta\chi_m^k] + \mathcal{D}_P \hat{B}(\mathsf{u}_m^{k-1}; P_{\mathrm{v}})[\delta P_m^k], \tag{67b}$$

where for a generic functional $\hat{L} \in \{\hat{A}, \hat{B}\}$ and a generic virtual field $\psi_{\mathrm{v}} \in \{\boldsymbol{V}_{\mathrm{v}}, P_{\mathrm{v}}\}$, $\mathcal{D}_\chi \hat{L}(\mathsf{u}_m^{k-1}; \psi_{\mathrm{v}})[\delta\chi_m^k]$ and $\mathcal{D}_P \hat{L}(\mathsf{u}_m^{k-1}; \psi_{\mathrm{v}})[\delta P_m^k]$ denote the Gâteaux derivatives of $\hat{L}$ with respect to the motion and pressure, evaluated at $(\mathsf{u}_m^{k-1}; \psi_{\mathrm{v}})$, and computed along the increments $\delta\chi_m^k$ and δP_m^k, respectively.

Upon enforcing the conditions $\hat{A}_{\mathrm{app}}(\delta\chi_m^k, \delta P_m^k; \boldsymbol{V}_{\mathrm{v}}) = 0$ and $\hat{B}_{\mathrm{app}}(\delta\chi_m^k, \delta P_m^k; P_{\mathrm{v}}) = 0$, the equations determining the increments $\delta\chi_m^k$ and δP_m^k at each time t_m and kth iteration of Newton's method, for $k \geq 1$, are given by[66, 88, 90]

$$\mathcal{D}_\chi \hat{A}(\mathsf{u}_m^{k-1}; \boldsymbol{V}_{\mathrm{v}})[\delta\chi_m^k] + \mathcal{D}_P \hat{A}(\mathsf{u}_m^{k-1}; \boldsymbol{V}_{\mathrm{v}})[\delta P_m^k] = -\hat{A}(\mathsf{u}_m^{k-1}; \boldsymbol{V}_{\mathrm{v}}), \tag{68a}$$

$$\mathcal{D}_\chi \hat{B}(\mathsf{u}_m^{k-1}; P_{\mathrm{v}})[\delta\chi_m^k] + \mathcal{D}_P \hat{B}(\mathsf{u}_m^{k-1}; P_{\mathrm{v}})[\delta P_m^k] = -\hat{B}(\mathsf{u}_m^{k-1}; P_{\mathrm{v}}). \tag{68b}$$

As is standard in linearization methods, the iterations stop for some positive integer $k_* \geq 1$ such that, for all $k \geq k_*$, the absolute values $|\hat{A}(\chi_m^k, P_m^k; \boldsymbol{V}_{\mathrm{v}})|$ and $|\hat{B}(\chi_m^k, P_m^k; P_{\mathrm{v}})|$ are smaller than a given tolerance.

Finally, there remains to determine the explicit expressions of the Gâteaux derivatives reported in Equations (68a) and (68b). In fact, the Gâteaux derivatives featuring in Equation (68a) are rather standard, and especially the one evaluated along $\delta\chi_m^k$ can be found in textbooks (see e.g.[91, 67]). However, in order to make our work self-contained, we show all the terms of Equations (68a) and (68b). To begin with, we notice that, due to the hypothesis of incompressibility of the solid and fluid phase, the stress tensor featuring in Equation (65a), which we write at time t_m and kth iteration as

$$\boldsymbol{T}_{\mathrm{Im}}^k := -J_m^k P_m^k [\boldsymbol{F}_m^k]^{-\mathrm{T}} + \boldsymbol{\mathcal{G}}^{\boldsymbol{T}_{\mathrm{sc}}}(\boldsymbol{F}_m^k), \tag{69}$$

can be obtained by employing the augmented energy density $W_{\mathrm{s}}^{\mathrm{a}}(\boldsymbol{F}_m, P_m) \equiv \Psi_{\mathrm{s}}^{\mathrm{a}}(\boldsymbol{C}_m, P_m)$, with $\Psi_{\mathrm{s}}^{\mathrm{a}}$ given in Equation (5a). Hence, upon writing

$$W_{\mathrm{s}}^{\mathrm{a}}(\boldsymbol{F}_m, P_m) = \tfrac{1}{2}\Phi_{\mathrm{sR}}\mu_{\mathrm{s}}[\mathrm{tr}\boldsymbol{C}_m - 3] - \Phi_{\mathrm{sR}}\mu_{\mathrm{s}} \log J_m + \tfrac{1}{2}\Phi_{\mathrm{sR}}\lambda_{\mathrm{s}}\,[\log J_m]^2 - [J_m - 1]P_m, \tag{70}$$

where we have highlighted the dependence on $\boldsymbol{F}_m$ (through $\boldsymbol{C}_m$ and J_m on the right-hand side) and P_m, it holds that

$$\begin{aligned}\boldsymbol{T}_{\mathrm{Im}}^k &\equiv \boldsymbol{\mathcal{G}}^{\boldsymbol{T}_{\mathrm{I}}}(\boldsymbol{F}_m^k, P_m^k) \\ &= \frac{\partial W_{\mathrm{s}}^{\mathrm{a}}}{\partial \boldsymbol{F}_m}(\boldsymbol{F}_m^k, P_m^k) = \underbrace{\Phi_{\mathrm{sR}}\mu_{\mathrm{s}}\boldsymbol{\eta}\boldsymbol{F}_m^k\boldsymbol{G}^{-1} - \Phi_{\mathrm{sR}}\mu_{\mathrm{s}}[\boldsymbol{F}_m^k]^{-\mathrm{T}} + \Phi_{\mathrm{sR}}\lambda_{\mathrm{s}}[\log J_m^k][\boldsymbol{F}_m^k]^{-\mathrm{T}}}_{\equiv \boldsymbol{\mathcal{G}}^{\boldsymbol{T}_{\mathrm{sc}}}(\boldsymbol{F}_m^k)} - J_m^k P_m^k [\boldsymbol{F}_m^k]^{-\mathrm{T}},\end{aligned} \tag{71}$$

where $\boldsymbol{G}$ is the material metric tensor. Accordingly, the Gâteaux derivatives $\mathcal{D}_\chi \hat{A}(\mathsf{u}_m^{k-1}; \boldsymbol{V}_{\mathrm{v}})[\delta\chi_m^k]$ and $\mathcal{D}_P \hat{A}(\mathsf{u}_m^{k-1}; \boldsymbol{V}_{\mathrm{v}})[\delta P_m^k]$ are given by

$$\mathcal{D}_\chi \hat{A}(\mathsf{u}_m^{k-1}; \boldsymbol{V}_{\mathrm{v}})[\delta\chi_m^k] = \int_{\mathscr{B}} \left[\frac{\partial^2 W_{\mathrm{s}}^{\mathrm{a}}}{\partial \boldsymbol{F}_m^2}(\boldsymbol{F}_m^{k-1}, P_m^{k-1}) : \mathrm{Grad}\,\delta\chi_m^k\right] : \mathrm{Grad}\boldsymbol{V}_{\mathrm{v}} =: [C_{\chi\chi}]_m^{k-1}(\delta\chi_m^k, \boldsymbol{V}_{\mathrm{v}}), \tag{72a}$$

$$\mathcal{D}_P\hat{A}(\mathsf{u}_m^{k-1};\boldsymbol{V}_\mathrm{v})[\delta P_m^k]=\int_{\mathscr{B}}\left[\frac{\partial^2 W_\mathrm{s}^\mathrm{a}}{\partial\boldsymbol{F}_m\partial P_m}(\boldsymbol{F}_m^{k-1},P_m^{k-1})\delta P_m^k\right]:\mathrm{Grad}\boldsymbol{V}_\mathrm{v}=:[C_{\chi P}]_m^{k-1}(\delta P_m^k,\boldsymbol{V}_\mathrm{v}),\tag{72b}$$

where the notation $[C_{\chi\chi}]_m^{k-1}(\delta\chi_m^k,\boldsymbol{V}_\mathrm{v})$ and $[C_{\chi P}]_m^{k-1}(\delta P_m^k,\boldsymbol{V}_\mathrm{v})$ is meant to highlight the influence of the motion on itself and the one of the pore pressure on the motion, respectively.

We recognize that the second derivative of W_s^a with respect to $\boldsymbol{F}_m$, hereafter denoted by $\mathbb{A}_{\mathrm{I}m}^{k-1}$, is the (augmented) *algorithmic first elasticity tensor*[91] of the mixture as a whole, while the mixed derivative of W_s^a with respect to $\boldsymbol{F}_m$ and P_m is representative of the presence of the pore pressure, intended as a Lagrange multiplier of the present theory, in the expression of the mixture's inner stress tensor. In explicit form, these derivatives read

$$\frac{\partial^2 W_\mathrm{s}^\mathrm{a}}{\partial\boldsymbol{F}_m^2}(\boldsymbol{F}_m^{k-1},P_m^{k-1})\equiv\mathbb{A}_{\mathrm{I}m}^{k-1}=\boldsymbol{\eta}\underline{\otimes}\boldsymbol{S}_{\mathrm{I}m}^{k-1}+[\boldsymbol{\eta}\boldsymbol{F}_m^{k-1}]\mathbb{C}_{\mathrm{I}m}^{k-1}:[(\boldsymbol{\eta}\boldsymbol{F}_m^{k-1})^\mathrm{T}\underline{\otimes}\boldsymbol{I}^\mathrm{T}],\tag{73a}$$

$$\frac{\partial^2 W_\mathrm{s}^\mathrm{a}}{\partial\boldsymbol{F}_m\partial P_m}(\boldsymbol{F}_m^{k-1},P_m^{k-1})=-J_m^{k-1}[\boldsymbol{F}_m^{k-1}]^{-\mathrm{T}}.\tag{73b}$$

where $\boldsymbol{S}_{\mathrm{I}m}^{k-1}=[\boldsymbol{F}_m^{k-1}]^{-1}\boldsymbol{\eta}^{-1}\boldsymbol{T}_{\mathrm{I}m}^{k-1}$ is the inner part of the mixture's second Piola-Kirchhoff stress tensor, and $\mathbb{C}_{\mathrm{I}m}^{k-1}$ is the elasticity tensor associated with it (i.e., $\mathbb{C}_{\mathrm{I}m}^{k-1}$ consists of the sum of the true elasticity tensor of the solid phase and of the pressure contribution stemming from the hypothesis of incompressibility)

$$\mathbb{C}_{\mathrm{I}m}^{k-1}=4\frac{\partial^2\Psi_\mathrm{s}^\mathrm{a}}{\partial\boldsymbol{C}_m^2}(\boldsymbol{C}_m^{k-1},P_m^{k-1}).\tag{74a}$$

Note that, in writing the last term of Equation (73a), the minor symmetry of $\mathbb{C}_{\mathrm{I}m}^{k-1}$ in its last pair of indices has been used. More explicitly, for the considered W_s^a, the first elasticity tensor is given by

$$\begin{aligned}\mathbb{A}_{\mathrm{I}m}^{k-1}=&\Phi_{\mathrm{sR}}\mu_\mathrm{s}\boldsymbol{\eta}\underline{\otimes}\boldsymbol{G}^{-1}+(\Phi_{\mathrm{sR}}\mu_\mathrm{s}-\Phi_{\mathrm{sR}}\lambda_\mathrm{s}\log J_m^{k-1}+J_m^{k-1}P_m^{k-1})[\boldsymbol{F}_m^{k-1}]^{-\mathrm{T}}\overline{\otimes}[\boldsymbol{F}_m^{k-1}]^{-1}\\&+(\Phi_{\mathrm{sR}}\lambda_\mathrm{s}-J_m^{k-1}P_m^{k-1})[\boldsymbol{F}_m^{k-1}]^{-\mathrm{T}}\otimes[\boldsymbol{F}_m^{k-1}]^{-\mathrm{T}}.\end{aligned}\tag{75}$$

Remark 5. In order to comply with the user interface of the "UMAT" subroutine in ABAQUS®, the Gâteaux derivative $\mathcal{D}_\chi\hat{A}(\mathsf{u}_m^{k-1};\boldsymbol{V}_\mathrm{v})[\delta\chi_m^k]$ in Equation (72a) is rephrased in such a way that its integrand is calculated with respect to the symmetrized increment of the deformation rate, defined as $\delta\boldsymbol{d}_m^k:=\mathrm{sym}\big(\boldsymbol{\eta}(\mathrm{Grad}\,\delta\chi_m^k)[\boldsymbol{F}_m^{k-1}]^{-1}\big)$, to the updated symmetrized "spatial" gradient of the Eulerian counterpart of $\boldsymbol{V}_\mathrm{v}$, which we write as $\boldsymbol{d}_{\mathrm{v}m}^k:=\mathrm{sym}\big(\boldsymbol{\eta}(\mathrm{Grad}\,\boldsymbol{V}_\mathrm{v})[\boldsymbol{F}_m^{k-1}]^{-1}\big)$, to the incremental deformation gradient tensor $\delta\boldsymbol{l}_m^k:=(\mathrm{Grad}\,\delta\chi_m^k)[\boldsymbol{F}_m^{k-1}]^{-1}$, and to the gradient of the Eulerian counterpart of $\boldsymbol{V}_\mathrm{v}$, which is $\boldsymbol{l}_{\mathrm{v}m}^k:=(\mathrm{Grad}\,\boldsymbol{V}_\mathrm{v})[\boldsymbol{F}_m^{k-1}]^{-1}$. To this end, we define the push-forward of the elasticity tensor $\mathbb{C}_{\mathrm{I}m}^{k-1}$ featuring in Equation (73a), i.e.,

$$[\mathbb{c}_{\mathrm{I}m}^{k-1}]^{spqr}:=\frac{1}{J_m^{k-1}}[\mathbb{C}_{\mathrm{I}m}^{k-1}]^{SPQR}[\boldsymbol{F}_m^{k-1}]^s{}_S[\boldsymbol{F}_m^{k-1}]^p{}_P[\boldsymbol{F}_m^{k-1}]^q{}_Q[\boldsymbol{F}_m^{k-1}]^r{}_R,\tag{76}$$

and we write the second Piola-Kirchhoff stress tensor as $\boldsymbol{S}_{\mathrm{I}m}^{k-1}=J_m^{k-1}[\boldsymbol{F}_m^{k-1}]^{-1}\boldsymbol{\sigma}_{\mathrm{I}m}^{k-1}[\boldsymbol{F}_m^{k-1}]^{-\mathrm{T}}$. Here, and in the sequel, the Cauchy stress tensor is defined with contravariant components, unless stated otherwise. Then, as required by the ABAQUS® "UMAT" subroutine, we provide the *algorithmic elasticity tensor*[91]

$$\mathbb{a}_m^{k-1}:=\mathbb{c}_{\mathrm{I}m}^{k-1}+\tfrac{1}{2}\big(\boldsymbol{\eta}^{-1}\underline{\otimes}\boldsymbol{\sigma}_{\mathrm{I}m}^{k-1}+\boldsymbol{\eta}^{-1}\overline{\otimes}\boldsymbol{\sigma}_{\mathrm{I}m}^{k-1}+\boldsymbol{\sigma}_{\mathrm{I}m}^{k-1}\underline{\otimes}\boldsymbol{\eta}^{-1}+\boldsymbol{\sigma}_{\mathrm{I}m}^{k-1}\overline{\otimes}\boldsymbol{\eta}^{-1}\big),\tag{77}$$

whereas Equation (72a) can be reformulated by expressing $\mathbb{A}_{\mathrm{I}m}^{k-1}$ in terms of the quantities $J_m^{k-1}\mathbb{c}_{\mathrm{I}m}^{k-1}$ and $J_m^{k-1}\boldsymbol{\sigma}_{\mathrm{I}m}^{k-1}$ (see section 4.6.1 of the Theory Manual of ABAQUS®[92]) as

$$[C_{\chi\chi}]_m^{k-1}(\delta\chi_m^k,\boldsymbol{V}_\mathrm{v})=\int_{\mathscr{B}}\boldsymbol{d}_{\mathrm{v}m}^k:[J_m^{k-1}\mathbb{c}_{\mathrm{I}m}^{k-1}]:\delta\boldsymbol{d}_m^k+\int_{\mathscr{B}}(\boldsymbol{\eta}\boldsymbol{l}_{\mathrm{v}m}^k):[\boldsymbol{\eta}^{-1}\underline{\otimes}J_m^{k-1}\boldsymbol{\sigma}_{\mathrm{I}m}^{k-1}]:(\boldsymbol{\eta}\delta\boldsymbol{l}_m^k)$$

$$=: [\hat{C}_{\boldsymbol{d}\boldsymbol{d}}]_m^{k-1}(\delta\boldsymbol{d}_m^k, \boldsymbol{d}_{\mathrm{v}m}^k) + [\hat{C}_{\boldsymbol{l}\boldsymbol{l}}]_m^{k-1}(\boldsymbol{\eta}\delta\boldsymbol{l}_m^k, \boldsymbol{\eta}\boldsymbol{l}_{\mathrm{v}m}^k). \tag{78}$$

Analogously, we can rewrite $[C_{\chi P}]_m^{k-1}(\delta\chi_m^k, \boldsymbol{V}_{\mathrm{v}})$ in the equivalent form

$$[C_{\chi P}]_m^{k-1}(\delta P_m^k, \boldsymbol{V}_{\mathrm{v}}) = -\int_{\mathscr{B}} \delta P_m^k\, [J_m^{k-1}\boldsymbol{\eta}^{-1}] : \boldsymbol{d}_{\mathrm{v}m}^k =: [\hat{C}_{\boldsymbol{d}P}]_m^{k-1}(\delta P_m^k, \boldsymbol{d}_{\mathrm{v}m}^k). \tag{79}$$

We compute now the Gâteaux derivatives $\mathcal{D}_\chi \hat{B}(\mathsf{u}_m^{k-1}; P_{\mathrm{v}})[\delta\chi_m^k]$ and $\mathcal{D}_P \hat{B}(\mathsf{u}_m^{k-1}; P_{\mathrm{v}})[\delta P_m^k]$, which constitute the part of the numerical procedure at hand containing the novelty of this work. To perform these calculations, we employ Equation (55), i.e., the time-discrete form of the fractional relationship between the (material) filtration velocity and the pressure gradient. This leads to

$$\begin{aligned}\mathcal{D}_\chi \hat{B}(\mathsf{u}_m^{k-1}; P_{\mathrm{v}})[\delta\chi_m^k] = &-\int_{\mathscr{B}} \frac{1}{\Delta t} J_m^{k-1}\{[\boldsymbol{F}_m^{k-1}]^{-\mathrm{T}} : [\mathrm{Grad}\,\delta\chi_m^k]\}P_{\mathrm{v}} \\ &+ \int_{\mathscr{B}} \left[\frac{\partial \boldsymbol{\mathcal{G}}^{\boldsymbol{\mathcal{Q}}_m}}{\partial \boldsymbol{F}_m}(\boldsymbol{F}_m^{k-1}, \mathrm{Grad}\,P_m^{k-1}) : \mathrm{Grad}\,\delta\chi_m^k\right]\mathrm{Grad}P_{\mathrm{v}}, \qquad (80a)\\ \mathcal{D}_P \hat{B}(\mathsf{u}_m^{k-1}; P_{\mathrm{v}})[\delta P_m^k] = &\int_{\mathscr{B}} \left[\frac{\partial \boldsymbol{\mathcal{G}}^{\boldsymbol{\mathcal{Q}}_m}}{\partial \mathrm{Grad}P_m}(\boldsymbol{F}_m^{k-1}, \mathrm{Grad}P_m^{k-1})\mathrm{Grad}\,\delta P_m^k\right]\mathrm{Grad}P_{\mathrm{v}}. \qquad (80b)\end{aligned}$$

We remark that, although an explicit expression of the function $\boldsymbol{\mathcal{G}}^{\boldsymbol{\mathcal{Q}}_m}$ is not available, and since it is only necessary to know the partial derivatives $\partial_{\boldsymbol{F}_m}\boldsymbol{\mathcal{G}}^{\boldsymbol{\mathcal{Q}}_m}(\boldsymbol{F}_m^{k-1}, \mathrm{Grad}\,P_m^{k-1})$ and $\partial_{\mathrm{Grad}P_m}\boldsymbol{\mathcal{G}}^{\boldsymbol{\mathcal{Q}}_m}(\boldsymbol{F}_m^{k-1}, \mathrm{Grad}\,P_m^{k-1})$, which are both evaluated at the $(k-1)$th Newton iteration, and are, thus, known, Dini's implicit function theorem permits to determine these derivatives exactly through Equations (64a) and (64b). Therefore, Equations (80a) and (80b) become

$$\begin{aligned}\mathcal{D}_\chi \hat{B}(\mathsf{u}_m^{k-1}; P_{\mathrm{v}})[\delta\chi_m^k] &\equiv [C_{P\chi}]_m^{k-1}(\delta\chi_m^k, P_{\mathrm{v}}) \\ &= -\int_{\mathscr{B}} \frac{1}{\Delta t} J_m^{k-1}\{[\boldsymbol{F}_m^{k-1}]^{-\mathrm{T}} : [\mathrm{Grad}\,\delta\chi_m^k]\}P_{\mathrm{v}} \\ &\quad -\int_{\mathscr{B}} \left\{\left[\frac{\partial \boldsymbol{\mathcal{Z}}}{\partial \boldsymbol{\mathcal{Q}}_m}(\sharp_m^{k-1})\right]^{-1}\left[\frac{\partial \boldsymbol{\mathcal{Z}}}{\partial \boldsymbol{F}_m}(\sharp_m^{k-1})\right] : \mathrm{Grad}\,\delta\chi_m^k\right\}\mathrm{Grad}P_{\mathrm{v}}, \qquad (81a)\\ \mathcal{D}_P \hat{B}(\mathsf{u}_m^{k-1}; P_{\mathrm{v}})[\delta P_m^k] &\equiv [C_{PP}]_m^{k-1}(\delta P_m^k, P_{\mathrm{v}}) \\ &= -\int_{\mathscr{B}} \left\{\left[\frac{\partial \boldsymbol{\mathcal{Z}}}{\partial \boldsymbol{\mathcal{Q}}_m}(\sharp_m^{k-1})\right]^{-1}\left[\frac{\partial \boldsymbol{\mathcal{Z}}}{\partial \mathrm{Grad}P_m}(\sharp_m^{k-1})\right]\mathrm{Grad}\,\delta P_m^k\right\}\mathrm{Grad}P_{\mathrm{v}}, \qquad (81b)\end{aligned}$$

where $\partial_{\boldsymbol{\mathcal{Q}}_m}\boldsymbol{\mathcal{Z}}$ has been determined in Equation (60), while the derivatives of $\boldsymbol{\mathcal{Z}}$ with respect to $\boldsymbol{F}_m$ and $\mathrm{Grad}\,P_m$ are given by

$$\begin{aligned}\frac{\partial \boldsymbol{\mathcal{Z}}}{\partial \boldsymbol{F}_m}(\sharp_m^{k-1}) = &\left(1 + \frac{\alpha t_{\mathrm{c}}^\alpha s^{1-\alpha}\zeta_\alpha}{\Delta t}\right)\left[\boldsymbol{\mathcal{Q}}_m^{k-1} \otimes \frac{\partial \mathcal{R}_{\mathrm{F}}}{\partial \boldsymbol{F}_m}(\boldsymbol{F}_m^{k-1}, \boldsymbol{\mathcal{Q}}_m^{k-1})\right] - \frac{\alpha t_{\mathrm{c}}^\alpha s^{1-\alpha}\zeta_\alpha}{\Delta t}\boldsymbol{\mathcal{Q}}_{m-1} \otimes \frac{\partial \mathcal{R}_{\mathrm{F}}}{\partial \boldsymbol{F}_m}(\boldsymbol{F}_m^{k-1}, \boldsymbol{\mathcal{Q}}_m^{k-1}) \\ &+ \alpha t_{\mathrm{c}}^\alpha J_m^{k-1}[\boldsymbol{F}_m^{k-1}]^{-1}\boldsymbol{\mathcal{F}}_\alpha(t_m) \otimes [\boldsymbol{F}_m^{k-1}]^{-\mathrm{T}} - \alpha t_{\mathrm{c}}^\alpha J_m^{k-1}[\boldsymbol{F}_m^{k-1}]^{-1} \otimes \{[\boldsymbol{F}_m^{k-1}]^{-1}\boldsymbol{\mathcal{F}}_\alpha(t_m)\} \\ &- \boldsymbol{\mathcal{G}}^{\boldsymbol{\mathcal{Q}}_{\mathrm{D}}}(\boldsymbol{F}_m^{k-1}, \mathrm{Grad}\,P_m^{k-1}) \otimes \frac{\partial \mathcal{R}_{\mathrm{D}}}{\partial \boldsymbol{F}_m}(\boldsymbol{F}_m^{k-1}) - \mathcal{R}_{\mathrm{D}}(\boldsymbol{F}_m^{k-1})\frac{\partial \boldsymbol{\mathcal{G}}^{\boldsymbol{\mathcal{Q}}_{\mathrm{D}}}}{\partial \boldsymbol{F}_m}(\boldsymbol{F}_m^{k-1}, \mathrm{Grad}P_m^{k-1}), \qquad (82a)\\ \frac{\partial \boldsymbol{\mathcal{Z}}}{\partial \mathrm{Grad}P_m}(\sharp_m^{k-1}) = &-\mathcal{R}_{\mathrm{D}}(\boldsymbol{F}_m^{k-1})\frac{\partial \boldsymbol{\mathcal{G}}^{\boldsymbol{\mathcal{Q}}_{\mathrm{D}}}}{\partial \mathrm{Grad}P_m}(\boldsymbol{F}_m^{k-1}, \mathrm{Grad}P_m^{k-1}) = (J_m^{k-1} - \Phi_{\mathrm{sR}})[\boldsymbol{C}_m^{k-1}]^{-1}, \qquad (82b)\end{aligned}$$

and, again, the notation $[C_{P\chi}]_m^{k-1}(\delta\chi_m^k, P_{\mathrm{v}})$ and $[C_{PP}]_m^{k-1}(\delta P_m^k, P_{\mathrm{v}})$ puts in evidence the influence of the pore pressure on the motion and the self-influence of the pore pressure. For completeness, we supply also the expressions of the derivatives of $\mathcal{R}_{\mathrm{F}}$, $\mathcal{R}_{\mathrm{D}}$, and $\boldsymbol{\mathcal{G}}^{\boldsymbol{\mathcal{Q}}_{\mathrm{D}}}$ with respect to $\boldsymbol{F}_m$. To this end, we write κ_{iso} and $\mathcal{A}_{\mathrm{iso}}$ as functions of J_m, i.e., we set $\kappa_{\mathrm{iso}} \equiv \hat{\kappa}_{\mathrm{iso}}(J_m)$ and $\mathcal{A}_{\mathrm{iso}} \equiv \hat{\mathcal{A}}_{\mathrm{iso}}(J_m)$, and we express $||\boldsymbol{\mathcal{Q}}_m||_{\boldsymbol{C}_m}$ as a function of $\boldsymbol{F}_m$, i.e., $||\boldsymbol{\mathcal{Q}}_m||_{\boldsymbol{C}_m} \equiv \hat{\mathfrak{Q}}(\boldsymbol{F}_m)$. Then, we obtain:

$$\frac{\partial \mathcal{R}_{\mathrm{D}}}{\partial \boldsymbol{F}_m}(\boldsymbol{F}_m^{k-1}) = \mathcal{R}_{\mathrm{D}}(\boldsymbol{F}_m^{k-1})\left[\frac{J_m^{k-1}}{J_m^{k-1} - \Phi_{\mathrm{sR}}} - \frac{J_m^{k-1}}{\hat{\kappa}_{\mathrm{iso}}(J_m^{k-1})}\frac{\partial \hat{\kappa}_{\mathrm{iso}}}{\partial J_m}(J_m^{k-1})\right][\boldsymbol{F}_m^{k-1}]^{-\mathrm{T}}, \tag{83a}$$

$$\frac{\partial\hat{\mathfrak{Q}}}{\partial\boldsymbol{F}_m}(\boldsymbol{F}_m^{k-1}) = -||\boldsymbol{Q}_m^{k-1}||_{\boldsymbol{C}_m^{k-1}}[\boldsymbol{F}_m^{k-1}]^{-\mathrm{T}} + \frac{1}{J_m^{k-1}||\boldsymbol{Q}_m^{k-1}||_{\boldsymbol{C}_m^{k-1}}}\frac{\boldsymbol{\eta}\boldsymbol{F}_m^{k-1}\boldsymbol{Q}_m^{k-1}}{J_m^{k-1}} \otimes \boldsymbol{Q}_m^{k-1}, \tag{83b}$$

$$\begin{aligned}\frac{\partial\mathcal{R}_{\mathrm{F}}}{\partial\boldsymbol{F}_m}(\boldsymbol{F}_m^{k-1},\boldsymbol{Q}_m^{k-1}) = \frac{\partial\mathcal{R}_{\mathrm{D}}}{\partial\boldsymbol{F}_m}(\boldsymbol{F}_m^{k-1})[1+\hat{\mathcal{A}}_{\mathrm{iso}}(J_m^{k-1})||\boldsymbol{Q}_m^{k-1}||_{\boldsymbol{C}_m^{k-1}}] \\ + \mathcal{R}_{\mathrm{D}}(\boldsymbol{F}_m^{k-1})\Bigg\{\frac{\partial\hat{\mathcal{A}}_{\mathrm{iso}}}{\partial J_m}(J_m^{k-1})J_m^{k-1}||\boldsymbol{Q}_m^{k-1}||_{\boldsymbol{C}_m^{k-1}}[\boldsymbol{F}_m^{k-1}]^{-\mathrm{T}} \\ + \hat{\mathcal{A}}_{\mathrm{iso}}(J_m^{k-1})\frac{\partial\hat{\mathfrak{Q}}}{\partial\boldsymbol{F}_m}(\boldsymbol{F}_m^{k-1})\Bigg\},\end{aligned} \tag{83c}$$

$$\begin{aligned}\frac{\partial\boldsymbol{\mathcal{G}}^{\boldsymbol{Q}_{\mathrm{D}}}}{\partial\boldsymbol{F}_m}(\boldsymbol{F}_m^{k-1},\mathrm{Grad}\,P_m^{k-1}) = \frac{J_m^{k-1}}{\hat{\kappa}_{\mathrm{iso}}(J_m^{k-1})}\frac{\partial\hat{\kappa}_{\mathrm{iso}}}{\partial J_m}(J_m^{k-1})\boldsymbol{Q}_{\mathrm{D}m}^{k-1}\otimes[\boldsymbol{F}_m^{k-1}]^{-\mathrm{T}} \\ - [\boldsymbol{F}_m^{k-1}]^{-1}\otimes\boldsymbol{Q}_{\mathrm{D}m}^{k-1} - [\boldsymbol{C}_m^{k-1}]^{-1}\underline{\otimes}\,\boldsymbol{\eta}\boldsymbol{F}_m^{k-1}\boldsymbol{Q}_{\mathrm{D}m}^{k-1}.\end{aligned} \tag{83d}$$

Finally, we notice that the definitions supplied in Equations (72a), (72b), (81a) and (81b) allow to rewrite Equations (68a) and (68b) in the more suggestive form

$$[C_{\chi\chi}]_m^{k-1}(\delta\chi_m^k,\boldsymbol{V}_{\mathrm{v}}) + [C_{\chi P}]_m^{k-1}(\delta P_m^k,\boldsymbol{V}_{\mathrm{v}}) = -\hat{A}(\mathrm{u}_m^{k-1};\boldsymbol{V}_{\mathrm{v}}), \tag{84a}$$

$$[C_{P\chi}]_m^{k-1}(\delta\chi_m^k,P_{\mathrm{v}}) + [C_{PP}]_m^{k-1}(\delta P_m^k,P_{\mathrm{v}}) = -\hat{B}(\mathrm{u}_m^{k-1};P_{\mathrm{v}}), \tag{84b}$$

with $[C_{\chi P}]_m^{k-1}(\,\cdot\,,\,\cdot\,)$ and $[C_{P\chi}]_m^{k-1}(\,\cdot\,,\,\cdot\,)$ being related through the identity[66, 17]

$$\begin{aligned}[C_{P\chi}]_m^{k-1}(\delta\chi_m^k,P_{\mathrm{v}}) = &\frac{1}{\Delta t}[C_{\chi P}]_m^{k-1}(P_{\mathrm{v}},\delta\chi_m^k) \\ &- \int_{\mathscr{B}}\left\{\left[\frac{\partial\boldsymbol{\mathcal{Z}}}{\partial\boldsymbol{Q}_m}(\sharp_m^{k-1})\right]^{-1}\left[\frac{\partial\boldsymbol{\mathcal{Z}}}{\partial\boldsymbol{F}_m}(\sharp_m^{k-1})\right] : \mathrm{Grad}\delta\chi_m^k\right\}\mathrm{Grad}P_{\mathrm{v}}.\end{aligned} \tag{85}$$

Equations (84a) and (84b) are a "prelude" to their associated algebraic form, which is achieved by introducing the finite element discretization of the problem at hand and the interpolation functions for the unknown increments $\delta\chi_m^k$ and δP_m^k as well as for the virtual fields $\boldsymbol{V}_{\mathrm{v}}$ and P_{v}. In fact, each summand on the left-hand side of Equations (84a) and (84b) gives rise to a specific block of the matrix of the coefficients of the system of algebraic equations associated with Equations (68a) and (68b).

It is important to emphasize that, while Equation (84a) is essentially the same as the one studied in[66, 88, 17], the main differences between these previous studies and our work are condensed in Equation (84b). The first difference is given by the second term of the functional $[C_{P\chi}]_m^{k-1}(\,\cdot\,,\,\cdot\,)$, which collects all the modifications to the Darcian model that are associated both with Forchheimer's correction and with its fractionalization (it can be proven, in this respect, that Darcy's model is retrieved by setting $\alpha = 0$ and $\mathcal{A}_{\mathrm{iso}} = 0$ identically). This term, in fact, describes a coupling between pressure and deformation that, because of the Jacobian $\partial\boldsymbol{\mathcal{Z}}/\partial\boldsymbol{Q}_m$ and of the derivative $\partial\boldsymbol{\mathcal{Z}}/\partial\boldsymbol{F}_m$, is much more intricate than the Darcian one, and, in addition, it takes into account the non-locality in time of the model under investigation through $\boldsymbol{\mathcal{F}}_\alpha(t_m)$. The second difference with the Darcian model addressed in[66, 88, 17] is related to the definition of the functional $[C_{PP}]_m^{k-1}(\,\cdot\,,\,\cdot\,)$, which, again, keeps track of the non-locality in time and of all the interactions between the flow and the deformation through the inverse of the Jacobian $\partial\boldsymbol{\mathcal{Z}}/\partial\boldsymbol{Q}_m$ (cf. Equation (60)).

In spite of the differences just discussed, for the purpose of implementation in ABAQUS®, and, in particular, due to the limitation of the "UMAT" and "UMATHT" subroutines present in the adopted software, in the numerical tests performed in this work, we neglect the second integral defining $[C_{P\chi}]_m^{k-1}(\delta\chi_m^k,P_{\mathrm{v}})$ on the far right-hand side of Equations (81a) and (85). Hence, for the forthcoming simulations, we substitute the term $[C_{P\chi}]_m^{k-1}(\delta\chi_m^k,P_{\mathrm{v}})$ in Equation (84b) with its approximated counterpart

$$\begin{aligned}[C_{P\chi}^{\mathrm{app}}]_m^{k-1}(\delta\chi_m^k,P_{\mathrm{v}}) &:= -\int_{\mathscr{B}}\frac{1}{\Delta t}J_m^{k-1}\{[\boldsymbol{F}_m^{k-1}]^{-\mathrm{T}} : [\mathrm{Grad}\,\delta\chi_m^k]\}P_{\mathrm{v}} \\ &= -\int_{\mathscr{B}}\frac{1}{\Delta t}J_m^{k-1}\mathrm{tr}[\boldsymbol{\eta}^{-1}\delta\boldsymbol{d}_m^k]P_{\mathrm{v}}\end{aligned}$$

$$=: [\hat{C}^{\mathrm{app}}_{P\boldsymbol{d}}]^{k-1}_m(\delta\boldsymbol{d}^k_m, P_{\mathrm{v}}), \tag{86}$$

and we solve the approximated system

$$[C_{\chi\chi}]^{k-1}_m(\delta\chi^k_m, \boldsymbol{V}_{\mathrm{v}}) + [C_{\chi P}]^{k-1}_m(\delta P^k_m, \boldsymbol{V}_{\mathrm{v}}) = -\hat{A}(\mathsf{u}^{k-1}_m; \boldsymbol{V}_{\mathrm{v}}), \tag{87a}$$

$$[C^{\mathrm{app}}_{P\chi}]^{k-1}_m(\delta\chi^k_m, P_{\mathrm{v}}) + [C_{PP}]^{k-1}_m(\delta P^k_m, P_{\mathrm{v}}) = -\hat{B}(\mathsf{u}^{k-1}_m; P_{\mathrm{v}}). \tag{87b}$$

Analogously to Equation (86), also the term $[C_{PP}]^{k-1}_m(\delta P^k_m, P_{\mathrm{v}})$ can be recast in the equivalent form

$$\begin{aligned}[C_{PP}]^{k-1}_m(\delta P^k_m, P_{\mathrm{v}}) &= -\int_{\mathscr{B}} \{(\mathrm{Grad}\delta P^k_m)[\boldsymbol{F}^{k-1}_m]^{-1}\}[J^{k-1}_m \boldsymbol{\mathfrak{B}}^{k-1}_m]\{(\mathrm{Grad}P_{\mathrm{v}})[\boldsymbol{F}^{k-1}_m]^{-1}\} \\ &=: [\hat{C}_{PP}]^{k-1}_m(\delta p^k_m, p_{\mathrm{v}}),\end{aligned} \tag{88}$$

where $p^k_m(\chi(X,t),t) := P^k_m(X,t)$, $p_{\mathrm{v}}(\chi(X,t),t) := P_{\mathrm{v}}(X,t)$ is the spatial counterpart of the virtual pressure field, and we have set

$$\boldsymbol{\mathfrak{B}}^{k-1}_m := \frac{1}{J^{k-1}_m}\boldsymbol{F}^{k-1}_m\left[\frac{\partial\boldsymbol{\mathcal{Z}}}{\partial\boldsymbol{Q}_m}(\sharp^{k-1}_m)\right]^{-1}\left[\frac{\partial\boldsymbol{\mathcal{Z}}}{\partial\mathrm{Grad}P_m}(\sharp^{k-1}_m)\right][\boldsymbol{F}^{k-1}_m]^{\mathrm{T}}. \tag{89}$$

Clearly, this way of proceeding has the drawback that not all the interactions introduced by our model are equally considered in the algorithm employed. However, the algorithm makes it still possible to account for those deviations from Darcy's regime that the fractional version of Forchheimer's correction studied in our work unfolds in the term $[C_{PP}]^{k-1}_m(\delta P^k_m, P_{\mathrm{v}})$ through $\boldsymbol{\mathfrak{B}}^{k-1}_m$ and in the residue $\hat{B}(\mathsf{u}^{k-1}_m; P_{\mathrm{v}})$.

Finally, by solving Equations (87a) and (87b) for $\delta\chi^k_m$ and δP^k_m, reconstructing the motion and fluid pressure at the kth iteration as $\chi^k_m = \chi^{k-1}_m + \delta\chi^k_m$ and $P^k_m = P^{k-1}_m + \delta P^k_m$, and computing the functionals $\hat{A}(\mathsf{u}^k_m, \boldsymbol{V}_{\mathrm{v}})$ and $\hat{B}(\mathsf{u}^k_m, P_{\mathrm{v}})$, the pair (χ_m, P_m) that solves Equations (65a) and (65b) is found, as anticipated above, when, for some $k_* \in \mathbb{N}$, the absolute values $|\hat{A}(\mathsf{u}^k_m, \boldsymbol{V}_{\mathrm{v}})|$ and $|\hat{B}(\mathsf{u}^k_m, P_{\mathrm{v}})| \equiv |B(\chi^k_m, P^k_m, \boldsymbol{Q}^k_m; P_{\mathrm{v}})|$ remain smaller than a given threshold for all $k > k_*$.

There is, however, a last step of the algorithm employed here that has to be commented. Indeed, to solve Equations (87a) and (87b), it is necessary to know the residue

$$\hat{B}(\mathsf{u}^{k-1}_m; P_{\mathrm{v}}) \equiv \hat{B}(\chi^{k-1}_m, P^{k-1}_m; P_{\mathrm{v}}) = B(\chi^{k-1}_m, P^{k-1}_m, \boldsymbol{Q}^{k-1}_m; P_{\mathrm{v}}), \qquad k \geq 1. \tag{90}$$

Yet, this quantity is unknown for all $k \geq 2$, because $\boldsymbol{Q}^{k-1}_m$ has still to be determined. On the other hand, $\boldsymbol{Q}^{k-1}_m$ is known only for $k = 1$, since $\boldsymbol{Q}^0_m$ is either guessed or computed by solving Equation (57c) through another Newton-Raphson procedure (see next paragraph). Hence, since χ^0_m and P^0_m are supplied by the initial guess, also the residue $B(\chi^0_m, P^0_m, \boldsymbol{Q}^0_m; P_{\mathrm{v}})$ is entirely defined. In conclusion, the filtration velocity $\boldsymbol{Q}^{k-1}_m$ must be computed at each $k \geq 2$. This is done by applying, again, the Newton-Raphson method shown in the next paragraph, and, with this procedure, also $\boldsymbol{Q}^k_m$ is obtained. Therefore, the filtration velocity $\boldsymbol{Q}_m$ at time t_m can be approximated with the value of $\boldsymbol{Q}^k_m$ for $k > k_*$, with $k_* \in \mathbb{N}$ being such that $|\boldsymbol{\mathcal{Z}}(\boldsymbol{F}^k_m, \mathrm{Grad}\, P^k_m, \boldsymbol{Q}^k_m)|$ is smaller than a given threshold for all $k > k_*$.

Determination of $\boldsymbol{Q}_m$. The separate determination of $\boldsymbol{Q}_m$ is necessary for computing the residues $\hat{B}(\chi^{k-1}_m, P^{k-1}_m; P_{\mathrm{v}}) \equiv B(\chi^{k-1}_m, P^{k-1}_m, \boldsymbol{Q}^{k-1}_m; P_{\mathrm{v}})$, for all $k \geq 2$. For $k = 1$, instead, the residue $B(\chi^0_m, P^0_m, \boldsymbol{Q}^0_m; P_{\mathrm{v}})$ is entirely defined by the initial triple $(\chi^0_m, P^0_m, \boldsymbol{Q}^0_m)$. In this work, to simplify the computational burden, we have opted to prescribe $\boldsymbol{Q}^0_m$ arbitrarily through an "educated guess", since this does not affect considerably the convergence to the value of $\boldsymbol{Q}_m$ that solves approximately Equation (57c).

To compute the residue $\hat{B}(\chi^{k-1}_m, P^{k-1}_m; P_{\mathrm{v}}) \equiv B(\chi^{k-1}_m, P^{k-1}_m, \boldsymbol{Q}^{k-1}_m; P_{\mathrm{v}})$, for all $k \geq 2$, we determine $\boldsymbol{Q}^{k-1}_m$ as follows. First, for each $k \geq 2$, we write $\boldsymbol{Q}^{k-1}_m$ as $\boldsymbol{Q}^{k-1,l}_m := \boldsymbol{Q}^{k-1,l-1}_m + \delta\boldsymbol{Q}^{k-1,l}_m$. Here, $l \geq 1$, $l \in \mathbb{N}$, is the counter of the Newton-Raphson procedure *"nested"*[89] in the kth iteration of the outer procedure, employed to calculate χ^k_m and P^k_m, while $\delta\boldsymbol{Q}^{k-1,l}_m$ is the increment of the filtration velocity at the lth iteration nested in the $(k-1)$th iteration of the outer scheme. We notice that, for $l = 1$, the

quantity $\boldsymbol{Q}_m^{k-1,0}$ is a guessed value of the filtration velocity that can be taken equal to $\boldsymbol{Q}_m^{k-2}$. Then, we approximate the function $\boldsymbol{\mathcal{Z}}$ with its Taylor polynomial of the first grade in $\delta\boldsymbol{Q}_m^{k-1,l}$, thereby writing

$$\begin{aligned}&\boldsymbol{\mathcal{Z}}_{\text{app}}(\boldsymbol{F}_m^{k-1}, \text{Grad}\, P_m^{k-1}, \boldsymbol{Q}_m^{k-1,l-1} + \delta\boldsymbol{Q}_m^{k-1,l})\\ &:= \boldsymbol{\mathcal{Z}}(\boldsymbol{F}_m^{k-1}, \text{Grad}\, P_m^{k-1}, \boldsymbol{Q}_m^{k-1,l-1}) + \left[\frac{\partial \boldsymbol{\mathcal{Z}}}{\partial \boldsymbol{Q}_m}(\boldsymbol{F}_m^{k-1}, \text{Grad}\, P_m^{k-1}, \boldsymbol{Q}_m^{k-1,l-1})\right]\delta\boldsymbol{Q}_m^{k-1,l}, \qquad l \geq 1. \end{aligned} \tag{91}$$

Next, by setting $\boldsymbol{\mathcal{Z}}_{\text{app}}(\boldsymbol{F}_m^{k-1}, \text{Grad}\, P_m^{k-1}, \boldsymbol{Q}_m^{k-1,l-1} + \delta\boldsymbol{Q}_m^{k-1,l}) = \boldsymbol{0}$ for $l \geq 1$, $\delta\boldsymbol{Q}_m^{k-1,l}$ is obtained as

$$\delta\boldsymbol{Q}_m^{k-1,l} = -\left[\frac{\partial \boldsymbol{\mathcal{Z}}}{\partial \boldsymbol{Q}_m}(\boldsymbol{F}_m^{k-1}, \text{Grad}\, P_m^{k-1}, \boldsymbol{Q}_m^{k-1,l-1})\right]^{-1} \boldsymbol{\mathcal{Z}}(\boldsymbol{F}_m^{k-1}, \text{Grad}\, P_m^{k-1}, \boldsymbol{Q}_m^{k-1,l-1}), \qquad l \geq 1, \tag{92}$$

and $\boldsymbol{Q}_m^{k-1,l}$ can be reconstructed according to its definition. As usual, the iterations stop when, for some $l_*(k) \in \mathbb{N}$, the absolute value $|\boldsymbol{\mathcal{Z}}(\boldsymbol{F}_m^{k-1}, \text{Grad}\, P_m^{k-1}, \boldsymbol{Q}_m^{k-1,l})|$ remains smaller than a given tolerance for all $l > l_*(k)$. Accordingly, $\boldsymbol{Q}_m^{k-1}$ is formally identified with the limit $\boldsymbol{Q}_m^{k-1} := \lim_{l\to+\infty} \boldsymbol{Q}_m^{k-1,l}$. This permits to calculate the residue $\hat{B}(\chi_m^{k-1}, P_m^{k-1}; P_v) \equiv B(\chi_m^{k-1}, P_m^{k-1}, \boldsymbol{Q}_m^{k-1}; P_v)$ as

$$B(\chi_m^{k-1}, P_m^{k-1}, \boldsymbol{Q}_m^{k-1}; P_v) = -\int_{\mathscr{B}} \frac{J_m^{k-1} - J_{m-1}}{\Delta t} P_v + \int_{\mathscr{B}} \boldsymbol{Q}_m^{k-1} \text{Grad}\, P_v. \tag{93}$$

To conclude this paragraph, we notice that $\boldsymbol{Q}_m^k$ is calculated with the same scheme employed for $\boldsymbol{Q}_m^{k-1}$, after determining the pair $(\boldsymbol{F}_m^k, \text{Grad}\, P_m^k)$ by solving Equations (87a) and (87b), so that the quantity $|\boldsymbol{\mathcal{Z}}(\boldsymbol{F}_m^k, \text{Grad}\, P_m^k, \boldsymbol{Q}_m^k)|$ remains smaller than a given threshold. We also remark that, at a given time t_m, the stopping criterion for the aforementioned scheme is the convergence within a certain tolerance of (χ_m^k, P_m^k), which is assured for $k > k_*$. To summarize, one more nested Newton-Raphson procedure is required to calculate $\boldsymbol{Q}_m$. In fact, after determining the approximated solution $(\chi_m^k, P_m^k) \equiv (\chi_m, P_m)$ of Equations (65a) and (65b), the value $\boldsymbol{Q}_m^k = \lim_{l\to+\infty} \boldsymbol{Q}_m^{k,l}$ is formally found by calling for the nested Newton-Raphson method (see, e.g., [89]), and $\boldsymbol{Q}_m$ is found as $\boldsymbol{Q}_m^k \equiv \boldsymbol{Q}_m$, for $k > k_*$.

7 Summary of the model and benchmark tests

In this section, we describe the initial and boundary value problem (IBVP) employed for our numerical experiments, which will be conducted in ABAQUS® by following the numerical procedure explained in section 6.

Our simulations refer to the mathematical model conceived in the previous sections, which aims at describing a class of media characterized, on the one hand, by non-negligible pore scale inertial effects of the fluid and, on the other hand, by a complex microstructure of the pore network that gives rise to flow laws modeled as non-local in time[38, 43, 31]. In particular, the class of media we are referring to include bio-mimetic scaffolds that have elastic parameters comparable to those of a biological tissue, and that are known to give rise to flow regimes compatible with Forchheimer's correction[87]. For the purpose of studying this kind of media, we concentrate on simulating Equations (43a)-(43c), so that it is possible to highlight how the overall behavior of the system under evaluation is influenced by the fractional constitutive law of $\boldsymbol{Q}$ specified in Equation (42). In this respect, we notice that the standard Darcy-Forchheimer model, represented by Equations (35a) and (35b), can be recovered from the fractional one by setting $\alpha = 0$, while standard Darcy's model can be obtained by setting $c_0 = 0$ and $\alpha = 0$ in Equation (32).

In the following simulations, we replicate the setup of an experimentally relevant uni-axial compression test in which, before the application of the load, a cylindrical sample of the hypothetical material under study is put in a compression chamber, situated in the inner part of the experimental apparatus. Inside the chamber, the sample is positioned between two impermeable plates, made of steel or, more generally, of a material that does not allow for adhesion bonds with the sample itself. Moreover, in the inner chamber, warm water circulates and maintains the sample in isothermal conditions. Then, the

experiment is conducted in control of displacement: the movement of the upper plate is controlled, and exerts a prescribed compression on the sample. When the maximum prescribed displacement is reached, the load is kept constant in order to study the relaxation of the material.

We perform the simulation of the just described unconfined compression test by solving Equations (43a)-(43c) for a cylindrical sample over the time interval $[t_{\text{in}}, t_{\text{fin}}] \equiv [0, t_{\text{fin}}]$. The specimen has initial radius $R = 30\,\text{mm}$ and initial height $H = 20\,\text{mm}$, as shown in Fig 1. Since we do not simulate the plates, boundary conditions are applied directly on the specimen's boundary, which coincides with the boundary of its reference placement, $\partial\mathscr{B}$, and can be partitioned as $\partial\mathscr{B} = \Gamma_{\text{U}} \cup \Gamma_{\text{L}} \cup \Gamma_{\text{B}}$, with Γ_{U}, Γ_{L}, and Γ_{B} being the specimen's upper, lateral, and bottom surface, respectively. We recall that, since the constitutive framework has been set, the system (43a)-(43c) is equivalent to seven scalar equations in the seven unknowns given by the three components of the motion χ, pore pressure P, and the three components of the material filtration velocity $\boldsymbol{Q}$.

To assign the boundary conditions, we introduce a reference frame, associated with $\mathscr{B}$, and having origin at the center X_{O} of Γ_{B}, and axes directed along the unit vectors of the triad $\mathscr{E}_{\text{O}} := \{\boldsymbol{E}_1, \boldsymbol{E}_2, \boldsymbol{E}_3\} \subset T_{X_{\text{O}}}\mathscr{B}$, in which $\boldsymbol{E}_3$ identifies the axial direction of the specimen, while $\boldsymbol{E}_1$ and $\boldsymbol{E}_2$ span the transversal plane. We also introduce the co-normals $\boldsymbol{N}_{\text{U}}$, $\boldsymbol{N}_{\text{L}}$, and $\boldsymbol{N}_{\text{B}}$ to Γ_{U}, Γ_{L}, and Γ_{B}, and we notice that $\boldsymbol{N}_{\text{U}}$ and $\boldsymbol{N}_{\text{B}}$ are parallel and anti-parallel to the co-vector $\boldsymbol{E}^3$ of the co-vector basis dual to $\mathscr{E}_{\text{O}}$. Hence, for every time $t \in [0, t_{\text{fin}}]$, the experimental setup illustrated above is represented by the boundary conditions

$$\chi^3(X,t) = \chi^3_{\text{U}}(X_1, X_2, t), \qquad [\boldsymbol{T}_{\text{I}}\boldsymbol{N}_{\text{U}}]\boldsymbol{E}_1 = 0, \qquad [\boldsymbol{T}_{\text{I}}\boldsymbol{N}_{\text{U}}]\boldsymbol{E}_2 = 0, \qquad \text{on } \Gamma_{\text{U}}, \tag{94a}$$

$$\boldsymbol{Q}\boldsymbol{N}_{\text{U}} = 0, \qquad \text{on } \Gamma_{\text{U}}, \tag{94b}$$

$$\boldsymbol{T}_{\text{I}}\boldsymbol{N}_{\text{L}} = \boldsymbol{0}, \qquad \text{on } \Gamma_{\text{L}}, \tag{94c}$$

$$P = 0, \qquad \text{on } \Gamma_{\text{L}}, \tag{94d}$$

$$\chi(X,t) = (X^1, X^2, 0), \qquad \text{on } \Gamma_{\text{B}}, \tag{94e}$$

$$\boldsymbol{Q}\boldsymbol{N}_{\text{B}} = 0, \qquad \text{on } \Gamma_{\text{B}}, \tag{94f}$$

where $\chi^3_{\text{U}}(X_1, X_2, t)$ is the time-dependent loading function, defined by[20, 30, 93]

$$\chi^3_{\text{U}}(X_1, X_2, t) \equiv \chi^3(X^1, X^2, H, t) := \begin{cases} H - u_{\text{T}}\dfrac{t}{t_{\text{ramp}}}, & t \in]0, t_{\text{ramp}}], \\ H - u_{\text{T}}, & t \in]t_{\text{ramp}}, t_{\text{fin}}]. \end{cases} \tag{95}$$

These prescriptions represent the fact that a prescribed axial compression is applied onto the upper surface of the specimen, while its bottom surface is clamped. The absolute value of the applied axial displacement $|\chi^3(X,t) - \chi^3_{\text{U}}(X_1, X_2, t)|$ increases in time until it reaches the maximum $u_{\text{T}} = 7\,\text{mm}$ at $t = t_{\text{ramp}} = 2\,\text{s}$ and, afterwards, it is kept constant until the final time of the simulated experiment $t = t_{\text{fin}} = 10\,\text{s}$.

The second and third conditions in Equation (94a) indicate that no tangential tractions are applied on Γ_{U}. In addition, Equations (94c) and (94d) mean that the lateral surface of the specimen Γ_{L} is traction-free and that the pore pressure is atmospheric. Finally, Equations (94b) and (94f) show that the upper and lower surfaces are both insulated, so that no fluid flow may occur through them. The fluid, however, is free to escape through the lateral surfaces of the specimen during compression.

A schematic representation of the cylindrical specimen and of the boundary conditions discussed above is shown in Fig 1.

The prescribed initial conditions for the IBVP are

$$\chi(X,0) = \chi_{\text{in}}(X), \qquad \text{in } \mathscr{B}, \tag{96a}$$

$$P(X,0) = 0, \qquad \text{in } \mathscr{B}, \tag{96b}$$

$$\boldsymbol{Q}(X,0) = \boldsymbol{0}, \qquad \text{in } \mathscr{B}, \tag{96c}$$

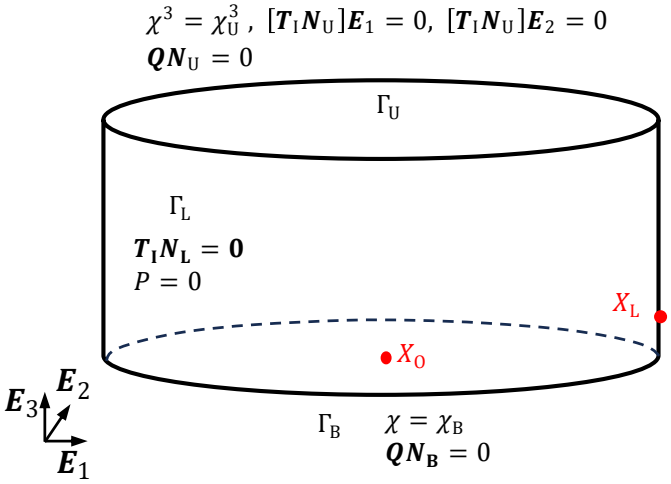

Figure 1: Geometry and boundary conditions for unconfined compression test

where, again, with a slight abuse of notation, we set $\chi_{in}(X) = (X^1, X^2, X^3)$ for all the inner points of $\mathscr{B}$. We remark that, at the initial time $t = t_{in} = 0\,s$, Equations (43a)-(43c) are identically satisfied, whereas, for $t \in]0, t_{fin}]$, it is necessary to have $\boldsymbol{Q}(X,t) \neq \boldsymbol{0}$ in order to meet the hypotheses of Dini's Theorem, as explained in subsection 6.2. Hence, for coding purposes, to avoid the explicit separation of the case $t = 0\,s$ from the case $t \in]0, t_{fin}]$, the initial condition for the filtration velocity $\boldsymbol{Q}$ is taken near the machine precision.

Under the initial and boundary conditions (94a)-(94e) and (96a)-(96c), we study the evolution of the system for different values of the fractional order α, and of the characteristic time t_c in order to simulate the evolution of the flux, of the deformation, and of the stress field over time. In particular, we perform two sets of simulations: for the first one, we assign the characteristic time $t_c = 3\,s$ and we let α vary as $\alpha \in \{0.0, 0.2, 0.4, 0.6, 0.8, 0.99\}$, and, for $\alpha = 0.0$, we recover the non-fractional Darcy-Forchheimer model; for the second set, we take $\alpha = 0.4$, and we assign the characteristic time as $t_c \in \{1\,s, 3\,s, 50\,s\}$. With these test cases, we aim to observe the effects of the two parameters related to the fractional model, α and t_c, on the behavior of the biphasic medium as a whole. The values of the material parameters adopted in the model are reported in Table 1.

The model is solved in ABAQUS® by having recourse to the subroutine "UMAT" for implementing Equation (43a), to the subroutine "UMATHT" for implementing (43b), and by selecting the option *"Fully coupled thermal-stress analysis"* in order to solve simultaneously for the deformation and the pore pressure. The latter option is selected to insert the terms $C^{app}_{P\chi}$ and $C_{\chi P}$, which introduce the coupling between the deformation and the pore pressure in the linearization of the fractional Forchheimer model. We remark that the "UMATHT" subroutine, although originally meant for energy conservation, is used for implementing the mass conservation equation (43b) by using the similarity between these equations [45] (see Appendix C for detailed information).

For the simulations, a quarter of cylinder is simulated and C3D8T elements are used, which are 3D brick elements with three displacements and one "temperature" degree of freedom, which, by analogy, as shown in Appendix C, is employed to simulate the one of pore pressure. Each element has eight integration points. The model has 47372 elements and 43850 nodes. A backward time integration scheme is adopted, with constant time increment of $\Delta t = 1\,s$.

8 Results and discussion

In this section, we present and discuss the numerical simulations of the compression tests described in the previous section. Emphasis will be placed on commenting the memory effects introduced by fractional Forchheimer's correction (43c). Our aim is to contextualize the effects introduced by the

Parameter	Symbol	Numerical value	Unit of measure	Reference
Initial radius	R	30	mm	-
Initial height	H	20	mm	-
Referential solidity	Φ_s	0.2	-	[36]
Reference permeability	k_{ref}	$4 \cdot 10^{-4}$	mm^2	[87]
Material parameter	m_0	0.0848	-	[94]
Material parameter	m_1	4.6380	-	[94]
First Lamé's constant	λ_s	$5.55 \cdot 10^5$	Pa	[20]
Second Lamé's constant	μ_s	$2.22 \cdot 10^5$	Pa	[20]
Density fluid phase	ϱ_f	$1 \cdot 10^3$	kg/m^3	-
Fluid viscosity	μ	$0.89 \cdot 10^{-9}$	$MPa \cdot s$	-
Forchheimer's parameter	c_0	0.363	-	[87]
Forchheimer's parameter	c_1	-5.5	-	[30]
Forchheimer's parameter	c_2	-0.5	-	[30]
Characteristic time	t_c	3	s	-
Prescribed displacement	u_T	7	mm	-
Loading time	T_{ramp}	2	s	-

Table 1: Values of the material parameters used for the numerical simulations.

fractional law through the comparison of the numerical simulations performed in the fractional case with those done under the assumption either of Darcy's law or of non-fractional Darcy-Forchheimer's law. We will focus on the description of the filtration velocity and on its coupling with the deformation of the solid phase through the visualization of the system's evolution. In this respect, we recall that the filtration velocity is, by definition, the product of the velocity of the fluid relative to the solid with the fluid phase volumetric fraction, which, because of the hypothesis of saturation, coincides with the porosity. Therefore, for a specimen under compression, the filtration velocity of the fluid is not a mere consequence of its kinematics relative to the solid, since there exists also a direct feedback of the deformation on the fluid volumetric fraction. The latter, indeed, decreases under compression until the compaction limit, which, in turn, places a lower bound on the volumetric deformation itself. As noticed, e.g., in[19], the natural condition $\Phi_f(X,t) = J(X,t) - \Phi_s(X) \geq 0$ yields the *"unilateral constraint"* $J(X,t) \geq \Phi_s(X)$ at all points $X \in \mathscr{B}$ and at all times.

We remark that the simulated specimen consists of a hypothetical tissue, which, as anticipated above, borrows some of its mechanical and structural properties from articular cartilage, since it features a complex microstructure, and exhibits memory effects[57, 58], while possessing a high permeability that is commonly associated with Forchheimer's correction in biological scaffolds[87].

8.1 Flow through the lateral surface of the specimen

The maximum of the magnitude of the filtration velocity is attained on a locus of points that, due to the axial symmetry of the problem under study, coincides with the circle defined by the lower edge, i.e., $\mathscr{C}_{BL} := \overline{\Gamma}_B \cap \overline{\Gamma}_L$, where the superimposed bar denotes the topological closure of the set to which it is applied (note that, if reinforcing fibers were included in the model, this behavior would be different in general; e.g., in articular cartilage the fibers being parallel to the sample's symmetry axis at the bottom would contrast the transversal filtration velocity in this region). However, since the conditions on the motion imposed on the Dirichlet nodes of the mesh lying on Γ_B have led to small numerical artifacts in the computation of the filtration velocity, we study the evolution of the magnitude of this quantity in a relatively small, stripe-shaped subset of Γ_L, containing $\mathscr{C}_{BL}$. In particular, in this subset, we select the point of coordinates $X_L = (30,\, 0\,, 2.8) \in \Gamma_L$ (length units are given in millimetres), and we observe the evolution of the magnitude of the filtration velocity at this point, i.e., of $\|\boldsymbol{q}(X_L, t)\|$, for different values of α and t_c.

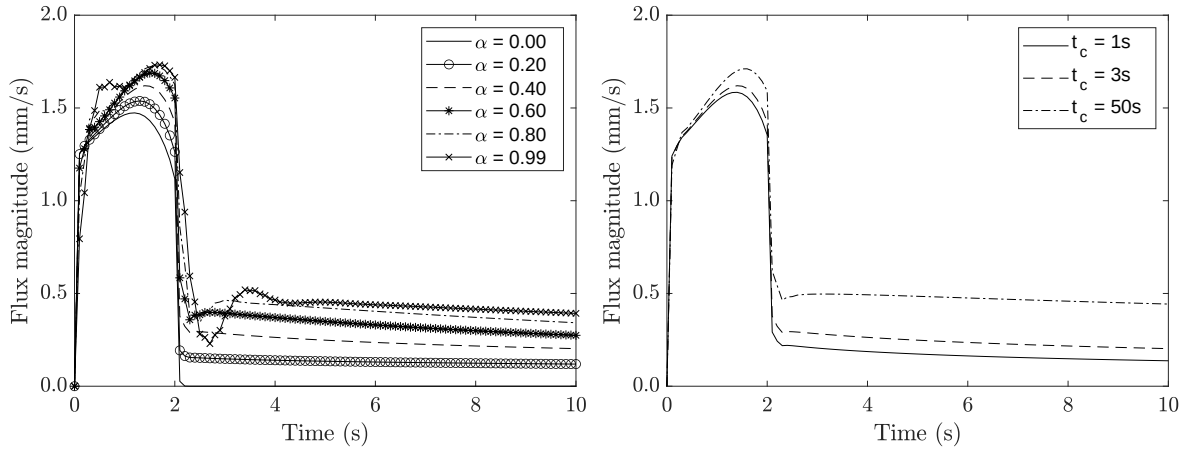

(a) Flow through the lateral surface: influence of α

(b) Flow through the lateral surface: influence of t_c

Figure 2: Time evolution of the Euclidean norm $\|\boldsymbol{q}(X_L, t)\|$ of the filtration velocity ("flux magnitude" in the figures), evaluated at the node corresponding to the point $X_L = (30,\ 0\,, 2.8) \in \Gamma_L$, for $\alpha = 0$ (i.e., standard Darcy-Forchheimer case) and for varying $\alpha \in \{0.2, 0.4, 0.6, 0.8, 0.99\}$ with $t_c = 3$ s (left panel), and for $t_c \in \{1\,\text{s}, 3\,\text{s}, 50\,\text{s}\}$ with $\alpha = 0.4$ (right panel)

.

By computing $\|\boldsymbol{q}(X_L, t)\|$ for various values of α (see Figure 2), we notice that the behavior of the filtration velocity depends noticeably on the fractional order α, whereas the value of t_c scales the trend imposed by α. In fact, in the Darcy model and in the Darcy-Forchheimer model, the maximum of $\|\boldsymbol{q}(X_L, t)\|$ is registered at relatively close time instants $t^* \in [0, t_{\text{ramp}}]$ (see Figure 3). Yet, for the fractional Forchheimer model, the maximum of $\|\boldsymbol{q}(X_L, t)\|$ is observed at times larger than t^*. Moreover, by setting $t_{\max}(\alpha) := \text{argmax}_{t\in[0,t_{\text{fin}}]}\{\|\boldsymbol{q}_\alpha(X_L, t)\|\}$, where $\boldsymbol{q}_\alpha$ indicates the filtration velocity computed for a given fractional order α, we notice that $t_{\max}(\alpha)$ increases with α. As a consequence of this behavior, we also observe a widening of the time interval over which $\|\boldsymbol{q}(X_L, t)\|$ grows monotonically in time. This result constitutes a delay in the attainment of $q_{\max} := \max_{t\in[0,t_{\text{fin}}]}\{\|\boldsymbol{q}_\alpha(X_L, t)\|\}$, and is an expected feature of the model. Its physical interpretation could be related to the complexity of the microstructure, which manifests itself, for instance, through the tortuosity of the pore network, or to some inertial effects of the fluid taking place at the pore scale. Looking at Figure 3, we observe that, for the considered problem, Forchheimer's correction does not affect significantly the dynamics of the interstitial fluid, since $\|\boldsymbol{q}(X_L, t)\|$ in Darcy-Forchheimer's case is only slightly different from the one computed with the equivalent Darcy model (i.e., same setting and same parameters, but $\alpha = 0$ and $c_0 = 0$).

Moreover, it can be observed that there is a trend reversal of the magnitude of the outflow when passing from the very first instants of loading (for t close to 0 s), in which fractional Forchherimer's fluid velocity is lower than the Darcian one, to the subsequent times, where, on average, the magnitude of the outflow increases with the fractional order. Such behavior can be correlated with the evolution of the pressure field, since it does not increase monotonically during the loading phase, as shown in Figure 3(b). The presence of such a "breaking point" suggests a transition from a Darcian-like flow to an alternative flow regime, whose existence depends on whether or not memory related effects are present in the model.

Finally, it can be observed that the increase in the fractional order entails that the flux magnitude relaxes more slowly towards the stationary state, as it is seen in Figures 2 and 3. In addition, the outflow registered while the load is being maintained, i.e., for t greater than T_{ramp}, depends both on α and on t_c. For higher values of the fractional order, e.g. $\alpha = 0.80, 0.99$, fluctuations in the flux are visible after the loading phase, and are quickly reabsorbed. We remark that the presence of oscillatory behavior with exponential decay is typical, for example, of the Mittag-Leffler functions, which can be found as the analytic solution of various integral equations and fractional models[95].

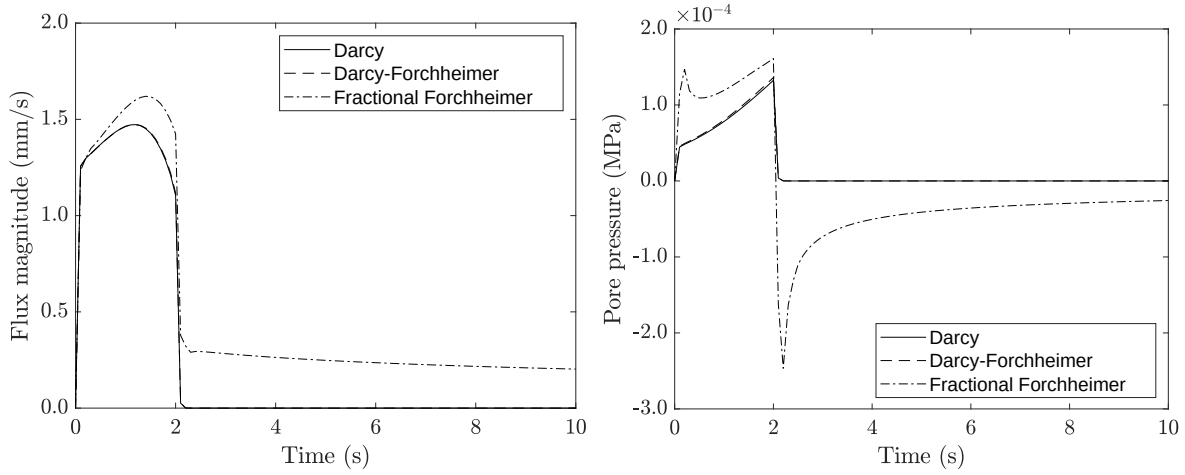

(a) Flux magnitude (b) Pore pressure

Figure 3: Comparison between the Darcy, the Darcy-Forchheimer and the fractional Forchheimer models of the time evolution of the Euclidean norm of the filtration velocity $\|\boldsymbol{q}(X_{\mathrm{L}}, t)\|$ ("Flux magnitude" in Figure 3(a)), evaluated at the node corresponding to the point $X_{\mathrm{L}} = (30,\, 0\,, 2.8) \in \Gamma_{\mathrm{L}}$, and of the pore pressure $P(X_{\mathrm{O}}, t)$ ("Pore pressure" in Figure 3(b)), evaluated at the node corresponding to the point $X_{\mathrm{O}} = (0, 0, 0) \in \Gamma_{\mathrm{B}}$, located at center of the bottom surface Γ_{B}. For the simulation of the fractional Forchheimer model we selected $\alpha = 0.4$ and $t_{\mathrm{c}} = 3$ s.

8.2 Fractional effects in the central region

Next, we move on to analyze the dynamics of the interstitial fluid in the central region of the specimen. Initially, in the center X_{O} of the bottom surface Γ_{B}, the fractional Forchheimer correction induces values of the pore pressure that are even higher than those attained with the non-fractional Forchheimer model, which, in turn, predicts values already higher than in Darcy's model, as shown in Figure 3(b). However, for $\alpha \in [0.40, 0.99]$, the pressure evolution is not monotonic, and for $\alpha = 0.80, 0.99$, the fluctuations of the pressure field induced by the fractional flow model exceed the values in the Darcy-Forchheimer case. Hence, upon this choice of permeability and Forchheimer's parameters, the pressure field evolves and decays mainly because of the memory effects.

Figure 4 displays the magnitude, predicted by the fractional Darcy-Forchheimer model, of the fluid radial filtration velocity evaluated at $X_{\mathrm{O}} \in \Gamma_{\mathrm{B}}$. This magnitude coincides with that of the total filtration velocity since Γ_{B} is in contact with the lower plate, which is impermeable. We notice that, in general, the filtration velocity of the fluid is comparable or slightly greater than the one obtained with the non-fractional Darcy model, i.e., for $c_0 = 0$ and $\alpha = 0$ (see Figure 3). However, while the loading is being maintained, and in response to the value of α, there exist cases in which the fluid filtration velocity is higher than the one computed with the non-fractional Darcy-Forchheimer model (see Figure 4a). In particular, the major oscillations in the pressure values translate into small swings in the tangential filtration velocity that quickly decays while the compression is held. Depending on the tissue under investigation, this result could be interpreted, for example, either as an accumulation of fluid in some regions of the pore network, which, because of tortuosity or other inhibitors of the hydraulic conductivity, may act as slowly emptying "buffers", or as the manifestation at the tissue scale of inertial or viscous effects and fluid-solid interactions at the pore scale. It is also interesting to note that, in $X_{\mathrm{O}} \in \Gamma_{\mathrm{B}}$, pore pressure does not increase monotonically for $\alpha \in [0.40, 0.99]$ (see Figures 3(b) and 4c), while for $\alpha = 0.2$ the behavior resembles the standard Darcy one, as the fractional effects do not induce swings in the pressure fields in the specimen.

Under the steady state loading, ($t > t_{\mathrm{ramp}}$), as time goes by, the history effect decreases, and the flux comes closer to the non-fractional model (see Figure 4a). Finally, only a very marginal impact of α on normal stress is observed (see Figure 4d), apart for the case $\alpha = 0.99$, in which, after the compression

phase ends, the negative pressure exerted on the pores affects the registered stress.

If some chemical substances, like salts or drugs, were considered in our models, and if one were interested in studying the situation in which such substances, dissolved in the fluid, are for some reason concentrated in the lower region of the specimen, then the radial filtration velocity of the fluid would be responsible for their transport towards the outer region of the specimen itself.

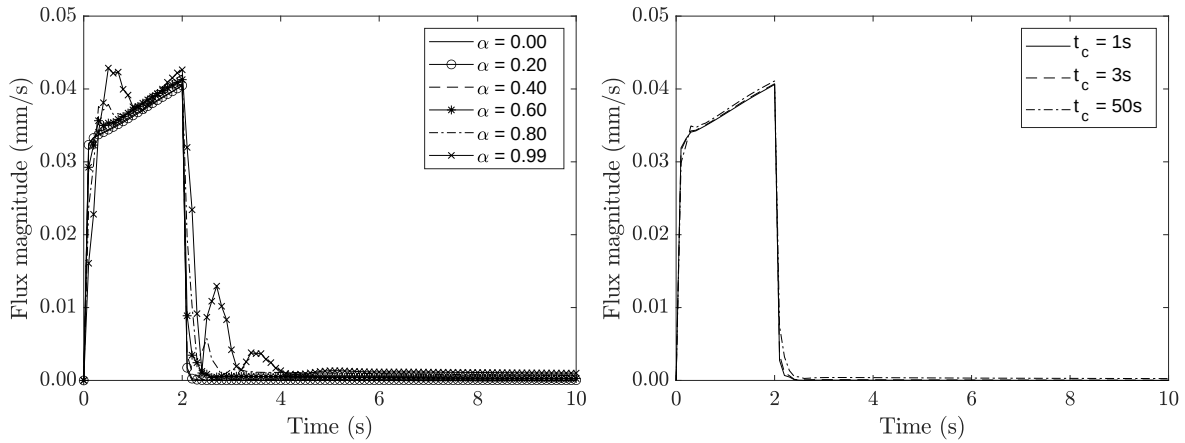

(a) Radial flow at the bottom surface: effect of α

(b) Radial flow at the bottom surface: effect of t_c

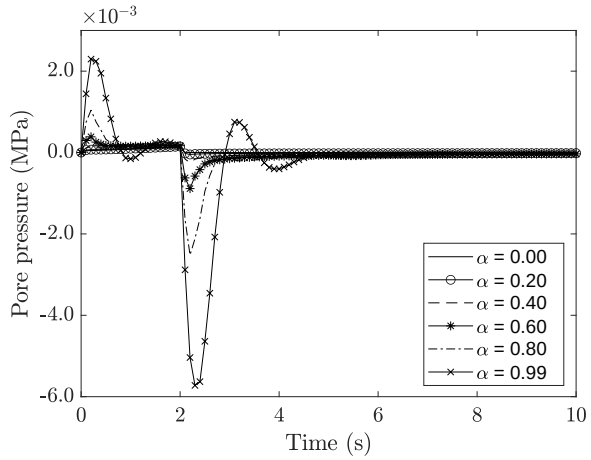

(c) Pore pressure at the bottom surface

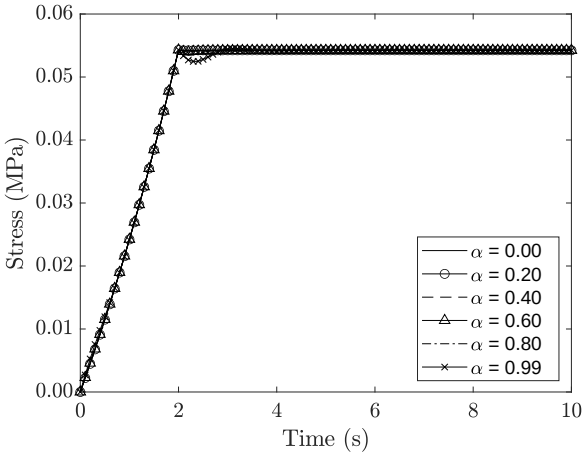

(d) Stress at the bottom surface

Figure 4: Time evolution of the Euclidean norm of the filtration velocity $\|\boldsymbol{q}(X_O, t)\|$ ("flux magnitude" in Figure 4(a) and 4(b)), pore pressure $P(X_O, t)$ ("pore pressure" in Figure 4(c)), and absolute value of the axial component of Cauchy stress, $|\sigma_3{}^3(X_O, t)|$ ("Stress" in Figure 4(d)), evaluated at the node $X_O = (0, 0, 0) \in \Gamma_B$, located at center of the bottom surface Γ_B (corresponding to the origin of the given reference frame) for $\alpha = 0$ (non-fractional Darcy-Forchheimer case) and for varying $\alpha \in \{0.20, 0.40, 0.60, 0.80, 0.99\}$, with characteristic time $t_c = 3$ s (Figures 4(a), 4(c) and 4(d)), and for $t_c \in \{1\,\text{s}, 3\,\text{s}, 50\,\text{s}\}$, with $\alpha = 0.4$ (Figure 4(b)).

8.3 A "zoom in" on the system's behavior for different material parameters

We now consider the case reported in[30], in which Forchheimer's correction is considered to extend the range of applicability of a given description of the flow by allowing to pass from a permeability formulation to a different one. With respect to Table 1, in order to make a comparison with the results observed in [30], this amounts to consider the following parameters: $R = 1.5\,\text{mm}$, $H = 1\,\text{mm}$, $k_{\text{ref}} = 1.88 \cdot 10^{-11}\,\text{mm}^2$, $c_0 = 1.44 \cdot 10^9$ and a loading ramp with the same shape as the one considered before, but with $u_T = 0.2\,\text{mm}$ and $T_{\text{ramp}} = 20\,\text{s}$. In this case, the simulations of the quarter of cylinder are

carried out with the aid of the software ABAQUS® by employing C3D8T elements, with 23800 nodes and 26535 elements.

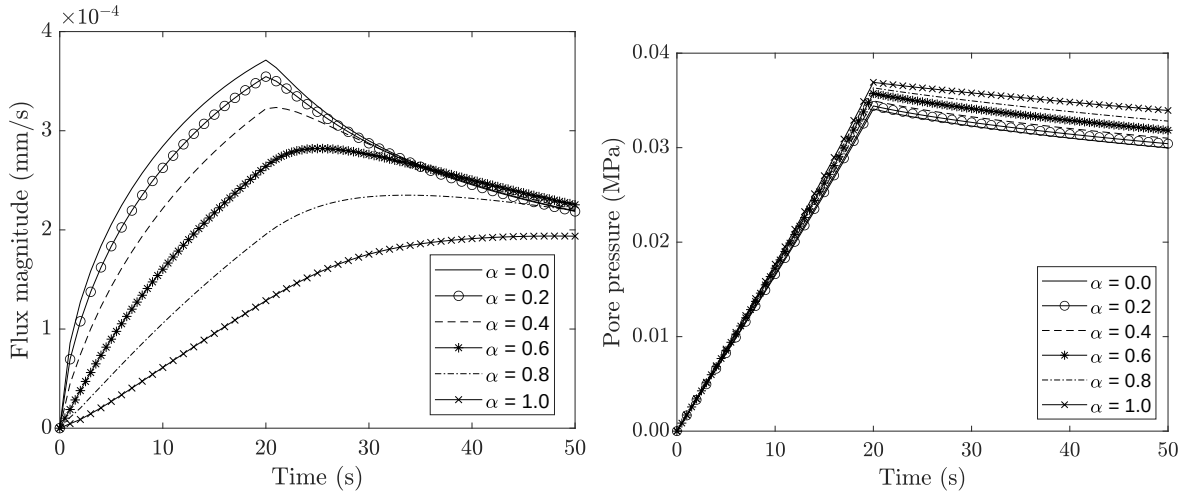

(a) Flux magnitude

(b) Pore pressure

Figure 5: Time evolution of the Euclidean norm of the filtration velocity $\|\boldsymbol{q}(X_{\mathrm{L}}, t)\|$ ("Flux magnitude" in Figure 5(a)), evaluated at the node corresponding to the point $X_{\mathrm{L}} = (1.5, 0, 0.14) \in \Gamma_{\mathrm{L}}$, and of the pore pressure $P(X_{\mathrm{O}}, t)$ ("Pore pressure" in Figure 5(b)), evaluated at the node corresponding to the point $X_{\mathrm{O}} = (0, 0, 0) \in \Gamma_{\mathrm{B}}$, located at center of the bottom surface Γ_{B}, for different values of $\alpha \in \{0, 0.2, 0.4, 0.6, 0.8, 1.0\}$. For the simulation of the fractional Forchheimer model we selected $t_{\mathrm{c}} = 50\,\mathrm{s}$.

In [30], the nonlinear effects associated with standard Forchheimer's model have been interpreted as a correction to the "true" permeability, while the physics of the process described by the model presented in our work is different, and shows that those conclusions can be limiting. Indeed, the analogy with the correction of the permeability is evident only as long as we limit ourselves to a specific time frame in which the recent history of the filtration velocity is monotonically increasing or decreasing. Indeed, if we study $\|\boldsymbol{q}(X_{\mathrm{L}}, t)\|$ for $t \in]0, T_{\mathrm{ramp}}]$, Figure 5(a) shows that the flow's history in the time integral affects the determination of the flux itself in a predictable way. During the loading ramp, the outflow grows because of the increasing compression, and the time derivative of the filtration velocity inside the integral of Equation (43c) is positive, and it does exert an antagonistic action with respect to equivalent Darcy's velocity. In this case, the filtration velocity $\|\boldsymbol{q}(X_{\mathrm{L}}, t)\|$ is lower than the one in the corresponding standard Darcy-Forchheimer model, i.e., under the same boundary and initial conditions. However, for t much greater than $t_{\max}$, the outflow decreases in time, and, thus, the time derivative of the filtration velocity becomes negative, thereby producing results that could be associated with a higher permeability. Hence, depending on the history of the fluid flow, the tissue could be more or less permeable.

This way of framing the study of the filtration velocity makes sense if the equivalent Darcian velocity is still comparable with the filtration velocity in the Darcian case, i.e., if the pressure field evolves in a similar way to the one in Darcy's case. However, this is not necessarily true, as reported in Figure 3(b). In fact, in this case, the analogy with the purely Darcian case holds only in the instants subsequent to the start of the compression, during which the registered values of the outflow in the fractional Forchheimer case are lower than the non-fractional Darcy-Forchheimer ones.

We have already observed in Figure 2(a) that, in fractional Forchheimer's model, the maximum of $\|\boldsymbol{q}(X_{\mathrm{L}}, t)\|$ is reached at a later time than in the standard Darcy-Forchheimer one. In order to quantify this time delay, we report in Figure 6 the time of the simulation in which the maximum outflow is computed as a function of the fractional parameter. Although the trend is clearly influenced by the material parameters considered for the benchmark, it is increasing in both cases.

Finally, a visual comparison between the non-fractional Forchheimer correction (which corresponds

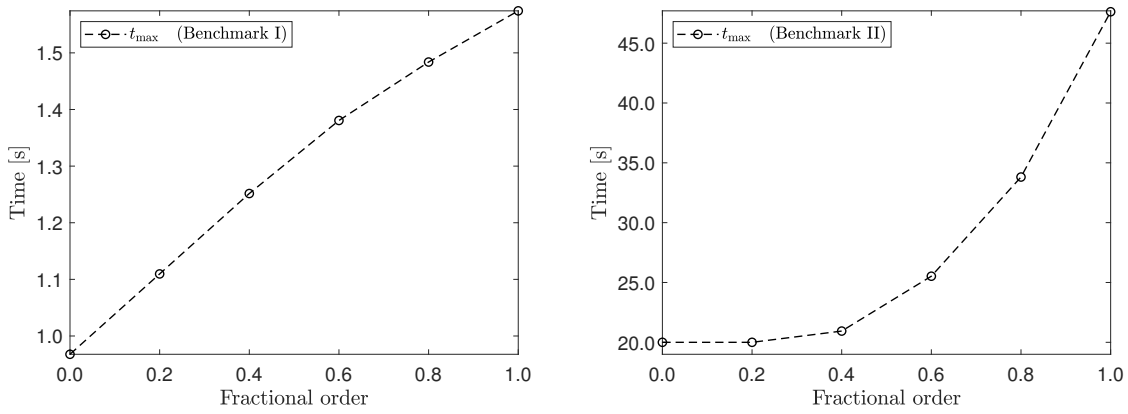

(a) Benchmark I (b) Benchmark II

Figure 6: Time at which the maximum value of the Euclidean norm of the filtration velocity $\|\boldsymbol{q}(X_L, t)\|$ is reached, evaluated at the node corresponding to the point $X_L = (1.5,\ 0\,, 0.14) \in \Gamma_L$, by varying $\alpha \in]0, 1[$.

to the case $\alpha = 0$) and the fractional Forchheimer correction can be drawn by looking at Figures 7 and 8. At the time $t = t_{ramp}$, we plot the spatial distributions of pore pressure, magnitude of the filtration velocity, magnitude of the displacement field, and von Mises stress both for the non-fractional Darcy-Forchheimer model and for the fractional Forchheimer model with $\alpha = 0.4$ and $t_c = 50\,\text{s}$, at the time $t = 20\,\text{s}$. The plots for the pore pressure and for the magnitude of the filtration velocity confirm that the region of interest for understanding the behavior of the fluid are the lower central region, where the overpressure area is located, and the lower lateral surface. The effect of the fractional order α on the coupling of the fluid with the solid phase is weak, since the spatial distribution of the total deformation and von Mises stress are barely affected (Figure 8) by α, and the evolution of the normal stress on the center of the bottom surface is similar (see Figure 4d).

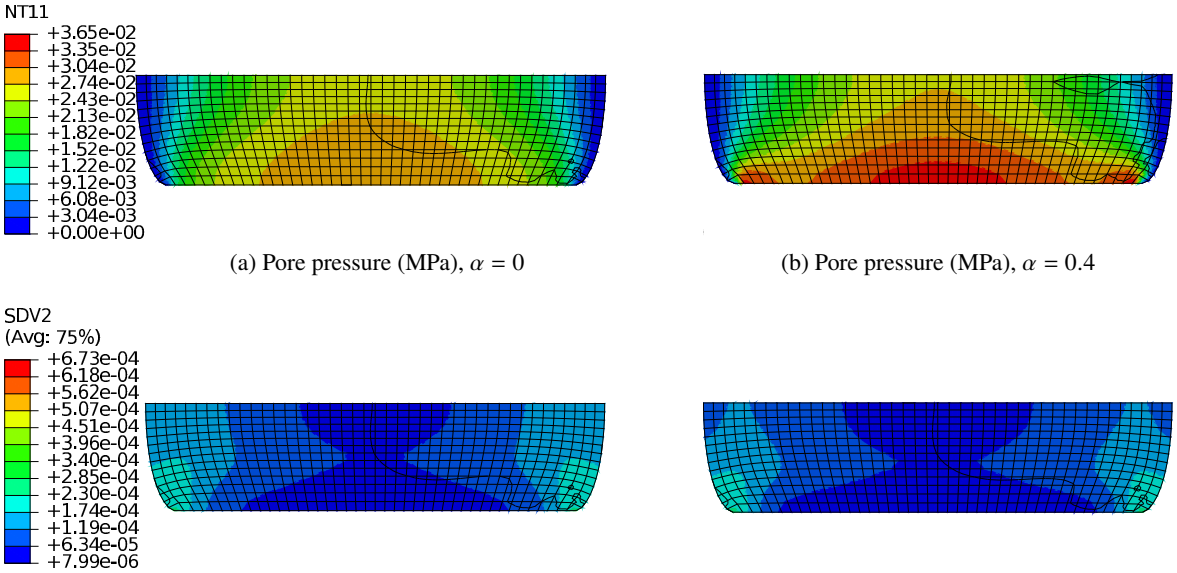

(a) Pore pressure (MPa), $\alpha = 0$ (b) Pore pressure (MPa), $\alpha = 0.4$

(c) Flux magnitude (mm/s), $\alpha = 0$ (d) Flux magnitude (mm/s), $\alpha = 0.4$

Figure 7: Comparison between the standard Darcy-Forchheimer model and the fractional Forchheimer model, with the choice of parameters $\alpha = 0.4$ and $t_c = 50\,\text{s}$, at time $t = 20\,\text{s}$, of the spatial distributions of the pore pressure (Figures 7a and 7b) and flux magnitude (Figures 7c and 7d). The black solid lines in the plots represent different layers of elements of the finite element discretization.

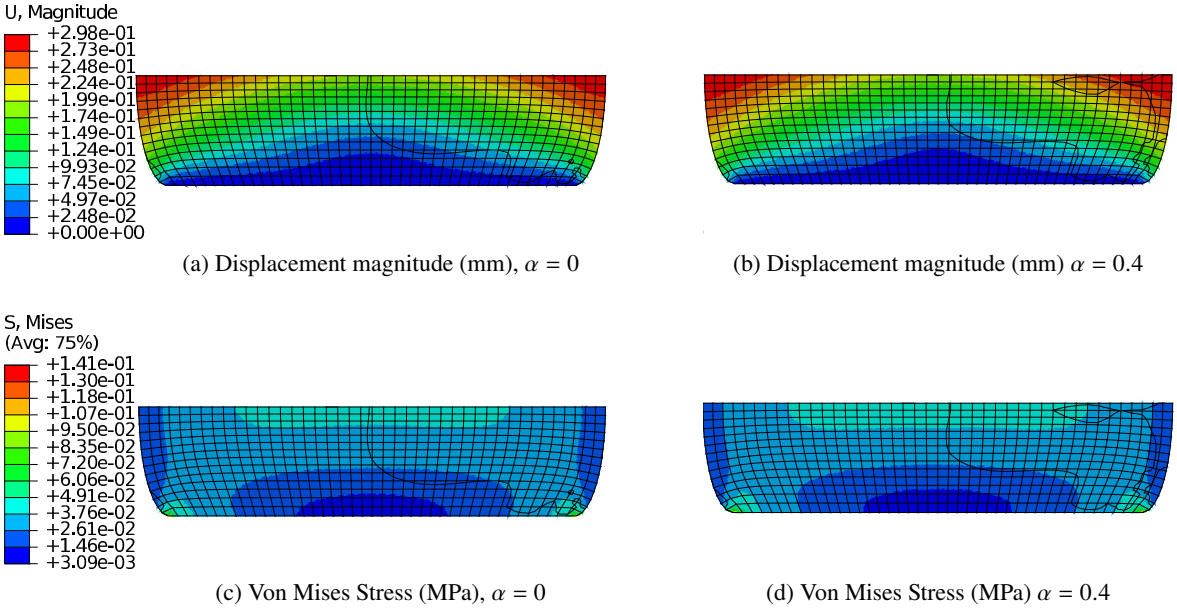

(a) Displacement magnitude (mm), $\alpha = 0$

(b) Displacement magnitude (mm) $\alpha = 0.4$

(c) Von Mises Stress (MPa), $\alpha = 0$

(d) Von Mises Stress (MPa) $\alpha = 0.4$

Figure 8: Comparison between the standard Darcy-Forchheimer model and the fractional Forchheimer model, with the choice of parameters $\alpha = 0.4$ and $t_c = 50\,\mathrm{s}$, at time $t = 20\,\mathrm{s}$, of the spatial distributions of the displacement magnitude (Figures 8a and 8b) and of the von Mises stress (Figures 8c and 8d). The black solid lines in the plots represent different layers of elements of the finite element discretization.

9 Conclusions

In this work, we have described a hypothetical biological tissue, viewed as a saturated and hydrated porous medium, by formulating a mechanical model having the fractionalization of Forchheimer's correction to Darcy's law in finite deformations as target. This amounts to considering the concomitant effect of two deviations from the "classical" Darcian regime, and has been done with the purpose of studying a scenario that may originate in a tissue with a complex microstructure, like articular cartilage, when memory effects have to be combined with flow velocities that do not justify Darcy's approximation. The main motivation for undertaking this study is the generalization of a class of flow models already existing in the literature, and aiming at describing Darcy's law with memory, to the case in which the interactions of the fluid with the solid matrix require to include inertial effects.

With the recent development of numerical methods coupled with image analysis (CFD-IA,[96]), the image-based simulations from high-resolution x-ray tomography and multiphoton microscopy of native meniscal tissue [97, 98] can reveal the fluid flow at the pore scale. Ongoing work on FSI (fluid-structure interaction) - AI, which couples FEM and meshless fluid flow solvers (such as SPH), will give rise to running simulation of deforming the solid and fluid phases of native tissue architecture, retaining the complexity of the pores' morphology. These simulations will provide the data to verify the model proposed here and elsewhere [44] as well as contribute to one of the main questions when dealing with fractional models, i.e., what the relation between the fractional parameters and the architecture of the tissue is. In other words, can we give a physical meaning to the fractional parameters?

To assess what our model predicts for a very typical benchmark problem, we have solved an initial and boundary value problem that simulates the uni-axial compression of a cylindrical specimen of the hypothetical tissue under investigation, and, to this end, we have devised a numerical procedure capable of framing fractional and highly nonlinear flow laws within the context of finite deformation poro-elasticity, and we implemented it in ABAQUS®.

In spite of the fact that, by applying the fractional operator only to the filtration velocity, we have particularized the constitutive picture presented in[38], our research encompasses two essential

generalizations. The first one pertains to the definition of the fractional operator applied to the filtration velocity, and describes the non-linearity of the flow model related to the passage from the Darcian to the Forchheimer regime. Indeed, in Equation (38) we define a generalized Caputo derivative in which the kernel of the integral operator features the resistivity tensor $\boldsymbol{r}_{\mathrm{F}}(\|\boldsymbol{q}(\tau)\|)$ applied to the Truesdell derivative of $\boldsymbol{q}$ at time τ, i.e., $\mathcal{T}_{\mathrm{s}}\boldsymbol{q}(\tau)$. This yields a modified Cattaneo's model for the filtration velocity $\boldsymbol{q}$ that weighs the evolution of $\boldsymbol{q}$ by means of a resistivity coefficient that depends on $\boldsymbol{q}$ itself in a non-linear way.

The second generalization is inherent to the coupling between flow and deformation and consists in the introduction of the Truesdell rate of the flow. Indeed, since our approach is entirely formulated for finite deformations, it requires to employ the *correct* objective derivative for the kinematic parameter chosen to describe the filtration motion of the fluid through the deforming solid matrix. In this respect, since we have chosen the filtration velocity $\boldsymbol{q}$, which is a pseudo-vector, we have reformulated Caputo's classical fractional derivative of $\boldsymbol{q}$ in such a way that the time derivative of $\boldsymbol{q}$, featuring under the integral operator in the classical definition, is replaced by its Truesdell derivative, $\mathcal{T}_{\mathrm{s}}\boldsymbol{q}$. Although the use of the objective rates is well established in Continuum Mechanics, its employment in the present context makes it clear how the deformation affects such reformulation. Indeed, looking at Equation (42), the pull-back of the "modified" Caputo derivative, i.e., with $\mathcal{T}_{\mathrm{s}}\boldsymbol{q}$ in lieu of $\dot{\boldsymbol{q}}$, transforms it into a Caputo-type fractional derivative for $\boldsymbol{Q}$, i.e., expressed in terms of $\dot{\boldsymbol{Q}}(\tau)$, at the price of introducing $J(t)\boldsymbol{F}^{-1}(t)$ and $J^{-1}(\tau)\boldsymbol{F}(\tau)$ in the kernel of the corresponding integral operator: the latter defines the push-forward of $\dot{\boldsymbol{Q}}(\tau)$ to the placement of the medium at time τ, whereas the former defines the pull-back, to the reference placement, of the integral in Equation (42), which captures the whole history of the medium from t_{in} to t.

We point out that the fractional order α, by analogy with Cattaneo's model[99], can be interpreted as a measure of how much the history of the process influences the filtration velocity $\boldsymbol{q}$. Depending on the history, such effect can be more or less antagonizing, and, in the latter case, it can lead to an outflow greater than the one obtainable in the standard Darcy-Forchheimer model under the same loading conditions. We have also observed that the introduction of the fractional law can lead to a significant alteration in the values of pressure in the central region with respect to the Darcy and Darcy-Forchheimer models, depending on the choice of parameters, and we did observe coupling effects that could alter significantly the stress state of the solid phase only for $\alpha = 0.99$. To this end, we remark that different couplings could be studied by considering a different fractional law [38], or by introducing remodeling effects, either structural or due to growth (a fractional model of which has been recently presented in[100]) or due to the spatial reorientation of fibers.

A different kind of nonlinear coupling that we would be interested to study in the future is the combined effect of a fractional Forchheimer's law for the flow and a fractional viscoelastic behavior of the solid phase. This approach would aim at a better characterization of the mechanical behaviour of biological tissues for which fractional models have been successful in describing the solid phase, but no fractional law has been proposed to describe the interstitial fluid.

Conflict of Interests

The Authors declare that they have no conflict of interests.

Authors' contributions

All authors have equally contributed to this work. This work is part of a joint research project conducted in equal measure by the authors Sachin Gunda and Alessandro Giammarini, and constitutes an intersection of their respective PhD programs.

Acknowledgments

This work is partially supported by MIUR (Italian Ministry of Education, Universities and Research) through the PRIN project n. 2017KL4EF3 on *"Mathematics of active materials: From mechanobiology to smart devices."* Sachin Gunda would like to acknowledge the financial support of the Prime Minister's Research Fellowship (PMRF ID: 2502381), Ministry of Education, Govt. of India, for his graduate study at the Indian Institute of Technology Madras. Sachin Gunda would like to acknowledge the International Immersion Experience Award, Office of Global Engagement, IIT Madras, for the financial support. Sachin Gunda and Sundararajan Natarajan acknowledge using the computing resources at HPCE, IIT Madras.

References

[1] G.A. Ateshian. On the theory of reactive mixtures for modeling biological growth. *Biomechanics and Modeling in Mechanobiology*, 6(6):423–445, jan 2007. doi: 10.1007/s10237-006-0070-x.

[2] M.H. Holmes and V.C. Mow. The nonlinear characteristics of soft gels and hydrated connective tissues in ultrafiltration. *Journal of biomechanics*, 23:1145–1156, 1990. ISSN 0021-9290. doi: 10.1016/0021-9290(90)90007-P.

[3] Jacques M. Huyghe, R. Van Loon, and F.T.P. Baaijens. Fluid-solid mixtures and electrochemo-mechanics: the simplicity of lagrangian mixture theory. *Computational & Applied Mathematics*, 23(2-3), dec 2004. doi: 10.1590/s0101-82052004000200008.

[4] B. Loret and F.M.F. Simões. A framework for deformation, generalized diffusion, mass transfer and growth in multi-species multi-phase biological tissues. *Eur. J. Mech. A*, 24:757–781, 2005. doi: 10.1016/j.euromechsol.2005.05.005.

[5] A. Grillo, S. Federico, and G. Wittum. Growth, mass transfer, and remodeling in fiber-reinforced, multi-constituent materials. *Int. J. Nonlinear Mech.*, 47:388–401, 2012. doi: 10.1016/j.ijnonlinmec.2011.09.026.

[6] A. Maroudas and P. Bullough. Permeability of articular cartilage. *Nature*, 219(5160):1260–1261, sep 1968. doi: 10.1038/2191260a0.

[7] Farshid Guilak. Compression-induced changes in the shape and volume of the chondrocyte nucleus. *Journal of Biomechanics*, 28(12):1529–1541, dec 1995. doi: 10.1016/0021-9290(95)00100-x.

[8] G.A. Holzapfel, T.C. Gasser, and R.W. Ogden. A new constitutive framework for arterial wall mechanics and a comparative study of material models. *J. Elast.*, 61(1-3):1–48, 2000.

[9] Juergen Mollenhauer, Matthias Aurich, Carol Muehleman, Giorgi Khelashvilli, and T. C. Irving. X-ray diffraction of the molecular substructure of human articular cartilage. *Connective Tissue Research*, 44(5):201–207, jan 2003. doi: 10.1080/03008200390244005.

[10] J. Merodio and R.W. Ogden. Mechanical response of fiber-reinforced incompressible non-linearly elastic solids. *Int. J. Nonlinear Mech.*, 40(2-3):213–227, 2005. doi: 10.1016/j.ijnonlinmec.2004.05.003.

[11] Kyriacos A. Athanasiou, Eric M. Darling, and Jerry C. Hu. *Articular Cartilage Tissue Engineering*. Springer International Publishing, 2010. doi: 10.1007/978-3-031-02578-5.

[12] Y. Lanir. Constitutive equations for fibrous connective tissues. *J. Biomech.*, 16:1–12, 1983.

[13] T.C. Gasser, R.W. Ogden, and G.A. Holzapfel. Hyperelastic modelling of arterial layers with distributed collagen fibre orientations. *J. R. Soc. Interface*, 3:15–35, 2006. doi: 10.1098/rsif.2005.0073.

[14] S. Federico and W. Herzog. Towards an analytical model of soft biological tissues. *J. Biomech.*, 41:3309–3313, 2008. doi: https://doi.org/10.1016/j.jbiomech.2008.05.039.

[15] S. Federico and W. Herzog. On the permeability of fibre-reinforced porous materials. *Int. J. Solids Struct.*, 45:2160–2172, 2008. doi: https://doi.org/10.1016/j.ijsolstr.2007.11.014.

[16] S. Federico and T.C. Gasser. Non-linear elasticity of biological tissues with statistical fibre orientation. *J. R. Soc. Interface*, 7:955–966, 2010. doi: 10.1098/rsif.2009.0502.

[17] M. Carfagna and A. Grillo. The spherical design algorithm in the numerical simulation of biological tissues with statistical fibre-reinforcement. *Comput. Vis. Sci.*, 18:157–184, 2017. doi: 10.1007/s00791-017-0278-6.

[18] G.A. Holzapfel, R.W. Ogden, and S. Sherifova. On fibre dispersion modelling of soft biological tissues: a review. *Proc. R. Soc. A*, 475(2224):1–22, 2019. doi: https://doi.org/10.1098/rspa.2018.0736.

[19] S. Federico and A. Grillo. Elasticity and permeability of porous fibre-reinforced materials under large deformations. *Mech. Mater.*, 44:58–71, 2012. doi: 10.1016/j.mechmat.2011.07.010.

[20] A. Tomic, A. Grillo, and S. Federico. Poroelastic materials reinforced by statistically oriented fibres — numerical implementation and application to articular cartilage. *IMA J. Appl. Math.*, 79:1027–1059, 2014. doi: 10.1093/imamat/hxu039.

[21] T.M. Quinn, P. Dierickx, and A.J. Grodzinsky. Glycosaminoglycan network geometry may contribute to anisotropic hydraulic permeability in cartilage under compression. *Journal of Biomechanics*, 34(11):1483–1490, nov 2001. doi: 10.1016/s0021-9290(01)00103-8.

[22] G.A. Ateshian and J.A. Weiss. Anisotropic hydraulic permeability under finite deformation. *J. Biomech. Engng.*, 132:111004–1–111004–7, 2010. doi: 10.1115/1.4002588.

[23] Gerhard A. Holzapfel and Ray W. Ogden. Constitutive modelling of arteries. *Proceedings of the Royal Society A: Mathematical, Physical and Engineering Sciences*, 466(2118):1551–1597, mar 2010. doi: 10.1098/rspa.2010.0058.

[24] David M. Pierce, Tim Ricken, and Gerhard A. Holzapfel. A hyperelastic biphasic fibre-reinforced model of articular cartilage considering distributed collagen fibre orientations: continuum basis, computational aspects and applications. *Computer Methods in Biomechanics and Biomedical Engineering*, 16(12):1344–1361, dec 2013. doi: 10.1080/10255842.2012.670854.

[25] K. Hashlamoun, A. Grillo, and S. Federico. Efficient evaluation of the material response of tissues reinforced by statistically oriented fibres. *Z. Angew. Math. Phys.*, 67:113–145, 2016. doi: 10.1007/s10237-006-0049-7.

[26] K. Li, R. W. Ogden, and G. A. Holzapfel. Computational method for excluding fibers under compression in modeling soft fibrous solids. *Eur. J. Mech. A/Solids*, 57:178–193, 2016. doi: 10.1016/j.euromechsol.2015.11.003.

[27] Alessio Gizzi, Anna Pandolfi, and Marcello Vasta. A generalized statistical approach for modeling fiber-reinforced materials. *Journal of Engineering Mathematics*, 109(1):211–226, nov 2017. doi: 10.1007/s10665-017-9943-5.

[28] Van C. Mow, Anthony Ratcliffe, and A. Robin Poole. Cartilage and diarthrodial joints as paradigms for hierarchical materials and structures. *Biomaterials*, 13(2):67–97, 1992. doi: 10.1016/0142-9612(92)90001-5.

[29] S.-K. Han, S. Federico, A. Grillo, G. Giaquinta, and W. Herzog. The mechanical behaviour of chondrocytes predicted with a micro-structural model of articular cartilage. *Biomechanics and Modeling in Mechanobiology*, 6(3):139–150, feb 2006. doi: 10.1007/s10237-006-0016-3.

[30] A. Grillo, M. Carfagna, and S. Federico. Non-Darcian flow in fibre-reinforced biological tissues. *Meccanica*, 52:3299–3320, 2017. doi: 10.1007/s11012-017-0679-0.

[31] G. Alaimo, V. Piccolo, A. Cutolo, L. Deseri, M. Fraldi, and M. Zingales. A fractional order theory of poroelasticity. *Mechanics Research Communications*, 100:103395, sep 2019. doi: 10.1016/j.mechrescom.2019.103395.

[32] S.M. Hassanizadeh. Derivation of basic equations of mass transp. porous med., part 2. generalized Darcy's and Fick's laws. *Adv. Water Resour.*, 9:207–222, 1986.

[33] J. Bear and Y. Bachmat. *Introduction to Modeling of Transport Phenomena in Porous Media*. Kluwer, Dordrecht, 1990.

[34] L.S. Bennethum, M.A. Murad, and J.H. Cushman. Macroscale thermodynamics and the chemical potential for swelling porous media. *Transport in Porous Media*, 39(2):187–225, 2000. doi: 10.1023/a:1006661330427.

[35] A.-R.A. Khaled and K. Vafai. The role of porous media in modeling flow and heat transfer in biological tissues. *International Journal of Heat and Mass Transfer*, 46(26):4989–5003, dec 2003. doi: 10.1016/s0017-9310(03)00301-6.

[36] A. Grillo, M. Carfagna, and S. Federico. The Darcy-Forchheimer law for modelling fluid flow in biological tissues. *Theoretical and Applied Mechanics (TEOPM7)*, 41(4):283–322, 2014.

[37] F. Thauvin and K. K. Mohanty. Network modeling of non-darcy flow through porous media. *Transport in Porous Media*, 31(1):19–37, 1998. doi: 10.1023/a:1006558926606.

[38] Luca Deseri and Massimiliano Zingales. A mechanical picture of fractional-order Darcy equation. *Communications in Nonlinear Science and Numerical Simulation*, 20(3):940–949, mar 2015. doi: 10.1016/j.cnsns.2014.06.021.

[39] JY. Jang and JL. Chen. Variable porosity and thermal dispersion effects on vortex instability of a horizontal natural convection flow in a saturated porous medium. *Wärme- und Stoffübertragung*, 29, 1994. doi: doi.org/10.1007/BF01548599.

[40] Raphaël Bulle, Gioacchino Alotta, Gregorio Marchiori, Matteo Berni, Nicola F. Lopomo, Stefano Zaffagnini, Stéphane P. A. Bordas, and Olga Barrera. The human meniscus behaves as a functionally graded fractional porous medium under confined compression conditions. *Applied Sciences*, 11(20), 2021. ISSN 2076-3417. doi: 10.3390/app11209405.

[41] Giampiero Iaffaldano, Michele Caputo, and Salvatore Martino. Experimental and theoretical memory diffusion of water in sand. *Hydrology and Earth System Sciences*, 10:93–100, 08 2005. doi: 10.5194/hessd-2-1329-2005.

[42] Michele Caputo. Models of flux in porous media with memory. *Water Resources Research*, 36 (3):693–705, mar 2000. doi: 10.1029/1999wr900299.

[43] Alberto Sapora, Pietro Cornetti, B. Chiaia, Ervin Lenzi, and Luiz Evangelista. Nonlocal diffusion in porous media: A spatial fractional approach. *Journal of Engineering Mechanics*, 143: D4016007, 03 2016. doi: 10.1061/(ASCE)EM.1943-7889.0001105.

[44] Sachin Gunda, Sundararajan Natarajan, and Olga Barrera. On the fractional transversely isotropic functionally graded nature of soft biological tissues: Application to the meniscal tissue. *Journal of the Mechanical Behavior of Biomedical Materials*, 143:105855, 2023.

[45] O. Barrera. A unified modelling and simulation for coupled anomalous transport in porous media and its finite element implementation. *Computational Mechanics*, 68:1267–1282, 2021.

[46] Michele Caputo and Wolfango Plastino. Diffusion in porous layers with memory. *Geophysical Journal International*, 158(1):385–396, jul 2004. doi: 10.1111/j.1365-246x.2004.02290.x.

[47] Sabri Uzuner, LePing Li, Serdar Kucuk, and Kaya Memisoglu. Changes in knee joint mechanics after medial meniscectomy determined with a poromechanical model. *Journal of Biomechanical Engineering*, 142(10), jul 2020. doi: 10.1115/1.4047343.

[48] Fabiana Amiri, Emanuela Bologna, Gianmarco Nuzzo, Lorenzo Moroni, and Massimiliano Zingales. Fractional-order poromechanics for a fully saturated biological tissue: Biomechanics of meniscus. *International Journal for Numerical Methods in Biomedical Engineering*, may 2023. doi: 10.1002/cnm.3732.

[49] A. Carpinteri and F. Mainardi, editors. *Fractals and Fractional Calculus in Continuum Mechanics*. Springer Vienna, 1997. ISBN 321182913X.

[50] M. Di Paola, A. Pirrotta, and A. Valenza. Visco-elastic behavior through fractional calculus: An easier method for best fitting experimental results. *Mechanics of Materials*, 43(12):799–806, dec 2011. doi: 10.1016/j.mechmat.2011.08.016.

[51] C. Ionescu, A. Lopes, D. Copot, J.A.T. Machado, and J.H.T. Bates. The role of fractional calculus in modeling biological phenomena: A review. *Communications in Nonlinear Science and Numerical Simulation*, 51:141–159, oct 2017. doi: 10.1016/j.cnsns.2017.04.001.

[52] Jason A. Maes and T.L. Haut Donahue. Time dependent properties of bovine meniscal attachments: Stress relaxation and creep. *Journal of Biomechanics*, 39(16):3055–3061, jan 2006. doi: 10.1016/j.jbiomech.2005.09.025.

[53] L. Camarda, E. Bologna, D. Pavan, F. Morello, F. Monachino, F. Giacco, and M. Zingales. Posterior meniscal root repair: a biomechanical comparison between human and porcine menisci. *Muscle Ligaments and Tendons Journal*, 09(01):76, mar 2019. doi: 10.32098/mltj.01.2019.03.

[54] E. Bologna, M. Di Paola, K. Dayal, L. Deseri, and M. Zingales. Fractional-order nonlinear hereditariness of tendons and ligaments of the human knee. *Philosophical Transactions of the Royal Society A: Mathematical, Physical and Engineering Sciences*, 378(2172):20190294, may 2020. doi: 10.1098/rsta.2019.0294.

[55] Christopher Norberg, Giovanni Filippone, Fotios Andreopoulos, Thomas M. Best, Michael Baraga, Alicia R. Jackson, and Francesco Travascio. Viscoelastic and equilibrium shear properties of human meniscus: Relationships with tissue structure and composition. *Journal of Biomechanics*, 120:110343, may 2021. doi: 10.1016/j.jbiomech.2021.110343.

[56] J. Pajerski. Nonlinear biphasic microstructural numerical analysis of articular cartilage and chondrocytes. *MSc Thesis*, 2010.

[57] Richard L. Magin and Thomas J. Royston. Fractional-order elastic models of cartilage: A multiscale approach. *Communications in Nonlinear Science and Numerical Simulation*, 15(3):657–664, mar 2010. doi: 10.1016/j.cnsns.2009.05.008.

[58] P. A. Smyth and I. Green. Fractional calculus model of articular cartilage based on experimental stress-relaxation. *Mechanics of Time-Dependent Materials*, 19(2):209–228, mar 2015. doi: 10.1007/s11043-015-9260-1.

[59] S. Quiligotti. On bulk growth mechanics of solid-fluid mixtures: kinematics and invariance requirements. *Theoret. Appl. Mech.*, 28-29:277–288, 2002.

[60] S. Quiligotti, G.A. Maugin, and F. dell'Isola. An eshelbian approach to the nonlinear mechanics of constrained solid-fluid mixtures. *Acta Mech.*, 160:45–60, 2003. doi: 10.1007/s00707-002-0968-z.

[61] S. Federico and W. Herzog. On the anisotropy and inhomogeneity of permeability in articular cartilage. *Biomech. Model. Mechanobiol.*, 7:367–378, 2008. doi: 10.1007/s10237-007-0091-0.

[62] Majid Hassanizadeh and William G Gray. General conservation equations for multi-phase systems: 1. averaging procedure. *Advances in Water Resources*, 2:131–144, mar 1979. doi: 10.1016/0309-1708(79)90025-3.

[63] J.E. Marsden and T.J.R. Hughes. *Mathematical Foundations of Elasticity*. Dover Publications, Inc., Mineola, New York, 1983.

[64] Salvatore Federico, Mawafag F. Alhasadi, and Alfio Grillo. Eshelby's inclusion theory in light of Noether's theorem. *Mathematics and Mechanics of Complex Systems*, 7(3):247–285, 2019. doi: dx.doi.org/10.2140/memocs.2019.7.247.

[65] Salvatore Federico, Alfio Grillo, and Reuven Segev. Material description of fluxes in terms of differential forms. *Continuum Mechanics and Thermodynamics*, 28(1-2):379–390, jun 2015. doi: 10.1007/s00161-015-0437-2.

[66] Alfio Grillo, Chiara Giverso, Marco Favino, Rolf Krause, Michael Lampe, and Gabriel Wittum. Mass transport in porous media with variable mass. In *Advanced Structured Materials*, pages 27–61. Springer Berlin Heidelberg, 2012. doi: 10.1007/978-3-642-30532-0_2.

[67] J. Bonet and R.D. Wood. *Nonlinear Continuum Mechanics for Finite Element Analysis*. Cambridge University Press, New York, 2008.

[68] S. Majid Hassanizadeh and Anton Leijnse. A non-linear theory of high-concentration-gradient dispersion in porous media. *Advances in Water Resources*, 18(4):203–215, jan 1995. doi: 10.1016/0309-1708(95)00012-8.

[69] S. Majid Hassanizadeh. Derivation of basic equations of mass transport in porous media, part 1. macroscopic balance laws. *Advances in Water Resources*, 9(4):196–206, dec 1986. doi: 10.1016/0309-1708(86)90024-2.

[70] L.S. Bennethum and T. Giorgi. Generalized Forchheimer equation for two-phase flow based on hybrid mixture theory. *Transport in Porous Media*, 26:261–275, 1997.

[71] M. Köpf, C. Corinth, O. Haferkamp, and T.F. Nonnenmacher. Anomalous diffusion of water in biological tissues. *Biophysical Journal*, 70(6):2950–2958, jun 1996. doi: 10.1016/s0006-3495(96)79865-x.

[72] Evren Özarslan, Peter J. Basser, Timothy M. Shepherd, Peter E. Thelwall, Baba C. Vemuri, and Stephen J. Blackband. Observation of anomalous diffusion in excised tissue by characterizing the diffusion-time dependence of the MR signal. *Journal of Magnetic Resonance*, 183(2):315–323, dec 2006. doi: 10.1016/j.jmr.2006.08.009.

[73] Richard L. Magin, Osama Abdullah, Dumitru Baleanu, and Xiaohong Joe Zhou. Anomalous diffusion expressed through fractional order differential operators in the bloch–torrey equation. *Journal of Magnetic Resonance*, 190(2):255–270, feb 2008. doi: 10.1016/j.jmr.2007.11.007.

[74] Richard L. Magin, Carson Ingo, Luis Colon-Perez, William Triplett, and Thomas H. Mareci. Characterization of anomalous diffusion in porous biological tissues using fractional order derivatives and entropy. *Microporous and Mesoporous Materials*, 178:39–43, sep 2013. doi: 10.1016/j.micromeso.2013.02.054.

[75] I.S. Liu. Method of lagrange multipliers for exploitation of the entropy principle. *Archive Rational Mech. Anal.*, 46:131–148, 1972.

[76] G.A. Ateshian and J.D. Humphrey. Continuum mixture models of biological growth and remodeling: Past successes and future opportunities. *Annual Review of Biomedical Engineering*, 14(1): 97–111, aug 2012. doi: 10.1146/annurev-bioeng-071910-124726.

[77] Teodor Atanacković, Sanja Konjik, Ljubica Oparnica, and Dušan Zorica. The Cattaneo type space-time fractional heat conduction equation. *Continuum Mechanics and Thermodynamics*, 24 (4-6):293–311, oct 2011. doi: 10.1007/s00161-011-0199-4.

[78] Velibor Želi and Dušan Zorica. Analytical and numerical treatment of the heat conduction equation obtained via time-fractional distributed-order heat conduction law. *Physica A: Statistical Mechanics and its Applications*, 492:2316–2335, feb 2018. doi: 10.1016/j.physa.2017.11.150.

[79] Salvatore Federico. The Truesdell rate in continuum mechanics. *Zeitschrift für angewandte Mathematik und Physik*, 73(3), apr 2022. doi: 10.1007/s00033-022-01738-4.

[80] Igor Podlubny. *Fractional Differential Equations: An Introduction to Fractional Derivatives, Fractional Differential Equations, to Methods of Their Solution and Some of Their Applications (ISSN Book 198)*. Academic Press, 1998. ISBN 9780080531984.

[81] Stephen Whitaker. The Forchheimer equation: A theoretical development. *Transport in Porous Media*, 25(1):27–61, oct 1996. doi: 10.1007/bf00141261.

[82] A. Grillo, D. Logashenko, S. Stichel, and G. Wittum. Forchheimer's correction in modelling flow and transport in fractured porous media. *Computing and Visualization in Science*, 15:169–190, 2012.

[83] M.R. Tek, K.H. Coats, and D.L. Katz. The effect of turbulence on flow of natural gas through porous reservoirs. *Journal of Petroleum Technology*, 14(07):799–806, jul 1962. doi: 10.2118/147-pa.

[84] J. Geertsma. Estimating the coefficient of inertial resistance in fluid flow through porous media. *Society of Petroleum Engineers Journal*, 14(05):445–450, oct 1974. doi: 10.2118/4706-pa.

[85] X. Wang, F. Thauvin, and K.K. Mohanty. Non-darcy flow through anisotropic porous media. *Chemical Engineering Science*, 54(12):1859–1869, jun 1999. doi: 10.1016/s0009-2509(99)00018-4.

[86] H. Huang and J. Ayoub. Applicability of the Forchheimer Equation for Non-Darcy Flow in Porous Media. *SPE Journal*, 13(01):112–122, March 2008. ISSN 1930-0220. doi: 10.2118/102715-pa.

[87] M. D. M. Innocentini, R. K. Faleiros, R. Pisani, I. Thijs, J. Luyten, and S. Mullens. Permeability of porous gelcast scaffolds for bone tissue engineering. *Journal of Porous Materials*, 17(5):615–627, October 2009. ISSN 1573-4854. doi: 10.1007/s10934-009-9331-2.

[88] A. Grillo, R. Prohl, and G. Wittum. A poroplastic model of structural reorganisation in porous media of biomechanical interest. *Continuum Mech. Therm.*, 28:579–601, 2016. doi: 10.1007/s00161-015-0465-y.

[89] Markus Knodel, Salvatore Di Stefano, Arne Nägel, and Alfio Grillo. An efficient algorithm for biomechanical problems based on a fully implicit nested newton solver. *Theoretical and Applied Mechanics*, 49(2):183–221, 2022. doi: 10.2298/tam221115012k.

[90] A. Grillo, R. Prohl, and G. Wittum. A generalised algorithm for anelastic processes in elastoplasticity and biomechanics. *Math. Mech. Solids*, 22(3):502–527, 2017. doi: 10.1177/1081286515598661.

[91] J.C. Simo and T.J.R. Hughes. *Computational Inelasticity*. Springer, New York, 1998.

[92] *Abaqus 6.11 Theory Manual*. Dassault Systèmes Simulia Corp, United States, 2011.

[93] Chiara Giverso, Salvatore Di Stefano, Alfio Grillo, and Luigi Preziosi. A three dimensional model of multicellular aggregate compression. *Soft Matter*, 15(48):10005–10019, 2019. doi: 10.1039/c9sm01628g.

[94] M. H. Holmes. Finite deformation of soft tissue: Analysis of a mixture model in uni-axial compression. *Journal of Biomechanical Engineering*, 108(4):372–381, nov 1986. doi: 10.1115/1.3138633.

[95] Ariel Ramírez-Torres, Raimondo Penta, and Alfio Grillo. Effective properties of fractional viscoelastic composites via two-scale asymptotic homogenization. *Mathematical Methods in the Applied Sciences*, 46(16):16500–16520, July 2023. ISSN 1099-1476. doi: 10.1002/mma.9457.

[96] J Waghorne, FP Bonomo, Arash Rabbani, Daniel Bell, and Olga Barrera. On the characteristics of natural hydraulic dampers: An image-based approach to study the fluid flow behaviour inside the human meniscal tissue. *arXiv preprint arXiv:2307.13060, Acta Biomaterialia, under review*, 2023.

[97] Greta Agustoni, Jared Maritz, James Kennedy, Francesco P Bonomo, Stéphane PA Bordas, and Olga Barrera. High resolution micro-computed tomography reveals a network of collagen channels in the body region of the knee meniscus. *Annals of Biomedical Engineering*, 49:2273–2281, 2021.

[98] V Vetri, K Dragnevski, M Tkaczyk, M Zingales, Gregorio Marchiori, NF Lopomo, Stefano Zaffagnini, A Bondi, JA Kennedy, DW Murray, et al. Advanced microscopy analysis of the micro-nanoscale architecture of human menisci. *Scientific Reports*, 9(1):18732, 2019.

[99] Albert Compte and Ralf Metzler. The generalized Cattaneo equation for the description of anomalous transport processes. *Journal of Physics A: Mathematical and General*, 30(21):7277–7289, nov 1997. doi: 10.1088/0305-4470/30/21/006.

[100] Ariel Ramírez-Torres, Salvatore Di Stefano, and Alfio Grillo. Influence of non-local diffusion in avascular tumour growth. *Mathematics and Mechanics of Solids*, 26(9):1264–1293, 2021. doi: 10.1177/1081286520975086.

[101] O Barrera, E Tarleton, HW Tang, and ACF Cocks. Modelling the coupling between hydrogen diffusion and the mechanical behaviour of metals. *Computational Materials Science*, 122:219–228, 2016.

[102] P Sreejith, K Srikanth, K Kannan, and KR Rajagopal. A thermodynamic framework for additive manufacturing of crystallizing polymers, part ii: Simulation of the printing of a stent. *International Journal of Engineering Science*, 184:103790, 2023.

[103] Michael Smith. *Abaqus 6.11 User Subroutines Reference Manual*. Dassault Systèmes Simulia Corp, United States, 2015.

10 Appendix A

We define the *apparent mass densities* $\varrho_\mathrm{s}\phi_\mathrm{s}$ and $\varrho_\mathrm{f}\phi_\mathrm{f}$, with ϱ_s and ϱ_f being the constant true mass densities of the solid and the fluid. Hence, we write the balance of mass for each phase in the mixture's current placement $\mathscr{B}_t$ as[1, 22, 36, 30]

$$\partial_t(\varrho_\mathrm{s}\phi_\mathrm{s}) + \mathrm{div}(\varrho_\mathrm{s}\phi_\mathrm{s}\boldsymbol{v}_\mathrm{s}) = 0 \quad \Rightarrow \quad \partial_t\phi_\mathrm{s} + \mathrm{div}(\phi_\mathrm{s}\boldsymbol{v}_\mathrm{s}) = 0, \quad \text{in } \mathscr{B}_t, \tag{97a}$$

$$\partial_t(\varrho_\mathrm{f}\phi_\mathrm{f}) + \mathrm{div}(\varrho_\mathrm{f}\phi_\mathrm{f}\boldsymbol{v}_\mathrm{f}) = 0 \quad \Rightarrow \quad \partial_t\phi_\mathrm{f} + \mathrm{div}(\phi_\mathrm{f}\boldsymbol{v}_\mathrm{f}) = 0, \quad \text{in } \mathscr{B}_t. \tag{97b}$$

The absence of terms on the right-hand side of Equations (97a) and (97b) means that, at the considered timescale, we see neither growth processes nor mass exchange between the constituents.

Since the mixture considered in our work is saturated, the condition $\phi_\mathrm{s} + \phi_\mathrm{f} = 1$ applies. Hence, the balance of mass for the solid phase and for the mixture as a whole, obtained by adding together Equations (97a) and (97b), can be rephrased as

$$\mathrm{D}_\mathrm{s}\phi_\mathrm{s} + \phi_\mathrm{s}\mathrm{div}\boldsymbol{v}_\mathrm{s} = 0, \quad \text{in } \mathscr{B}_t, \tag{98a}$$

$$\mathrm{div}\boldsymbol{v}_\mathrm{s} + \mathrm{div}\boldsymbol{q} = 0, \quad \text{in } \mathscr{B}_t, \tag{98b}$$

where the substantial derivative with respect to the motion of the solid phase has been introduced, i.e., $\mathrm{D}_\mathrm{s}\varsigma := \partial_t\varsigma + (\mathrm{grad}\varsigma)\boldsymbol{v}_\mathrm{s}$, for any differentiable field $\varsigma : \mathscr{B}_t \times \mathscr{I} \to \mathbb{S}$ valued in $\mathbb{S} \equiv \mathbb{R}$ or in higher-order vector or tensor spaces[5]. Hence, Equations (1a) and (1b) are obtained by considering the pull-back of Equations (98a) and (98b) in the reference placement.

Next, we introduce the balance of linear momentum in the current placement. Since, in the present framework, macroscopic inertial forces are assumed to be negligible from the outset, we write[19, 36, 30]

$$\begin{aligned} &\mathrm{div}\boldsymbol{\sigma}_\mathrm{s} + \boldsymbol{\pi}_\mathrm{s} + \varrho_\mathrm{s}\phi_\mathrm{s}\boldsymbol{g} = \boldsymbol{0}, \\ &\mathrm{div}\boldsymbol{\sigma}_\mathrm{f} + \boldsymbol{\pi}_\mathrm{f} + \varrho_\mathrm{f}\phi_\mathrm{f}\boldsymbol{g} = \boldsymbol{0}, \end{aligned} \quad \Longrightarrow \quad \begin{aligned} &\mathrm{div}(\boldsymbol{\sigma}_\mathrm{s} + \boldsymbol{\sigma}_\mathrm{f}) + (\varrho_\mathrm{s}\phi_\mathrm{s} + \varrho_\mathrm{f}\phi_\mathrm{f})\boldsymbol{g} = \boldsymbol{0}, \quad \text{in } \mathscr{B}_t, \\ &\mathrm{div}\boldsymbol{\sigma}_\mathrm{f} + \boldsymbol{\pi}_\mathrm{f} + \varrho_\mathrm{f}\phi_\mathrm{f}\boldsymbol{g} = \boldsymbol{0}, \quad \text{in } \mathscr{B}_t, \end{aligned} \tag{99a, 99b}$$

where $\boldsymbol{\sigma}_\mathrm{s}$ and $\boldsymbol{\sigma}_\mathrm{f}$ are the Cauchy stress tensors of the solid and of the fluid phase, $\boldsymbol{\pi}_\mathrm{s}$ and $\boldsymbol{\pi}_\mathrm{f}$ are the force densities due to the exchanges of linear momentum between the phases, and $\boldsymbol{g}$ is the gravity acceleration co-vector. Note that, in the equations of the first column, each balance law is associated with a single phase, i.e., either with the solid or with the fluid phase. In the second column, instead, the second equation is identical to its homologous of the first column, while the first equation expresses the balance of linear momentum for the mixture as a whole. Indeed, it is obtained by adding together the balance laws associated with each single phase and by using the hypothesis of the mixture being closed with respect to linear momentum, i.e., $\boldsymbol{\pi}_\mathrm{s} + \boldsymbol{\pi}_\mathrm{f} = \boldsymbol{0}$.

Since, according to Equation (1a), Φ_s is constant in the time interval over which the system is observed, and it is determined univocally by the initial condition Φ_sR, we set $\Phi_\mathrm{s}(X,t) = \Phi_\mathrm{sR}(X)$, and we eliminate it from the set of unknowns featuring in the balance equations. This result, indeed, permits to write the volumetric fractions of the solid and of the fluid phase as $\phi_\mathrm{s}(\chi(X,t),t) = \Phi_\mathrm{sR}(X)/J(X,t)$ and $\phi_\mathrm{f}(\chi(X,t),t) = 1 - \Phi_\mathrm{sR}(X)/J(X,t)$. Therefore, Equations (98b), (99a), and (99b) feature 7 scalar equations in 21 unknowns (assuming $\boldsymbol{\sigma}_\mathrm{s}$ and $\boldsymbol{\sigma}_\mathrm{f}$ to be symmetric): 3 for the components of the motion χ; 3 for the components of the filtration velocity $\boldsymbol{q}$; 6 for the components of $\boldsymbol{\sigma}_\mathrm{s}$; 6 for the components of $\boldsymbol{\sigma}_\mathrm{f}$; and 3 for the components of $\boldsymbol{\pi}_\mathrm{f}$. To these unknowns, however, a Lagrange multiplier accompanying the incompressibility constraint has to be added, so that the full number of unknowns raises to 22. Consequently, to close the model, we need to supply the Cauchy stress tensors $\boldsymbol{\sigma}_\mathrm{s}$ and $\boldsymbol{\sigma}_\mathrm{f}$ as well as the force density $\boldsymbol{\pi}_\mathrm{f}$ constitutively, thereby introducing the missing 15 scalar equations. This way, the *remaining unknowns* to be determined are:

$$\chi, \quad \boldsymbol{q}, \quad p, \tag{100}$$

where p is the pore pressure and represents the Lagrangian multiplier of the present theory.

11 Appendix B

It can be proved that, if the solid phase is hyperelastic and the macroscopic stress response of the fluid phase is not appreciably affected by the fluid viscosity, the Cauchy stress tensors are given by[32, 34, 1, 22, 19, 20, 30]

$$\boldsymbol{\sigma}_{\mathrm{s}} = -\phi_{\mathrm{s}} p \boldsymbol{\imath}^{\mathrm{T}} + \boldsymbol{\sigma}_{\mathrm{sc}}, \qquad \text{in } \mathscr{B}_t, \tag{101a}$$

$$\boldsymbol{\sigma}_{\mathrm{f}} = -\phi_{\mathrm{f}} p \boldsymbol{\imath}^{\mathrm{T}}, \qquad \text{in } \mathscr{B}_t, \tag{101b}$$

where p is pore pressure, $\boldsymbol{\sigma}_{\mathrm{sc}}$ is the constitutive part of $\boldsymbol{\sigma}_{\mathrm{s}}$, and $\boldsymbol{\imath}(x,t)$ is the identity tensor associated with $T_x\mathscr{S}$. Note that, in this work, the Cauchy stress tensors are taken as linear maps from $T_x^*\mathscr{S}$ into itself, i.e., $\boldsymbol{\sigma}_\alpha(x,t) : T_x^*\mathscr{S} \to T_x^*\mathscr{S}$, for all $x \in \mathscr{B}_t$, and, thus, the transpose of the identity tensor $\boldsymbol{\imath}$ is needed for consistency, since it applies that $\boldsymbol{\imath}^{\mathrm{T}}(x,t) : T_x^*\mathscr{S} \to T_x^*\mathscr{S}$, with $x \in \mathscr{B}_t$, and $\boldsymbol{\imath}^{\mathrm{T}}(x,t)\boldsymbol{\beta}(x,t) = \boldsymbol{\beta}(x,t)$, for every co-vector $\boldsymbol{\beta}(x,t) \in T_x^*\mathscr{S}$.

For a given hyperelastic strain energy density function $W_{\mathrm{s}}(\boldsymbol{F})$, the constitutive part of the Cauchy stress tensor associated with the solid phase is identified by

$$\boldsymbol{\sigma}_{\mathrm{sc}}(\chi(X,t),t) = \frac{1}{J(X,t)}\left[\frac{\partial W_{\mathrm{s}}}{\partial \boldsymbol{F}}(\boldsymbol{F}(X,t))\right]\boldsymbol{F}^{\mathrm{T}}(\chi(X,t),t). \tag{102}$$

Moreover, the balance laws (99a) and (99b) can be recast in the form

$$\mathrm{div}(-p\boldsymbol{\imath}^{\mathrm{T}} + \boldsymbol{\sigma}_{\mathrm{sc}}) + (\varrho_{\mathrm{s}}\phi_{\mathrm{s}} + \varrho_{\mathrm{f}}\phi_{\mathrm{f}})\boldsymbol{g} = \boldsymbol{0}, \qquad \text{in } \mathscr{B}_t, \tag{103a}$$

$$-\phi_{\mathrm{f}}\,\mathrm{grad}p + \boldsymbol{\pi}_{\mathrm{fd}} + \varrho_{\mathrm{f}}\phi_{\mathrm{f}}\boldsymbol{g} = \boldsymbol{0}, \qquad \text{in } \mathscr{B}_t, \tag{103b}$$

with $\boldsymbol{\sigma}_{\mathrm{sc}}$ being given in Equation (102), and $\boldsymbol{\pi}_{\mathrm{fd}} := \boldsymbol{\pi}_{\mathrm{f}} - p\,\mathrm{grad}\,\phi_{\mathrm{f}}$ being referred to as the *dissipative part* of $\boldsymbol{\pi}_{\mathrm{f}}$ [32, 34, 1, 5].

The stress tensor featuring in Equation (103a), i.e.,

$$\boldsymbol{\sigma}_{\mathrm{I}} := -p\boldsymbol{\imath}^{\mathrm{T}} + \boldsymbol{\sigma}_{\mathrm{sc}}, \tag{104}$$

represents the *inner part*[32] of the overall Cauchy stress tensor of the solid-fluid mixture under investigation, that is, the stress tensor of the mixture exclusive of the dynamic contributions, which are negligible in the considered regime[32, 19].

12 Appendix C

Equations (57a)-(57c) are solved within ABAQUS® by using some formal analogies among thermoelasticity, poroelasticity and mass diffusion, and by having recourse to the user subroutines "UMAT" and "UMATHT" in the same fashion as [101, 45, 44, 102]. ABAQUS™ "UMATHT" solves the energy balance equation (see Equation (107)). This is similar to the weak form of the mass conservation Equation (57b) that can be written as follows. Integration is taken over the reference placement $\mathscr{B}$, here assumed to coincide with the medium's initial placement, i.e.,

$$-\int_{\mathscr{B}} \frac{J_m - J_{m-1}}{\Delta t} P_{\mathrm{v}} + \int_{\mathscr{B}} \boldsymbol{Q}_m \mathrm{Grad} P_{\mathrm{v}} - \int_{\partial^P_{\mathrm{N}}\mathscr{B}} (\boldsymbol{Q}_m \boldsymbol{N}) P_{\mathrm{v}} = 0. \tag{105}$$

By converting the integrals in Equation (105) to the current placement $\mathscr{B}_t$, Equation (105) becomes

$$-\int_{\mathscr{B}_t} \frac{1}{\Delta t}\left[\left(\frac{J_m - J_{m-1}}{J_m}\right)\right] p_{\mathrm{v}} + \int_{\mathscr{B}_t} \boldsymbol{q}_m \mathrm{grad} p_{\mathrm{v}} - \int_{\partial^P_{\mathrm{N}}\mathscr{B}_t} (\boldsymbol{q}_m \boldsymbol{n}) p_{\mathrm{v}} = 0, \tag{106}$$

where, with a slight abuse of notation, the ratio $(J_m - J_{m-1})/J_m$ is understood here as a function of spatial points and time. The weak form of the energy balance equation given in ABAQUS® reference manual[103] reads

$$\underbrace{\frac{1}{\Delta t}\int_V \delta\theta\rho(U_{t+\Delta t} - U_t)dV}_{=0} = \int_V \delta g \cdot \underbrace{\mathbf{f}}_{\boldsymbol{q}_m} dV + \int_S \delta\theta \underbrace{q}_{-\boldsymbol{q}_m\boldsymbol{n}} dS + \int_V \delta\theta \underbrace{r}_{-\frac{J_m - J_{m-1}}{J_m\Delta t}} dV, \tag{107}$$

where $\delta\theta$ is a virtual variation of temperature, and, thus, plays the role of p_{v}, while δg stands for the spatial gradient of $\delta\theta$, and corresponds to our grad p_{v}. Further equivalences among the variables featuring in Equations (106) and (107) are made for making "UMATHT" suitable for solving Equations (43b) and (43c). The correspondences are as follows: the temperature θ of "UMATHT" plays the role of the pore pressure p; the rate of heat generation is identified with the rate of volumetric deformation, so that r corresponds to $-\big((J_m - J_{m-1})/(J_m\Delta t)\big)$; the heat flux $\mathbf{f}$ corresponds to the filtration velocity $\boldsymbol{q}_m$; the density ρ introduced in "UMATHT" is set equal to zero.

The pseudo-code for the implementation of our equations in ABAQUS® is provided in Algorithm 1. Within "UMATHT", the filtration velocity is solved from Equation (43c) by using the methodology explained in subsection 6.2. Variations of flux with respect to the gradient of pore pressure are calculated according to Equation (89). The information of the gradient required for calculating the filtration velocity through Equation (55) is passed to "UMATHT" from "UMAT" by storing it among the global variables. The terms that are calculated in "UMATHT", required as output to ABAQUS®, are given as

$$FLUX \text{ (see (92))} : \boldsymbol{q}_m^{k-1} = \frac{1}{J_m^{k-1}}\boldsymbol{F}_m^{k-1}\boldsymbol{Q}_m^{k-1}, \tag{108a}$$

$$DFDG \text{ (see (89))} : \mathfrak{B}_m^{k-1} := \frac{1}{J_m^{k-1}}\boldsymbol{F}_m^{k-1}\left[\frac{\partial \boldsymbol{\mathcal{Z}}}{\partial \boldsymbol{Q}_m}(\sharp_m^{k-1})\right]^{-1}\left[\frac{\partial \boldsymbol{\mathcal{Z}}}{\partial \mathrm{Grad}P_m}(\sharp_m^{k-1})\right][\boldsymbol{F}_m^{k-1}]^{\mathrm{T}}. \tag{108b}$$

The subroutine "UMAT" is used to solve the balance of linear momentum, and to define the coupling terms. The Neo-Hookean potential energy density is stated in Equation (70), and the *consistent Jacobian matrix* given in Equation (77) can be written for the problem solved in Section 7 as follows (see (77)):

$$DDSDDE :$$
$$\mathfrak{a}_m^{k-1} = \frac{\Phi_{\mathrm{sR}}\mu_{\mathrm{s}}}{2J_m^{k-1}}\big(\boldsymbol{\eta}^{-1}\underline{\otimes}\boldsymbol{B}_m^{k-1} + \boldsymbol{\eta}^{-1}\overline{\otimes}\boldsymbol{B}_m^{k-1} + \boldsymbol{B}_m^{k-1}\underline{\otimes}\boldsymbol{\eta}^{-1} + \boldsymbol{B}_m^{k-1}\overline{\otimes}\boldsymbol{\eta}^{-1}\big) + \left(\frac{\Phi_{\mathrm{sR}}\lambda_{\mathrm{s}}}{J_m^{k-1}} - P\right)\boldsymbol{\eta}^{-1}\otimes\boldsymbol{\eta}^{-1}. \tag{109}$$

Here, $\boldsymbol{B}$ is the left Cauchy-Green deformation tensor defined as $\boldsymbol{B} := \boldsymbol{F}.\boldsymbol{F}^{\mathrm{T}}$. Other terms that are calculated in "UMAT", required as output to ABAQUS®, are given as

$$STRESS : \boldsymbol{\sigma}_m^{k-1} = \frac{1}{J_m^{k-1}}\boldsymbol{\eta}^{-1}\boldsymbol{T}_{\mathrm{Im}}^{k-1}[\boldsymbol{F}_m^{k-1}]^{\mathrm{T}} \quad \text{(see (71))}, \tag{110a}$$

$$DDSDDT : -\boldsymbol{\eta}^{-1} \quad \text{(see (79))}, \tag{110b}$$

$$RPL := -\frac{J_m^{k-1} - J_{m-1}}{J_m^{k-1}\Delta t}, \tag{110c}$$

$$DRPLDE := -\frac{1}{\Delta t}\boldsymbol{\eta}^{-1} \quad \text{(see (86))}, \tag{110d}$$

$$DRPLDT = 0. \tag{110e}$$

Algorithm 1 Pseudo Code of "UMAT" and "UMATHT" for ABAQUS®

Common Module
Define global variables to store the deformation gradient in "UMAT" to be used by "UMATHT", and to store the history terms for the calculation of fractional integral.
UMATHT:
Inputs: Pore pressure, Increment of pore pressure, Current gradient of pore pressure and other terms.

Calculate permeability κ_{iso} from (36)
Calculate Forchheimer's coefficient $\mathcal{A}_{\text{iso}}$ from (33)
Compute $\mathcal{R}_{\text{F}}$ from (41)
Calculate $\mathcal{F}_{\alpha}$ from (54b)
Compute filtration velocity $\boldsymbol{Q}$ using the Newton-Raphson method as described in section 6.2
Compute flux rate $\dot{\boldsymbol{Q}}_{\text{app}}$ using (50)
Compute the contribution from the current time step to the History variable $\mathcal{F}_{\alpha}(t_m)$ using (54b) and store it in global variables.
Compute flux (108a), Variation of flux with respect to pore pressure gradient using (108b).
Output: Flux at the end of the increment (FLUX), Variation of the flux vector with respect to the spatial gradients of pore pressure (DFDG).
UMAT:
Input: Deformation gradient at the increment's start and end, Stress, Pore pressure at the start of the increment, increment of pore pressure and other terms.
Compute Stress (110a), Consistent Jacobian matrix (109), Variation of stress with pore pressure(110b), rate of volumetric deformation (110c) and its variation with strain increment (110d) and temperature increment (110e)
Store deformation gradient in the global variable.
Output: Stress at the end of the increment(STRESS), Consistent Jacobian matrix (DDSDDE), Volumetric heat generation per unit time (RPL), Variation of stress with respect to pore pressure(DDSDDT), Variation of RPL with Pore pressure(DRPLDT), Variation of RPL with strain increments(DRPLDE).